On the nature, interpretation, and application of electromagnetic reflections in cold ice

Zur Natur, Interpretation und Anwendung elektromagnetischer Reflexionen in kaltem Eis

---

Olaf Eisen

Ber. Polarforsch. Meeresforsch. 474 (2004)
ISSN 1618 - 3193

Zeit?

Nie Zeit –
Selten Zeit –
Gar keine Zeit –
Wer hat noch Zeit?
Wo bleibt die Zeit?
Ich nehme mir Zeit –
Ich suche Zeit –
Noch ist Zeit –
Viel Zeit – Zeit

für Klaus

Olaf Eisen
Stiftung Alfred-Wegener-Institut für Polar- und Meeresforschung Bremerhaven
Columbusstraße
Postfach 120161
D-27515 Bremerhaven

Die vorliegende Arbeit ist die inhaltlich unveränderte Fassung einer kumulativen Doktorarbeit, die 2002 dem Fachbereich Geowissenschaften der Universität Bremen vorgelegt wurde. Die Arbeit ist in elektronischer Form unter http://www.suub.uni-bremen.de verfügbar.

Contents

Zusammenfassung

Die Untersuchung von Gletschern und Eisschilden mit elektromagnetischen Reflexionsverfahren ist eine der gängisten geophysikalischen Methoden der Glaziologie geworden. Diese Doktorarbeit leistet mit neuen Ansätzen und Ergebnissen einen Beitrag zur Auswertung elektromagnetischer Reflexionen, die innerhalb kalter Eiskörper entstehen. Den Hauptteil bildet der direkte Vergleich von synthetischen Radargrammen mit gemessenen Radardaten und die Auslegung daraus abgeleiteter Ergebnisse, besonders hinsichtlich der klimatischen Interpretation von Eiskerndaten. Desweiteren werden neue Beurteilungen von Messtechniken und Datenauswertungen vorgestellt.

Mit Blickpunkt auf die Umgebung der EPICA-Eiskerntiefbohrung in Dronning-Maud-Land, Antarktis, werden zwei unterschiedliche numerische Verfahren zur Vorwärtsmodellierung angewendet: einfache Faltung eines Radarquellsignals mit einer Tiefenreihe der Reflexionskoeffizienten und Simulierung der Ausbreitung elektromagnetischer Wellen in Eis durch anspruchsvolle zweidimensionale finite Differenzen-Modellierung im Zeitbereich. Physikalische in-situ Eigenschaften werden von drei Flachbohrkernen übernommen, die in Dronning-Maud-Land abgeteuft wurden, und für welche Profile der komplexen dielektrischen Eigenschaften vorliegen. Referenzspuren der Radardaten für den Vergleich mit synthetischen Radargrammen werden aus Messungen bestimmt, die von der Oberfläche aus mit verschiedenen Geometrien und Frequenzen durchgeführt wurden.

Die Ergebnisse bestätigen den allgemeinen Ansatz, dass es möglich ist, Radarmessungen durch Vorwärtsmodellierung nachzubilden. Dieses Verfahren ist durch die räumliche Struktur der physikalischen Eiseigenschaften beschränkt. Hervorragende Übereinstimmung zwischen modellierten und Referenzradargrammen wird durch Vorwärtsmodellierung mit finiten Differenzen erzielt. Auch wenn die Faltungsmethode verwertbare Ergebnisse hervorbringt, ist die Übereinstimmung hierbei weniger deutlich. Gründe sind der implizite Einschluß von Wellenphänomenen bei finiten Differenzen-Rechnungen, die bei der Faltung nicht berücksichtigt werden können. Unabhängig von der zur numerischen Berechnung verwendeten Methode sind hochaufgelöste dielektrische Profile im Zentimeterbereich eine notwendige Voraussetzung für erfolgreiche Modellierung.

Die Anwendung kombinierter Eiskern- und Radarauswertungen konzentriert sich auf interne Reflexionshorizonte. Die erfolgreiche Vorwärtsmodellierung erlaubt Sensitiviätsstudien mit veränderten dielektrischen Eiskerndaten. Die Resultate bestätigen frühere Annahmen, dass Änderungen der Permitivität für beobachtete Reflexionshorizonte im oberen Bereich der Eisschilde verantwortlich sind. Obwohl die Variation der Leitfähigkeit als Ursache zu vernachlässigen ist, deutet die starke Korrelation zwischen Permitivität- und Leitfähigkeits-Signalen auf einen wechselseitigen Einfluß hin, was den isochronen Charakter der Reflexionshorizonte bestätigt. Auf Grundlage dieser Eigenschaft wird der Fehler abgeschätzt, welcher mit der Datierung von Reflexionshorizonten und dem Abgleich von Eiskernen verknüpft ist; für das Eisschild in Dronning-Maud-Land und zusätzlich für den kalten alpinen Sattel Colle Gnifetti (Monte Rosa, Walliser Alpen). Die Ergebnisse sind vielversprechend, da die in beiden Studien bestimmten Fehler nur bedingt größer sind als die mit der Eiskerndatierung zusammenhängenden anfänglichen Unsicherheit.

Abstract

The investigation of glaciers and ice sheets by means of ice penetrating radar has become one of the most commonly used geophysical techniques in glaciology. This doctoral thesis contributes new approaches and results to the analysis of electromagnetic reflections originating within cold ice bodies. Main subject is the direct comparison of synthetic radargrams with radar survey data and the explanation of results thereof, especially in view of climatic interpretation of ice core records. In addition, new evaluations of survey techniques and data analyses are presented.

Focusing on the region surrounding the EPICA ice core deep drilling location in Dronning Maud Land, Antarctica, two different numerical forward modeling techniques are used: first, the simple convolution of radar source signals with depth series of reflection coefficients; second, simulation of propagating electromagnetic waves in ice by means of sophisticated two-dimensional finite-difference time-domain modeling. Physical in-situ properties are taken from three shallow ice cores retrieved in Dronning Maud Land, for which profiles of the complex dielectric constant are available. Radar reference traces for comparison with the synthetic radargrams are determined from surface-based radar surveys recorded at various geometries and frequencies.

The results proof the general statement that it is possible to reconstruct radar survey data by forward modeling techniques. Limitations to this approach are set by the spatial characteristics of the physical properties of ice. Finite-difference forward modeling produces excellent agreement of modeled and reference radargrams. Although the convolution technique yields useful results, the correspondence is less clear. Reasons are the implicit inclusion of wave phenomena in the finite-difference calculations which cannot be taken into account by the convolution. Irrespective of the method utilized for numerical computations, high resolution dielectric profiles on the centimeter scale are a necessary requirement for successful modeling.

Application of combined ice core and radar analyses focus on internal reflection horizons. The successful forward modeling allows numerical sensitivity studies with altered dielectric ice core data. Findings confirm earlier assumptions that changes in permittivity are responsible for observed reflection horizons in the upper part of the ice sheet. Although variations in conductivity are negligible for causing reflections, strong correlations of permittivity and conductivity signals indicate a mutual influence, and validate the isochronous character of reflection horizons. Based on this property, the error involved in the dating of reflection horizons and synchronization of ice cores is evaluated for the ice sheet in Dronning Maud Land and additionally for the cold alpine saddle Colle Gnifetti (Monte Rosa, Valaisian Alps). The results are promising as the errors determined in both studies are only relatively larger than the initial uncertainty related to ice core dating.

1 Introduction

Interpretation of ice cores as paleoclimate archives and the significance of ice sheets for global sea level require detailed knowledge about the past and present glaciated environments. Different techniques have been developed that facilitate the determination of the present state as well as the reconstruction of past glaciological settings, in particular surrounding deep drilling locations. The raising number of deep ice cores being retrieved in Antarctica and Greenland as well as development of sophisticated spaceborne remote sensing techniques for mass balance studies come along with an increasing demand for ice core synchronization, improved numerical ice sheet modeling, and extended surface observations. Especially the representativity of individual ice core records deserves major attention. In this context, ice penetrating radar[1] as an active remote sensing technique provides a powerful tool to investigate properties of glaciers and ice sheets, having lead to its widespread application as a standard tool in glaciology [Bogorodsky et al., 1985].

The discovery that aircraft altimeters were subject to dangerously high errors when used over ice sheets [Waite and Schmidt, 1961] started the application of radar soundings in glaciology. Although internal reflections from ice sheets were already observed more than 30 years ago [Jiracek and Bentley, 1967, Robin et al., 1969] their origin is not yet fully understood. First direct comparisons of reflection coefficients calculated from acidity and density changes with measured radar data were carried out by Millar [1981]. By comparing radargrams with a high resolution electric conductivity measurement record of an ice core, Hempel and Thyssen [1992] found direct evidence of reflections being caused by acidic layers from volcanic eruptions.

From electromagnetic theory it is clear that reflections can only occur when dielectric properties within the ice sheet are subject to spatial changes. Based on numerous ice core studies, laboratory experiments, theoretical considerations, and analyses of radar data, the following picture on the origin of electromagnetic reflections in ice sheets is state of the art: discontinuities in the real part of the dielectric constant, the permittivity, are basically related to density and dominate reflections in the upper hundreds of meters; variations in the frequency-dependent imaginary part, proportional to conductivity and related to acidic impurities, are the governing cause for reflections in deeper regions of the ice; a third mechanism, proposed by Harrison [1973], involves dielectric anisotropy of the crystal fabric, but its significance is still heavily discussed, as direct evidence from ice core–radargram comparisons is still pending.

The main application of ice penetrating radar in polar environments has been ice thickness probing in relation to ice core deep drilling projects [Hempel and Thyssen, 1992, Dahl-Jensen et al., 1997, Steinhage et al., 1999, Kanagaratnam et al., 2001, Nixdorf and Göktaş, 2001, among others], mostly carried out with powerful airborne systems. As a matter of principle, ice penetrating radar is used as well to establish the stratigraphy of internal reflection horizons (IRHs). Studies of dielectric proper-

[1] I will use the term ice penetrating radar synonymously to other expressions like radio echo sounding and ground penetrating radar, as no common definition has been agreed on in the radar community.

ties of ice and IRHs suggested for long that most processes forming electromagnetic reflectors take place at the glacier's surface at approximately the same time, with the submergence rate of the isochronic surface being determined by interaction of the flow field and surface accumulation [Robin et al., 1969, Gudmandsen, 1975, Clough, 1977, Millar, 1981, Moore, 1988].

Mapping of IRHs, and thus englacial isochrones, at quasi-continuous scale therefore has been applied to manifold applications: IRHs allow to match ice core records [Jacobel and Hodge, 1995, Siegert et al., 1998]; depict vertical strain rates and history [Jacobel et al., 1993, Raymond et al., 1995, Vaughan et al., 1999, Hodgkins et al., 2000]; reconstruct snow and firn genesis [Frezzotti et al., 2002]; determine spatial distributions of accumulation [Richardson-Näslund and Holmlund, 1999, Siegert and Hodgkins, 2000, Nereson and Raymond, 2001]; and validate numerical ice sheet models [Huybrechts et al., 2000, Baldwin et al., 2003].

Whereas frequency dependent wave absorption and scattering are used to determine the inner fabric state of ice sheets and glaciers [Fujita et al., 1999] and separate certain thermal regimes [Moore et al., 1999, Murray et al., 2000], sophisticated detailed analyses of return signals yield information about basal properties and processes [Oswald and Robin, 1973, Arcone et al., 1995, Corr et al., 2002, among others]. Especially the analysis of the upper tens of meters of firn by high resolution surface-based radar will play a key role for validation and ground truthing of satellite data for constraining Antarctic and Greenland mass balance from space with upcoming CryoSat and ICESat missions [Wahr et al., 2000, Zwally et al., 2002]. Most applications related to internal structures, however, still depend on assumptions and require further information to enable unambiguous data interpretations.

The importance of accurate interpretations of IRHs for the above applications in terms of the underlying physical processes has motivated for some time several studies on forward modeling of radar data, utilizing ice core records of physical properties. Electrodynamic numerical forward modeling approaches are mainly developed in other fields of geophysics [Schoolmeester et al., 1995, Lázaro-Mancilla and Gómez-Treviño, 1996, Roberts and Daniels, 1997, Bergmann et al., 1998]. However, in those studies simplistic physical properties are usually attributed to the considered mediae.

In glaciology, two techniques are widely used to derive electric properties along ice cores: the direct current conductivity can be determined from electric conductivity measurements [Hammer, 1980]; the distribution of the dielectric constant as a function of depth is derived from dielectric profiling (DEP) [Moore and Paren, 1987]. While DEP was first designed to detect volcanic horizons [Moore et al., 1991] by measuring alternating current conductivity, it meanwhile developed to a sophisticated high precision method to determine an ice core's complex dielectric constant [Wilhelms et al., 1998], thus becoming a technique well renown in ice core analysis [Wolff, 2000].

Earlier approaches for ice core-based forward modeling involving direct comparison of glaciological survey and synthetic radar data, in principle providing the best means to directly investigate reflection mechanisms, were only of minor success [e.g. Moore, 1988, Blindow, 1994, Hildebrand, 1996, Miners et al., 1997, Miners, 1998].

Reasons are mainly shortcomings of ice core data, limited computational resources, but also brave assumptions on the characteristics of radar data. The recent establishment of an improved calibrated DEP device for simultaneous measurements of the real and imaginary part of the complex dielectric constant with a precision in the 1% range [Wilhelms, 2000] opened new opportunities to investigate physical processes leading to electromagnetic reflections. The studies presented here were significantly motivated by this development.

2 Towards Synthetic Radargrams

Starting point is the physical-chemical interpretation of electromagnetic reflections in cold ice. In this section I present the underlying line of thought, the red thread so to say, and introduce the approaches and applications dealt with in detail in the different studies attached at the end. The organization and sequential structure of the corresponding publications will be summarized in the last section.

During several EPICA[2] pre-site surveys for selection of a suitable deep drilling location in Dronning Maud Land Antarctica, a comprehensive data set was obtained on the physical and chemical properties of the upper 100-150 m of ice. High resolution DEP was performed along three ice cores (B31, B32, and B33), retrieved in 1997/98 [Oerter et al., 2000]. These data are the essential part of all studies, as the dielectric properties of the ice cores are assumed to represent the in-situ distribution in the ice sheet. In the field season 1998/99 a traverse connecting the locations of ice cores drilled in earlier seasons recorded surface-based radar profiles at different frequencies. In 2000/01 this radar data set was extended to cover especially the region surrounding the deep drilling location at the new Kohnen station and improve earlier – partly poor – data sets. The results achieved during the last years depend on three key factors: well coordinated field programs relating ice core drilling and radar surveys; availability of the precise dielectric profiles in high resolution; development of numerical models to suit ice radar applications.

Forward modeling of radargrams based on ice core DEP data is carried out by utilizing two different methods, namely the convolution and the finite-difference time-domain (FDTD) approach. The convolution technique requires knowledge of the electromagnetic wave speed distribution in the ice, motivating preliminary studies described first.

2.1 Radar- and DEP-based electromagnetic wave speeds

A initial step to evaluate the comparability of radar profiles in respect to ice core information is the comparison of traveltime–velocity and traveltime–depth profiles derived from radar common-midpoint (CMP) surveys at different frequencies (described in more detail in paragraph 2.5) with those calculated from ice DEP and density data [PAPER I: Eisen et al., 2002]. The finding that it is possible to convert radar traveltimes to depth with an error of only a few percent, independently of

[2]European Project for Ice Coring in Antarctica

any other than radar information, had the immediate consequence that during the expedition EPICA VI in 2000/01 a number of CMP surveys were carried out in the vicinity of the new deep drilling location. Although processing of the data is still under preparation, the regional distribution of radar traveltime–depth transfer functions will provide important information on the variation of physical properties and will decrease errors involved in calculation of accumulation rates and ice deformation from radar profiles.

2.2 Convolution technique

Preparatory studies for FDTD forward modeling include implementation of the convolution technique. As it only requires a low number of simple calculations which can be carried out rather fast, it is the means of choice to perform first investigations on interpolation and processing schemes of DEP data sets, evaluate their significance for forward modeling, and test different radar wavelet parameters.

The convolution approach generally considers the distribution of reflection coefficients with depth to be the impulse response function of the subsurface. Complex convolution of the source signal with the complex reflection coefficient, determined from the dielectric impedance contrast of adjacent DEP samples, results in a synthetic radargram.

Although several approximations are involved in the calculation of convolution radargrams, especially the explicit conversion of the DEP data from depth- to time-domain, results are already promising in view of the general suitability of the DEP data for forward modeling. Equally important, they also give first insights into the nature of electromagnetic reflections. In PAPER II [Eisen et al., 2003c] I demonstrate the possibility to reproduce prominent IRHs in a radargram by forward modeling with the convolution technique. Most of them are identified as isochrones, some of which are related to acidic signals like volcanic eruptions.

In addition to partly successful forward modeling, two important results are obtained: sensitivity studies with altered DEP data confirm earlier assumptions that permittivity is indeed the important physical variable causing reflections in the upper part of the ice sheet; in a number of cases the permittivity signals constituting the reflections significantly coincide with dominant peaks in the conductivity record, partly of volcanic origin, indicating that the observed reflections are isochrones. Despite these important results the question what causes the correlation of chemical impurities and permittivity, and if acidic layers affect the permittivity of the firn, cannot be definitely answered.

2.3 Finite-difference time-domain technique

Subsequent experiments brought along a milestone for forward modeling of ice penetrating radar surveys: the successful detailed reproduction of survey data by DEP-based numerical FDTD forward modeling [PAPER III: Eisen et al., 2003d]. The excellent agreement of synthetic and radar-based results demonstrates the capability of FDTD models to reproduce radargrams from ice core properties to a much

higher degree than convolution models. This emphasizes the exploitation of radar data for improved interpretations of glaciological climate proxys and indicates new approaches to overcoming limitations of radar survey data.

Advantages of the FDTD technique in comparison to convolution methods are the implicit inclusion of electromagnetic wave phenomena occuring during propagation, like multiple reflections, interferences, absorption, geometrical spreading, ray focusing, phase shifts, etc. However, the performance of FDTD forward modeling requires a huge number of model points and computing time, complicating simple implementation. The numerical model is based on a FDTD set of Maxwell's curl equations [Yee, 1966], implemented on a staggered grid with absorbing boundary conditions. Its general structure, special requirements for our purposes, and advantages of the developed implementation are describe in detail in appendix A.1.

2.4 Application: synchronization of ice cores

In conjunction with ice core data it is possible to obtain information about the internal structure of cold ice bodies, important to improve climatic interpretations in respect to the past and present glaciated environment. The transfer of age–depth relationships obtained from ice core records is not exclusively bound to polar regions, but can also be performed at cold alpine drill sites [PAPER IV: Eisen et al., 2003a], coming along with information on ice thickness and bedrock topography. The results show that the general lack of information on the reflector properties (i.e. constituting physical features) decreases accuracies of ice core synchronization, not only in alpine regions with their more difficult topographical settings, but also in ice sheets.

An immediate application of the developed DEP-based FDTD forward modeling technique therefore involves investigations on improving quantitative interpretation and utilization of isochrones [PAPER V: Eisen et al., 2003b]. Investigations include which errors are related to conventional IRH dating; how accurate the synchronization of ice cores and the extrapolation of ice core properties along IRHs can be performed; and if the combination of ice core dating and forward modeling of radar data provides advantages to conventional techniques.

Various methods are utilized, including conventional geophysical techniques to connect radar data and subsurface features. Novel sensitivity studies performed with altered ice core records reveal characteristic composition of individual radar reflections. Results demonstrate that the error involved in IRH dating in the upper hundreds of meters of the ice sheet is only slightly larger than the error coming along with initial ice core dating. The developed concept can be considered a first step towards extension of the forward modeling approach to deeper regions of the ice sheet where several physical processes leading to reflections of comparable magnitude show up.

2.5 Model validation and characteristics of radar survey data

Comparisons of modeled radargrams with measured radar data require suitable reference traces. These can either be derived from single point, common-offset or CMP radar surveys. Whereas the first two survey setups are carried out at a fixed transmitter–receiver distance, stationary in the first case and moving across the surface in the second, the CMP recording technique, adapted from seismic data acquisition, provides multifold coverage at several nonzero-offsets, thereby improving signal-to-noise ratio and yielding subsurface velocity information [Garotta and Michon, 1967, Yilmaz, 1987].

Different radar setups, data processing, and display methods are examined to evaluate the truth content of synthetic radargrams; for instance, comparing raw single radargrams, embedding synthetic traces in raw common-offset profiles, or opposing synthetic traces and stacked common-offset data in multi-trace wiggle format. Results indicate that noise content of individual radar traces in conjunction with the influence of small scale variability of physical properties impose a severe problem on objective reproducibility of survey radar data [PAPER V: Eisen et al., 2003b]. This is likely an additional reason why forward modeling approaches attempted in the past only had minor success.

Due to the relatively low signal-to-noise ration and lateral inhomogeneity of the firn pack it is difficult to locate the arrival time of IRH signals exactly when considering a single radar trace for comparison with a synthetic radargram. To decrease the noise content of the radar data for further analysis, and to minimise the influence of reflections from obstacles at the surface, another approach is based on creating a single trace radargram by stacking all traces from eleven different radar profiles located within a radius of 50 m of the borehole under consideration [PAPER II: Eisen et al., 2003c].

It is also possible, and of advantage, to make use of the specific characteristic of the CMP survey setup [PAPER III: Eisen et al., 2003d]. Based on the CMP velocity model [PAPER I: Eisen et al., 2002] a normal moveout correction is applied to each trace. Subsequent stacking of all normal moveout corrected traces results in one single reference trace. Advantages of this technique are the coverage of the same stationary center points, ideally at the borehole location, and reduction of noise from lateral inhomogeneities of the dielectric properties. Success of this method emphasizes the role of the small scale variation of physical properties during measurements and lays out a general approach for overcoming these difficulties.

3 Publication Synopsis

Finally, I want to complement the thematically structured description given above with a short account on the content of the five papers attached below. The accuracy of electromagnetic wave speeds derived from CMP radar surveys is estimated in PAPER I [Eisen et al., 2002]. Comparison with wave speeds calculated from ice core DEP and density profiles accentuates the benefit to be gained from the CMP technique for conversion of signal traveltime to depth. Yielding wave speeds that are only a couple of percent different from those derived from ice core profiles, which agree within the 1% range, the area-wide application of CMP surveys for improved radar interpretations is justified.

The successful forward modeling of radargrams by means of the convolution method from ice core DEP data prepares the ground for the interpretation of reflection horizons in PAPER II [Eisen et al., 2003c]. The origin of prominent reflection horizons is determined, simultaneously proving one of their most important properties, the isochronous character. The study also raises the question where the observed correlation between permittivity and conductivity is coming from, a significant point for future investigations.

PAPER III [Eisen et al., 2003d] demonstrates the possibility to reproduce survey radargrams to a high degree by applying FDTD forward modeling, a major enhancement to the convolution approach. The results emphasize the importance of suitable radar processing schemes in equal measure to high quality ice core data and numerical techniques. Sensitivity runs provide direct evidence for the dominating role of permittivity changes for electromagnetic reflections in the upper ice sheet.

The last two papers indicate several applications of radar analysis in different environments. The cold alpine saddle Colle Gnifetti (Monte Rosa, Swiss-Italian Alps) is the stage for investigating the potential of ice penetrating radar to provide mutual information to ice core data retrieved from cold ice bodies in the mid-latitudes, presented in PAPER IV [Eisen et al., 2003a]. The difficult settings in respect to bedrock topography and flow regime are overcome by sophisticated processing of radar data and cross-checking with ice core records. Advanced interpretation of the internal structure is thus accomplished and enables improved climatic interpretations of ice cores.

Dating of reflection horizons and synchronization of ice cores in Antarctic firn are evaluated in PAPER V [Eisen et al., 2003b]. This presentation is the linkage of expertise developed in the above studies and permits immediate application to climate pursuits. Employing numerical forward modeling yields an improved interpretation of reflection characteristics and ice core signals on a regional scale, thus reducing misinterpretation of unambiguous reflection horizons. The successful combination of different techniques in the upper part of the ice sheet point out a means how to gain better insights into the more difficult reflection processes occuring at greater depths.

A Related Software

This appendix provides a short overview of the main software developed for the studies referred to above. The main part is concerned with the numerical model EMICE. In addition, I will also briefly describe the module RAMACIN, which is the essential link between the RAMAC radar system and the DISCO processing software. Many other stand-alone shell scripts were developed for this thesis, e.g. for transformation of data for numerical models and data analyses. Instead of describing all of them here I decided to put together a comprehensive CD-ROM for future applications, including corresponding manuals and the source code of executables, software modules, and shell scripts.

A.1 The Finite-Difference Time-Domain Model EMICE

Different schemes were developed over the decades to employ numerical techniques for computational electrodynamics. Whereas several approaches are based on wave equation formulations of only the electric or magnetic field, the algorithm introduced by Yee [1966] solves for both electric and magnetic fields in time and space using the coupled Maxwell's curl equations. This provides a robust basis with several advantages over other realizations. In this section I describe the physical foundation of the FDTD program EMICE, including governing equations, and outline its implementation and performance to demonstrate what has been achieved. Details on the physical interpretations, other implementation approaches, and a variety of applications can be found in Taflove [1995].

Governing Equations

For a three-dimensional (3D) region in space without electric and magnetic current sources, but which might have properties for absorbing electric or magnetic field energy, the relationships between electric and magnetic fields can be given by the time dependent Maxwell equations in a differential form for a cartesian coordinate system in MKS units, reading

$$\frac{\partial \vec{B}}{\partial t} = -\nabla \times \vec{E} - \vec{J}_m \quad \text{(Faraday's Law)}, \tag{1a}$$

$$\frac{\partial \vec{D}}{\partial t} = \nabla \times \vec{H} - \vec{J}_e \quad \text{(Ampére's Law)}, \tag{1b}$$

$$\nabla \cdot \vec{D} = 0 \quad \text{(Gauss's Law for the electric field)}, \tag{1c}$$

$$\nabla \cdot \vec{B} = 0 \quad \text{(Gauss's Law for the magnetic field)}. \tag{1d}$$

Here, $\vec{E}$ is the electric field vector; $\vec{D}$ is the electric flux density vector; $\vec{H}$ is the magnetic field vector; and $\vec{B}$ is the magnetic flux density. The electric and magnetic conduction current densities are given by J_e and J_m, respectively. For the present application I consider the medium to consist of linear, isotropic, and non-dispersive materials. Introducing the magnetic permeability μ' and the electric permittivity

ε', two simple proportions relate $\vec{B}$ to $\vec{H}$ and $\vec{D}$ to $\vec{E}$, respectively:

$$\vec{B} = \mu'\vec{H}, \tag{2a}$$
$$\vec{D} = \varepsilon'\vec{E}. \tag{2b}$$

As the assumptions permit the possibility of electric and magnetic losses, dissipating electromagnetic fields in materials via conversion to heat energy, two equivalent magnetic and electric currents can be defined to account for the magnetic and electric loss mechanisms, respectively:

$$\vec{J}_m = \tau\vec{H}, \tag{3a}$$
$$\vec{J}_e = \sigma\vec{E}, \tag{3b}$$

with τ being the equivalent magnetic resistivity and σ the electric conductivity. Combination of (2) and (3) with substitution into (1) leads us to

$$\frac{\partial\vec{H}}{\partial t} = -\frac{1}{\mu'}\nabla\times\vec{E} - \frac{\tau}{\mu'}\vec{H}, \tag{4a}$$
$$\frac{\partial\vec{E}}{\partial t} = \frac{1}{\varepsilon'}\nabla\times\vec{H} - \frac{\sigma}{\varepsilon'}\vec{H}, \tag{4b}$$

This set of six partial differential equations, as $\vec{E} = (E_x, E_y, E_z)$ and $\vec{H} = (H_x, H_y, H_z)$, forms the basis of the FDTD numerical algorithm for electromagnetic wave interactions with general 3D mediae [Taflove, 1995, p. 55].

Numerous applications allow the reduction of this 3D set to two dimensions (2D), assuming that neither the field excitation nor the geometry has any variation in a distinguished direction. In our case the considered medium is assumed to extend to infinity in y-direction with no change in the material properties of its transverse cross section. Furthermore, all partial derivatives in respect to y are equal to zero and can therefore be neglected in the full set (4). In addition to considerably reducing the model space, thus requiring less CPU memory and computation time, another effect can be exploited to ease physical considerations, namely the decoupling of transverse magnetic (TM) and transverse electric (TE) modes[3] [Hohmann, 1988]. For example, the 2D TE mode in respect to the z-axis involves only H_x, H_z, and E_y with the set of equations

$$\frac{\partial\vec{H}_x}{\partial t} = \frac{1}{\mu'}\left(\frac{\partial\vec{E}_y}{\partial z} - \tau\vec{H}_x\right), \tag{5a}$$
$$\frac{\partial\vec{H}_z}{\partial t} = \frac{1}{\mu'}\left(-\frac{\partial\vec{E}_y}{\partial x} - \tau\vec{H}_z\right), \tag{5b}$$
$$\frac{\partial\vec{E}_y}{\partial t} = \frac{1}{\varepsilon'}\left(\frac{\partial\vec{H}_x}{\partial z} - \frac{\partial\vec{H}_z}{\partial x} - \sigma\vec{E}_y\right). \tag{5c}$$

Implementation of the operational FDTD model EMICE is based on these equations.

[3]Note that use of the terms TM and TE varies among authors, as different axes are considered to define transverse.

Finite Difference Formulation: the Yee Algorithm

The algorithm introduced by Yee [1966] solves for both electric and magnetic fields in time and space using the coupled Maxwell's curl equations. Both fields are calculated on different, but interleaved space lattices. The special choice of the space lattices implicitly enforces Gauss' relations, as every $\vec{E}$ component is surrounded by four circulating $\vec{H}$ components and vice versa.

Applying standard numerical approximations for differential operators accurate to second order in time and fourth order in space ($O[2,4]$), the components of the 2D Maxwell's curl equations in TE mode (5) can be rearranged to yield a formulation where new values of H_x, H_z, and E_y at a space point only depend on past values of H_x, H_z, and E_y surrounding the space point [e.g. Taflove, 1995, p. 71] (I omit the full formulation of the FDTD system for brevity). Based on this system of finite-difference equations past values of the complete fields can be used to calculate all values for the new time step, allowing the simulation of wave propagation in time.

Implementation for Radar Application

The original core of the Fortran source code was written for the commercial seismic and radar analysis PC software REFLEX (Sandmeier Software, Karlsruhe, Germany). For our special purposes, the module had to be decoupled from the main program and ported to more powerful UNIX-based architectures. Additional software was written to convert ice core DEP data to the desired numerical model space, including various methods for outlier correction, interpolation, and boundary conditions.

The transmitter is represented by a infinite electric line source in y-direction close to the surface, the y-component of the electric field E_y at a preselected position represents the signal recorded at the receiver location. For the operational model, duration and shape of the source function are determined from air waves of radar survey data and interpolated to the model time increment using an Akima spline.

Sensitivity Tests for Model Validation

Prior to computations with the operational model numerous sensitivity studies were carried out. In particular, these included tests of different absorbing boundary conditions, interpolation schemes for DEP data, and runs with different analytical and measured source signals. The findings emphasized that operation of the model at a space increment of 1 cm and time steps of 0.01 ns sufficiently minimizes diffusion from numerical approximations and still satisfies stability criteria.

Boundary conditions were implemented by an absorbing range with exponential increase of the imaginary part of the dielectric constant towards the boundary, ensuring dissipation of the propagating wave. Although this approach artificially enlarges the model space, implementation of other types of boundary conditions (e.g. Mur- or Berenge-types) face the problem that the boundary is not in free space, i.e. the medium displays variations of its physical parameters. Comparison of synthetic traces with measured radar data produced best results for using the air

wave, i.e. the direct wave between transmitter and receiver, as the source signal.

Data I/O and Model Derivatives

As the original source code required the REFLEX PC program for analyses, new input-output-(I/O-)routines had to be developed to increase efficiency. The large number of data points required for reproducing measured ice penetrating radar data requires a fast writing module with a compact output format. I decided to use the extensive netCDF package provided by Unidata (http://www.unidata.ucar.edu), as it fulfils these requirements and moreover enables easy portation of the program to different architectures.

Several other subroutines for calculating propagation of Maxwell's equations in different dimensions and grades of numerical approximations are also implemented already, including a fully coupled mode in 2D accurate to $O[2,2]$, and in 3D two fully coupled modes accurate to $O[2,2]$ and $O[2,4]$, respectively. Although sensitivity studies were performed with all subroutines, only the 2D TE mode representation so far permits operational studies on the scale necessary to cover the desired $\sim$100 m vertical column of ice.

Computing Requirements and Parallelization

First performance test were carried out under Solaris 2.8 on a SUN Blade 100 in a single processor version and on the 8-processor SGI Origin-2000 system at AWI using three processors. The parallel version utilizes OpenMP (http://www.openmp.org) multi-platform shared-memory programming. As computing time and especially CPU memory requirements soon reached the physical limits of these systems, it was decided to implement and further develop the model on the new NEC SX-6 supercomputer at the Deutsches Klimarechenzentrum (DKRZ, Hamburg, Germany). With support from DKRZ staff it was finally possible to further increase effective parallelization of the 2D TE model.

Model dimensions for the standard runs for the studies carried out so far [Eisen et al., 2003b,d] are 10 m in horizontal direction ($x \in [-5\text{ m}, 5\text{ m}]$) and 120 m in vertical direction ($z \in [-20\text{ m}, 100\text{ m}]$), with an isotropic space increment $\Delta = 0.01$ m, a time increment $\Delta t = 0.01$ ns, and 5 m exponential absorbing range. The total model contains 2.6×10^7 data points. Computation of 1000 ns of wave propagation with this parameter set took less than 1 h, required 1.5 GBytes RAM memory, and 7 h of CPU time at 3.7 GFlops on 8 dedicated CPUs. According to the DKRZ, EMICE is currently the program with the best performance on the NEC SX-6 with almost 30 concurrent GFlops, and is even used by DKRZ for benchmarking.

A.2 RAMACIN: DISCO-Module for Importing Radar Data

RAMACIN is a module complementing the seismic programming software FOCUS/DISCO version 4.2 (Paradigm Geophysical). I developed it to enable the analysis of radar data recorded with the RAMAC system (Malå Geoscience, Sweden) in the standard seismic processing stream utilized at AWI. This section reproduces the manual page of RAMACIN which should be used in conjunction with the standard FOCUS/DISCO manuals.

Overview

RAMACIN is an input module for RAMAC radar trace files. RAMACIN assigns the following trace header entries to the seismic traces input:

> The header entries SEGSTR and SEGEND are intended to be used for the insertion of empty traces in profile plots. This should be done to distinguish between traces from different files of the same profile.

RAMACIN was compiled for use under Solaris 2.x. Portation to other systems, e.g. IRIS 64 on the SGI Origin, requires careful checking of the data type byte assignments.

Requirements and Restrictions

RAMACIN is an input module, it is not reentrant; i.e., it must not be run more than once in the same job. No other input module must be run in the same job as RAMACIN.

Output

Output are the traces in DISCO internal format. Input traces are passed on for further processing.

Parameter Table

	1-8	9-48	49-64
Req.	*CALL	RAMACIN	
Opt.	FILRAD		
Opt.	FILRD3		

General Execution Parameters - Required

	1-8	9-48	49-64
Req.	***CALL**	**RAMACIN**	

***CALL** Execution directive.
Columns: 1-8

RAMACIN Program name.
Columns: 9-48

Directive FILRAD - Optional

	1-8	9-48	49-64
Opt.	**FILRAD**	NAME	

FILRAD Operation Name.
Columns: 1-8

NAME Name of the input header file (*.rad) to read the parameters from. The name should include the directory path and the full name of the input header file, including the extension .rad.
Columns: 9-48
Type of value: Character*40

Directive FILRD3 - Optional

	1-8	9-48	49-64
Opt.	**FILRD3**	NAME	

FILRD3 Operation Name.
Columns: 1-8

NAME Name of the input data file (*.rd3) to read the data from. The name should include the directory path and the full name of the input data file including the extension .rd3.
Columns: 9-48
Type of value: Character*40

B List of Acronyms

AGC	:	automatic gain control
ALPCLIM	:	Environmental and climate records from high elevation alpine glaciers (EU project)
CMP	:	common-midpoint
CO	:	common-offset
CPU	:	central processing unit
DC	:	dielectric constant
DEP	:	dielectric profiling
DKRZ	:	Deutsches Klimarechenzentrum
DML	:	Dronning Maud Land
ECM	:	electric conductivity measurements
EM	:	electromagnetic
EMICE	:	electromagnetic reflections in ice (numerical FDTD model)
EPICA	:	European Project for Ice Coring Antarctica (joint ESF/EU project)
FD	:	finite-difference
FDTD	:	finite-difference time-domain
GPR	:	ground penetrating radar
IPR	:	ice penetrating radar
IRH	:	internal reflection horizon
NMO	:	normal moveout
RES	:	radio echo sounding
RX	:	receiver
SNR	:	signal-to-noise ratio
TE	:	transverse electric
TM	:	transverse magnetic
TWT	:	two-way traveltime
TX	:	transmitter
WE	:	water equivalent

References

S. Arcone, D. Lawson, and A. Delaney. Short-pulse wavelet recovery and resolution of dielectric contrasts within englacial and basal ice of Matanuska Glacier, Alaska, U.S.A. *J. Glaciol.*, 41(137):68–86, 1995.

D. J. Baldwin, J. L. Bamber, A. J. Payne, and R. L. Layberry. Using internal layers from the Greenland Ice Sheet, identified from radio echo sounding data, with numerical models. *Ann. Glac.*, 37, -in press-, 2003.

T. Bergmann, J. O. A. Robertsson, and K. Holliger. Finite-difference modeling of electromagnetic wave propagation in dispersive and attenuating media. In *Geophysics*, volume 63, pages 856–867. Soc. of Expl. Geophys., 1998.

N. Blindow. Reflection amplitudes of 40 MHz monopulse radio echo sounding: correlation with ice core data and ice dynamics. *Filchner-Ronne Ice Shelf Programme, Report No.8 (1994)*, pages 5–8, 1994.

V. Bogorodsky, C. Bentley, and P. Gudmandsen. *Radioglaciology.* D. Reidel Publishing Company, Dordrecht, Holland, 1985.

J. W. Clough. Radio echo sounding: reflections from internal layers in ice sheets. *J. Glaciol.*, 18(78):3–14, 1977.

H. F. J. Corr, A. Jenkins, K. W. Nicholls, and C. S. M. Doake. Precise measurement of changes in ice-shelf thickness by phase-sensitive radar to determine basal melt rates. *Geophys. Res. Letters*, 29(8):73-1–74-4, 2002.

D. Dahl-Jensen, N. Gundestrup, K. Keller, S. Johnsen, S. Gogineni, C. Allen, T. Chuah, H. Miller, S. Kipfstuhl, and E. Waddington. A search in North Greenland for a new ice-core drill site. *J. Glaciol.*, 43(144):300–306, 1997.

O. Eisen, U. Nixdorf, L. Keck, and D. Wagenbach. Alpine ice cores and ground penetrating radar: Combined investigations for glaciological and climatic interpretations of a cold Alpine ice body. *Tellus*, 55B:1007–1017, 2003a.

O. Eisen, U. Nixdorf, F. Wilhelms, and H. Miller. Electromagnetic wave speed in polar ice: Validation of the CMP technique with high resolution DEP and γ-density measurements. *Ann. Glac.*, 34:150–156, 2002.

O. Eisen, U. Nixdorf, F. Wilhelms, and H. Miller. Ice core synchronization and reflection characteristics: combined analyses of survey and synthetic radar data. *J. Geophys. Res.*, -submitted-, 2003b.

O. Eisen, F. Wilhelms, U. Nixdorf, and H. Miller. Identifying isochrones in GPR profiles from DEP-based forward modelling. *Ann. Glac.*, 37, -in press-, 2003c.

O. Eisen, F. Wilhelms, U. Nixdorf, and H. Miller. Revealing the nature of radar reflections in ice: DEP-based FDTD forward modeling. *Geophys. Res. Letters*, 30 (5), 2003d.

M. Frezzotti, S. Gandolfi, and S. Urbini. Snow megadunes in Antarctica: Sedimentary structure and genesis. *J. Geophys. Res.*, 107(0):ACL X-1–X-12, 2002.

S. Fujita, H. Maeno, S. Uratsuka, T. Furukawa, S. Mae, Y. Fujii, and O. Watanabe. Nature of radio echo layering in the Antarctic ice sheet detected by a two-frequency experiment. *J. Geophys. Res.*, 104(B6):13,013–13,024, 1999.

R. Garotta and D. Michon. Continuous analysis of the velocity function and the move out corrections. *Geophysical Prospecting*, 15(4):584–597, 1967.

P. Gudmandsen. Layer echoes in polar ice sheets. *J. Glaciol.*, 15(73):95–101, 1975.

C. Hammer. Acidity of polar ice cores in relation to absolute dating, past volcanism, and radio-echoes. *J. Glaciol.*, 25(93):359–372, 1980.

C. H. Harrison. Radio echo sounding of horizontal layers in ice. *J. Glaciol.*, 12(66): 383–397, 1973.

L. Hempel and F. Thyssen. Deep Radio Echo Soundings in the vicinity of GRIP and GISP2 Drill Sites, Greenland. *Polarforschung*, 62(1):11–16, 1992.

A. Hildebrand. *Untersuchung der Laufzeit- und Amplitudenverhalten elektromagnetischer Impulse bei glaziologischen Radarmessungen.* PhD thesis, Westfälische Wilhelmsuniversität Münster, 1996.

R. Hodgkins, M. J. Siegert, and J. A. Dowdeswell. Geophysical investigations of ice-sheet internal layering and deformation in the Dome C region of central East Antarctica. *J. Glaciol.*, 46(152):161–166, 2000.

G. W. Hohmann. Numerical modeling for electromagnetic methods of geophysics. In M. N. Nabighian, editor, *Electromagnetic methods in applied geophysics*, volume 1 of *Geophysical monograph series*, pages 313–364. Soc. of Expl. Geophys., 1988.

P. Huybrechts, D. Steinhage, F. Wilhelms, and J. Bamber. Balance velocities and measured properties of the Antarctic ice sheet from a new compilation of gridded data for modeling. *Ann. Glac.*, 30:52–60, 2000.

R. Jacobel and S. Hodge. Radar internal layers from the Greenland summit. *Geophys. Res. Letters*, 22(5):587–590, 1995.

R. W. Jacobel, A. M. Gades, D. L. Gottschling, S. M. Hodge, and D. L. Wright. Interpretation of radar-detected internal layer folding in West Antarctic ice streams. *J. Glaciol.*, 39(133):528–537, 1993.

K. C. Jiracek and C. R. Bentley. Velocity of electromagnetic waves in Antarctic ice. In A. P. Crary et al., editors, *Antarctic Snow and Ice Studies II*, volume 16 of *Antarctic Research Series*, pages 199–208. American Geophysical Union, 1967.

P. Kanagaratnam, S. Gogineni, N. Gundstrup, and L. Larsen. High-resolution radar mapping of internal layers at the North Greenland Ice Core Project. *J. Geophys. Res.*, 106(D24):33,799–33,812, 2001.

O. Lázaro-Mancilla and E. Gómez-Treviño. Synthetic radargrams from electrical conductivity and magnetic permeability variations. *J. Appl. Geophys.*, 34:283–290, 1996.

D. H. H. Millar. Radio echo layering in polar ice sheets and past volcanic activity. *Nature*, 292:441–443, 1981.

W. Miners, A. Hildebrand, S. Gerland, N. Blindow, D. Steinhage, and E. Wolff. Forward Modelling of the Internal Layers in Radio Echo Sounding Using Electrical and Density Measurements from Ice Cores. *J. Phys. Chem. B*, 101(32):6201–6204, 1997.

W. D. Miners. *Electromagnetic reflections inside ice sheets.* PhD thesis, Open University, 1998.

J. Moore. Dielectric variability of a 130 m Antarctic ice core: implications for radar sounding. *Ann. Glac.*, 11:95–99, 1988.

J. Moore, A. Pälli, F. Ludwig, H. Blatter, J. Jania, B. Gadek, P. Glowacki, D. Mochnacki, and E. Isaksson. High-resolution hydrothermal structure of Hansbreen, Spitsbergen, mapped by ground-penetrating radar. *J. Glaciol.*, 45(151): 524–532, 1999.

J. Moore and J. Paren. New technique for dielectric logging of Antarctic ice cores. *Journal de Physique (Colloque C1)*, 48(3):155–160, 1987.

J. C. Moore, H. Narita, and N. Maeno. A continuous 770-year record of volcanic activity from East Antarctica. *J. Geophys. Res.*, 96(D9):17,353–17,359, September 1991.

T. Murray, G. W. Stuart, P. J. Miller, J. Woodward, A. M. Smith, P. R. Porter, and H. Jiskoot. Glacier surge propagation by thermal evolution at the bed. *J. Geophys. Res.*, 105(B6):13,491–13,507, 2000.

N. A. Nereson and C. F. Raymond. The elevation history of ice streams and the spatial accumulation pattern along the Siple Coast of West Antarctica inferred from ground-based radar data from three inter-ice-stream ridges. *J. Glaciol.*, 47 (157):303–313, 2001.

U. Nixdorf and F. Göktaş. Spatial depth distribution of the subglacial bed and internal layers in the ice around NGRIP, Greenland, derived with airborne RES. *J. Appl. Geophys.*, 47:175–182, 2001.

H. Oerter, F. Wilhelms, F. Jung-Rothenhäusler, F. Göktas, H. Miller, W. Graf, and S. Sommer. Accumulation rates in Dronning Maud Land as revealed by dielectrical-profiling measurements at shallow firn cores. *Ann. Glac.*, 30:27–34, 2000.

G. K. A. Oswald and G. d. Q. Robin. Lakes beneath the Antarctic ice sheet. *Nature*, 245(5423):251–254, 1973.

C. F. Raymond, N. Nereson, A. M. Gades, H. Conway, R. Jacobel, and T. Scambos. Geometry and stratigraphy of Siple Dome, Antarctica. *Antarct. J. U.S.*, 30(5): 91–93, 1995. 1996 Review.

C. Richardson-Näslund and P. Holmlund. Spatial variablility in shallow snow-layer depths in central Dronning Maud Land, East Antarctica. *Ann. Glac.*, 29:10–16, 1999.

R. Roberts and J. Daniels. Modeling near-field GPR in three dimensions using FDTD method. *Geophysics*, 62(4):1114–1126, 1997.

G. d. Q. Robin, S. Evans, and J. T. Bailey. Interpretation of radio echo sounding in polar ice sheets. In *Philosophical Transactions of the Royal Society of London*, volume 146 of *A*, pages 437–505. Royal Society of London, 1969.

J. Schoolmeester, E. Slob, and J. Fokkema. Forward modeling of ground penetrating radar data for a horizontally layered earth. In *The First latin American Geophysical Conference and Exposition*, page 4, http://www.mp.tudeflt.nl/~jws/rio/riohtml.html, 1995.

M. J. Siegert and R. Hodgkins. A stratigraphic link across 1100 km of the Antarctic ice sheet between the Vostok ice-core site and Titan Dome (near South Pole). *Geophys. Res. Letters*, 27(14):2133–2136, 2000.

M. J. Siegert, R. Hodgkins, and J. A. Dowdeswell. A chronology for the Dome C deep ice-core site through radio-echo layer correlation with the Vostok ice core, Antarctica. *Geophys. Res. Letters*, 25(7):1019–1022, 1998.

D. Steinhage, U. Nixdorf, U. Meyer, and H. Miller. New maps of the ice thickness and subglacial topography in Dronning Maud Land, Antarctica, determined by means of airborne radio echo sounding. *Ann. Glac.*, 29:267–272, 1999.

A. Taflove. *Computational Electrodynamics: The Finite-Difference Time-Domain Method.* Artech House, Boston, 1995.

D. Vaughan, H. Corr, C. Doake, and E. D. Waddington. Distortion of isochronous layers in ice revealed by ground-penetrating radar. *Nature*, 398:323–326, 1999.

J. Wahr, D. Wingham, and C. Bentley. A method of combining ICESat and GRACE satellite data to constrain Antarctic mass balance. *J. Geophys. Res.*, 105(B7): 16,279–16,294, 2000.

A. H. Waite and S. J. Schmidt. Gross errors in height indication from pulsed radar altimeters operating over thick ice or snow. *Institute of radio engineers. International Convention Record*, (5):38–54, 1961.

F. Wilhelms. *Measurement of dielectric properties of polar ice cores (in German)*, volume 367 of *Berichte zur Polarforschung*. Alfred-Wegener-Institut für Polar- und Meeresforschung, 2000.

F. Wilhelms, J. Kipfstuhl, H. Miller, K. Heinloth, and J. Firestone. Precise dielectric profiling of ice cores: a new device with improved guarding and its theory. *J. Glaciol.*, 44(146):171–174, 1998.

E. Wolff. Electrical stratigraphy of polar ice cores: principles, methods, and findings. In T. Hondoh, editor, *Physics of Ice Core Records. International Symposium on Physics of Ice Core Records, 14–17 September 1998, Shikotsukohan, Japan*, pages 155–184, Kita 9, Nishi 8, Kita-ku, Sapporo 060-0809, Japan, 2000. Hokkaido University Press.

K. S. Yee. Numerical solution of initial boundary value problems involving Maxwell's equations in isotropic media. *IEEE Transactions on Antennas and Propagation*, 14(3):302–307, 1966.

O. Yilmaz. *Seismic data processing*, volume 2 of *Investig. Geophys.* Society of Exploration Geophysicist, 1987.

H. Zwally, B. Schutz, W. Abdalati, J. Abshirend, C. Bentley, A. Brenner, J. Bufton, J. Dezio, D. Hancock, D. Harding, T. Herring, B. Minster, K. Quinn, S. Palm, J. Spinhirne, and R. Thomas. ICESat's laser measurements of polar ice, atmosphere, ocean, and land. *J. Geodynamics*, 34(3-4):405–445, 2002.

Acknowledgements

Prof. Will Harrison (University of Alaska Fairbanks) first exposed me to glaciology as well as science as a business and introduced me to pragmatic reality and administrative battles. The opportunities he provided me with, his experience in the art of writing and critical questioning not only accompanied me over the last six years in one way or another, but also significantly influenced and improved my own scientific everyday life. I greatly appreciate his support.

The advice of Prof. Christoph Kottmeier (University of Karlsruhe) during and after my Diploma encouraged my decision to stay in science and start a doctoral thesis. I greatly acknowledge the continuation of our good cooperation during the last years.

Prof. Heinrich Miller (AWI) offered me the possibility to carry out work in a field of science I have been interested in for years, leaving me the freedom I wanted to perform my studies and pursuit my ideas. His support did – and still does – enable many interesting acquaintances world wide. I greatly thank him for these opportunities and becoming my doctoral advisor. Prof. Heinrich Villinger (University Bremen) deserves thanks for his readiness to take over the additional report.

The Studienstiftung des Deutschen Volkes supported my thesis with a doctoral scholarship. In addition, participation in summer schools and discussions with local tutors enriched my experiences.

Special thanks is expressed to Uwe Nixdorf. His interest in radar techniques provided the actual opportunity for this work. Likewise to Frank Wilhelms. It was stimulating to share an office with him and I picked up a lot; programming techniques, physics problems – and telephone calls. The good cooperation among the three of us over the last years helped me in several aspects. Many thanks to Dietmar Wagenbach for the fruitful cooperation and jovial working atmosphere. The hard tasks related to parallel programming would not have been accomplished without the support from Stephan Frickenhaus and Klaus Ketelsen, thank you.

Johannes Freitag and Wolfgang Rack gave valuable comments for final improvements. Furthermore, the AWI glaciology group provided a terrific environment for working, but there are too many people to name them all for their contributions. Despite the tight expedition schedules, people are usually able to enjoy whatever is up.

The reprint of the papers was made possible by the International Glaciological Society, the American Geophysical Union, and Blackwell Munksgaard.

PAPER I

PAPER I is reprinted from the Annals of Glaciology with permission of the International Glaciological Society.

Annals of Glaciology 34, 150-156, 2002.

Electromagnetic wave speed in polar ice: Validation of the CMP technique with high-resolution dielectric profilling and γ-density measurements

Olaf Eisen, Uwe Nixdorf, Frank Wilhelms, and Heinrich Miller

Alfred-Wegener-Institut für Polar- und Meeresforschung Bremerhaven, Bremerhaven, Germany

Abstract. The accuracy of the traveltime–velocity and traveltime–depth profile derived from ground-penetrating radar (GPR) common-midpoint (CMP) surveys at different frequencies is investigated for the first time ever by direct comparison with the profile calculated from high resolution dielectric-profiling (DEP) ice core data. In addition, we compare two traveltime profiles calculated from ice core density data by means of different dielectrical mixture models with the DEP based profile. CMP surveys were carried out at frequencies of 25, 50, 100 and 200 MHz near the new European deep drilling site DML05 in Dronning Maud Land, Antarctica, during the 1998/99 field season. An improved scanning capacitor for high resolution DEP and a γ-densiometer for density measurements were used to determine the complex dielectric constant and the density at 5 mm increments along the ice core B32, retrieved in 1997/98 at DML05. The comparisons with DEP and density based velocity series show that the CMP velocity series are slightly higher, but asymptotically approach the core based velocities with depth. Root-mean-square differences of the DEP velocity series range between 8% for the 25 MHz CMP and 2% in the case of the 200 MHz survey. Density based velocities differ from the DEP velocities by less than 1%. The traveltime–depth series calculated from the interval velocities show a better agreement between all series than the velocity series. Differences are between 5.7 and 1.4% for the 25 and 200 MHz CMP measurements, and less than 0.6% for the density data. Based on these comparisons we evaluate the accuracy with which the depth of electromagnetic reflectors observed in common-offset profiles can be determined and discuss reasons for the observed differences between CMP- and core based profiles. Moreover, we compare the errors determined from the field measurements with those estimated from GPR system characteristics to provide a measure that can be used to estimate the accuracy of GPR analyses for the planning of GPR campaigns. Our results show that CMP surveys are a useful technique to determine the depth of radar reflectors in combination with common-offset measurements, especially on a region-wide basis.

Introduction

Radio-echo sounding (RES) is an active remote sensing method that has become a major tool for glaciological investigations [*Bogorodsky et al.*, 1985]. Whereas satellite-borne radar devices operating in the GHz bands yield information about the upper few centimeters to meters of the ice and snow surface, RES performed in the MHz to GHz bands is capable to penetrate up to several tens of meters to kilometers of ice.

RES devices are used to determine the inner state of the ice sheet [*Fujita et al.*, 1999], bottom topography [*Steinhage et al.*, 1999; *Nixdorf and Göktaş*, 2001], to separate certain thermal regimes [*Murray et al.*, 2000], transfer datings from ice cores to electromagnetic reflectors [*Hempel et al.*, 2000], and get information about the accumulation [e.g. *Richardson-Näslund et al.*, 1997; *Nereson et al.*, 2000; *Siegert and Hodgkins*, 2000] and strain history [*Vaughan et al.*, 1999]. Whereas some surveys try to make

use of the frequency dependence of the dielectrical properties [*Fujita et al.*, 1999], most applications analyse the depth and shape of internal reflectors. As the return signals are recorded as a function of traveltime of the transmitted radar pulse, the latter application requires knowledge of the variation of the wave speed with depth in order to be able to convert the observed reflections from time to depth domain.

In this paper we compare the velocity of electromagnetic wave propagation in ice and the deduced traveltime–depth relationship derived from four common-midpoint (CMP) surveys carried out at various frequencies at the site DML05 in Dronning Maud Land (DML), Antarctica, with results from new high resolution dielectric-profiling (DEP) data and two simple density based mixture models, the classical *Looyenga* [1965] model, which is based on theoretical considerations, and the empirical fit derived from field data given by *Kovacs et al.* [1995].

Methods have been developed to determine the velocity–depth function of electromagnetic waves propagating through ice. The most direct method involves the measurement of dielectrical properties along ice cores by means of DEP [*Moore and Paren*, 1987; *Wilhelms et al.*, 1998], from which interval velocities can be calculated directly. Instead of the dielectrical properties, density profiles of an ice core can also be used to determine the electromagnetic wave speed from mixture models [*Kovacs et al.*, 1995; *Richardson-Näslund et al.*, 1997].

Indirect techniques are usually carried out with ground penetrating radar (GPR) systems, using different approaches. The down-hole radar technique makes use of a borehole to record traveltimes as a function of depth of a reflecting target *Jezek and Roeloffs* [e.g. 1983]; *Clarke and Bentley* [e.g. 1994]. Interval velocities can then be derived from the transmitter–target–receiver traveltime as a function of depth. Although this type of measurement and the subsequent analysis is straightforward and less time consuming than those referred to previously, it still makes use of an existing hole.

A special case of radar wide-angle and reflection measurements is the common-midpoint (CMP) survey technique, well known from reflection seismic exploration [*Yilmaz*, 1987]. As an indirect method this technique has been widely applied to single and multichannel GPR measurements in recent years [e.g. *Fisher et al.*, 1992; *Hempel et al.*, 2000; *Murray et al.*, 2000]. The CMP technique makes use of a special linear geometry setup such that the points of reflection at a certain depth remain the same for all transmitter–receiver offsets. The velocity-depth function can be inferred from the increase of traveltime with offset, assuming near-horizontal reflectors.

Whereas the errors involved in calculating the velocity–depth profile from DEP and density models are rather small, a fair amount of time and logistic support for retrieving and processing the core is required. CMP measurements, on the other hand, can be carried out rapidly and with little logistic support. As the dielectric properties depend in principle on temperature, the CMP technique has the advantage to take the in-situ temperature into account, compared to ice core data that are processed at an ambient processing temperature. However, wavelengths typically on the order of meters result in lower resolution, and theoretical assumptions for CMP analysis introduce errors, when establishing a traveltime–velocity profile from GPR measurements. The results of our investigations are used to evaluate the accuracy of the CMP traveltime–velocity and traveltime–depth functions with regard to the other methods, and to assess if the lower expenditure in the field justifies CMP application to determine the depth of electromagnetic reflectors.

Data, Equipment and Methods

Data basis and GPR system

The European Project for Ice Coring in Antarctica (EPICA) aims to retrieve deep ice cores from two different regions of the Antarctic ice

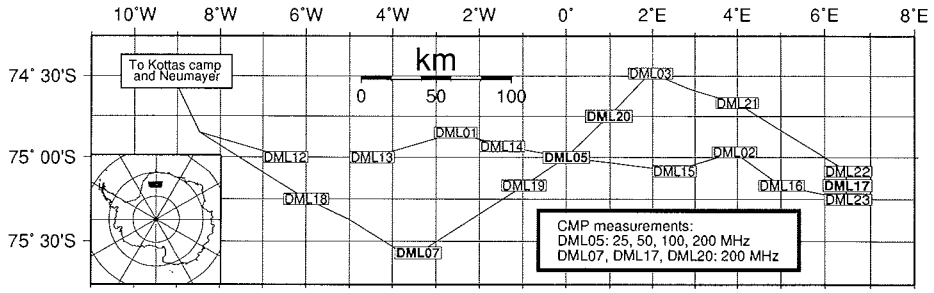

Figure 1. Location map of the study area in Dronning Maud Land. The 1998/99 traverse radar profiles are drawn as solid lines. The location of firn cores at which CMP surveys were carried out are in bold typescript. The inset displays the location of the study area on the Antarctic continent.

Table 1. Geometric setup and wavelet characteristics of the CMP surveys

f	x_0	x_N	Δx	λ_{ice}	λ_{ice}^w
MHz	m	m	m	m	m
25	10.0	290	5.0	6.7	20.1
50	4.0	300	4.0	3.4	11.8
100	1.0	98	1.0	1.7	8.4
200	1.0	70	0.5	0.8	4.2

f: TX, RX antennae frequency
x_0: minimum offset
x_N: maximum offset
Δx: shot increment
λ_{ice}: wavelength in ice
λ_{ice}^w: length of transmitted wavlet in ice
(assuming $c_{\text{ice}} = 168$ m $(\mu\text{s})^{-1}$)

sheet (Dome Concordia and DML). During the 1998/99 EPICA pre-site survey in DML, GPR measurements were carried out simultaneously at two different frequencies on a traverse connecting the locations of ice cores drilled in earlier seasons. In addition to more than 4000 km of common-offset GPR profiles, six CMP measurements were obtained at different frequencies at several borehole locations along the traverse (Figure 1). Most CMP surveys were measured at the site DML05, close to the location of the forthcoming ice coring, from which a shallow 150 m ice core was retrieved during the 1997/98 season. The field processing of the ice core, hereafter refered to as B32, included high-resolution DEP and density measurements [*Oerter et al.*, 2000]. Together with the CMP data they form the basis for the investigations carried out in this paper.

The radar measurements were performed with a commercial RAMAC GPR set of the Swedish company Malå Geoscience. The GPR device is a monopulse bistatic radar system with a maximum sample rate of 200 scans/s, a dynamic range of 150 dB, and can be operated at several frequencies. The data acquisition is organised by software from the same company, using a Husky PX5 personal computer. The antennae are connected to the control unit via fibre-optics cables, thus avoiding disturbing interferences of the transmitted wave with ohmic connectors. For all field measurements discussed here a linear profile line was set up with an azimuth of approximately 130° and ~100 m SE of the location of the core B32. Four CMPs were carried out with anntenna frequencies of 25, 50, 100 and 200 MHz, using 512 stacks per trace and the geometric setup as given in Table 1.

CMP method with GPR

The CMP recording technique is usually employed to improve the signal-to-noise ratio with redundant recording during reflection seismic data acquisition [*Garotta and Michon*, 1967; *Yilmaz*, 1987], and has also been applied successfully to GPR surveys [*Fisher et al.*, 1992; *Greaves et al.*, 1996]. In addition, multifold coverage with nonzero-offset recording yields velocity information about the subsurface. In the case of single-channel GPR, the redundancy is achieved by multiple offset coverage of the same subsurface point with one transmitter–receiver pair, positioned at the same distance from the center of a linear profile. Since the geometry of the setup is essential for the analysis, the offset x between both antennae is, for the sake of simplicity, usually increased in N equidistant intervals Δx, starting from a minimum offset x_0 up to a maximum offset $x_N = x_0 + N\,\Delta x$. At a given offset x from the profile center, the traveltime $t(x)$ along the raypath from the transmitter to the depth point and back to the receiver at the surface is

$$t(x) = \sqrt{t^2(0) + x^2/v^2}, \qquad (1)$$

where v is the velocity of the medium above the reflecting interface, and $t(0)$ is twice the traveltime along the vertical path. Equation (1) describes a hyperbola in the plane of two-way traveltime (TWT) vs offset. The difference between the two-way time $t(x)$ at a given offset x and the two-way zero offset time $t(0)$ is called normal moveout (NMO). When $t(x)$ and $t(0)$ are known, the velocity v can be calculated from Equation (1). With an estimated NMO velocity the traveltimes can be corrected to remove the influence of the offset, thus turning the reflection hyperbola in the radargram into a flat reflector.

To derive an expression for the vertical velocity distribution, assume a lateral homogeneous medium consisting of J horizontal layers of constant interval velocities v_1, v_2, ..., v_J. The traveltime from the transmitter to the depth point at the j-th layer and back to the receiver then becomes a function of layer thickness, velocity, and higher orders of the offset x. The root-mean-square (rms) velocity v_{rms} down to the j-th reflector is defined as [*Yilmaz*, 1987]

$$v_{rms,j} = \sqrt{\frac{1}{t(0)} \sum_{i=1}^{j} v_i^2 \Delta t_i(0)}, \qquad (2)$$

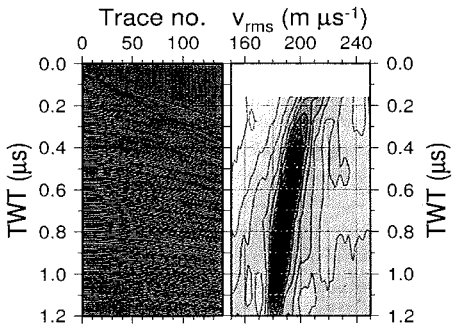

Figure 2. Radargram of a CMP, carried out with the 200 MHz antennae, after bandpass filtering and applying an automatic gain control, and the corresponding spectrum of the rms velocity, calculated from stacked amplitudes. The direct wave, the ground wave, and more than 20 reflectors consisting of several phases are clearly visible in the radargram. In the velocity spectrum, the upper 0.18 ns are muted to avoid errors in the calculation from the overlapping of the first reflection and the ground wave.

where $\Delta t_i(0)$ is the traveltime through the i-th layer and $t(0) = \sum_{k=1}^{i} \Delta t_k(0)$. When the offset is small compared to depth, the traveltime can be approximated by

$$t(x) = \sqrt{t^2(0) + x^2/v_{rms}^2}. \qquad (3)$$

Comparing Equations (1) and (3), it can be seen that, in the so-called small-spread approximation, the velocity required for NMO correction is equal to the rms velocity.

CMP data processing

Data processing is carried out using Paradigm Geophysical FOCUS version 4.2 software. The processing stream for all measurements includes bandpass filtering and automatic gain control. An example for the CMP measured with the 200 MHz antennae after these processing steps is shown in Figure 2. These steps are followed by the definition of the trace geometry and a first estimate of the TWT–rms-velocity profile from the velocity spectrum using a stacked amplitude contour plot (Figure 2). Velocity estimates are not reliable at times greater than that at which the last coherent reflection occurs (e.g. below 1.2 μs in Figure 2). To improve the velocity model, reflection hyperbolae are manually fitted to prominent reflectors in the radargram by selecting points in the v_{rms} vs TWT domain. A final check of the velocity distribution is performed by investigating the NMO-corrected radargrams in the offset vs TWT domain, i.e. if all hyperbolic reflectors are transformed into flat events. As the final step we use the TWT–rms-velocity distribution to successiveley invert Equation (2) to obtain the interval velocities [*Dix*, 1955], which in turn are used to perform the traveltime to depth conversion of the prominent horizons.

High-resolution DEP

The complex relative dielectric constant (DC) can be written as

$$\epsilon = \epsilon' - i\epsilon'' = \epsilon' - i\frac{\sigma}{\epsilon_0 \omega}, \qquad (4)$$

where the real part ϵ' is the ordinary relative permittivity of the medium. The imaginary part ϵ'' is the dielectric loss factor and can be expressed as a function of conductivity σ, circular frequency ω and the permittivity of vacuum ϵ_0. The DC can be determined along an ice core by means of DEP [*Moore and Paren*, 1987]. An improved DEP device developed by *Wilhelms et al.* [1998], essentially a calibrated guarded scanning capacitor, was used at a frequency of 250 kHz to determine the complex DC along the ice core in 5 mm increments. The new version of the DEP device has a systematic accuracy of about 1% for each complex permittivity component. Sections with poor core quality, such as cracks or missing pieces, were removed from the data set.

The electromagnetic wave speed c in snow and ice obeys the general equation

$$c = c_0/\sqrt{\epsilon}, \qquad (5)$$

with c_0 being the electromagnetic wave speed in vacuum. The DEP measurements indicate that the conductivity is of the order of 10^{-5} Sm^{-1}, implying that the imaginary part of the DC calculated from Equation (4) is about two orders of magnitude smaller than the real part. It can thus essentially be neglected for determining c from Equation (5) and the DEP data.

For each point of the DC–depth series we calculate the wave speed, resulting in a velocity–depth distribution. The linear interpolation of the velocity between the data points and the subsequent integration of the velocity distribution yields a propagation time for each data point, which, in analogy to the propagation of a transmitted radar pulse in ice, can be converted to a TWT.

γ-absorption density and mixture models

In dry ice density is the main factor affecting the real part of the DC [*Robin et al.*, 1969]. With the use of a mixture model that relates the ice density to the DC it is therefore possible to calculate the electromagnetic wave speed from the measured density. In addition to the DEP device, the measuring bench hosts a γ-densiometer as well, allowing quasi simultaneous measurements of the DC and density. The density of the core, being an air-ice mixture, was recorded in 5 mm increments with an accuracy of 10 kg m^{-3}, corresponding to $\sim$1.1% for solid ice [*Wilhelms*, 2000]. For the application of the γ-density to calculating the wave speed two relations are considered that connect density and permittivity; the model by *Looyenga* [1965] and the relation given by *Kovacs et al.* [1995].

Looyenga [1965] derived a relation that connects density and permittivity of a constant mixture from a theoretical model. Application to polar ice yields an expression for the permittivity of the mixture:

$$\epsilon' = \left(\frac{\rho}{\rho_{\mathrm{ice}}}\left[\sqrt[3]{\epsilon'_{\mathrm{ice}}} - 1\right] + 1\right)^3 \qquad (6)$$

Here, $\epsilon'_{\mathrm{ice}} = 3.17$ is the permittivity and $\rho_{\mathrm{ice}} = 917$ kg m^{-3} is the density of ice [*Robin et al.*, 1969].

The empirical formula published by *Robin et al.* [1969] was improved by *Kovacs et al.* [1995] by comparing field measurements of the DC with density. Their study leads to the relation

$$\epsilon' = (1 + 0.845\rho)^2, \qquad (7)$$

with a standard error of ± 0.031 for ϵ' ($\sim$1% for ϵ'_{ice}).

Using the γ-density–depth series together with Equations (6) and (7) provides two series for ϵ' of the mixture. These are used to determine the velocity from Equation (5) and the TWT as explained for the DEP measurements.

Comparison of the Electromagnetic Wave Speeds

The CMP-processing sequence is performed for each of the four CMP measurements. Together with the DEP and density based interval velocity distributions, this results in seven different data sets for the TWT–interval velocity and TWT–depth distributions for the site of the ice core B32. For the sake of brevity the interval velocity is referred to as velocity, as only the interval velocities are considered.

Interval velocity

The spatial resolution of the three methods, DEP, mixture model and CMP analysis, varies between 5 mm for the ice core data to several tens of meters for the 25 MHz-CMP measurement (Table 1). In order to estimate the accuracy of the methods, it is appropriate to smooth the ice core based data series as follows.

The DEP and γ-density velocities are resampled with a linear interpolation on an equidistant sample interval of 1 ns, and then smoothed with a cosine time domain filter with a filter length of 0.2 μs. The CMP velocities are plotted on mid-interval points and connected by straight lines representing a linear velocity

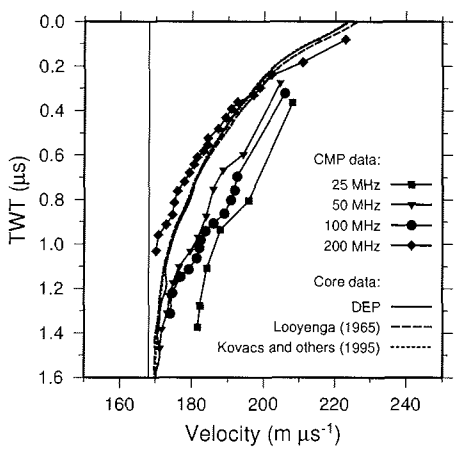

Figure 3. Two-way traveltime (TWT) vs velocity calculated from the CMP and ice core data, as described in the text. The raw velocity profile calculated from DEP measurements is plotted in light grey to illustrate the different resolutions and the effect of the filtering procedure. The vertical line at 168 m $(\mu s)^{-1}$ indicates the electromagnetic wave speed in solid ice.

gradient. Except for the 25 MHz-CMP the course of the velocities with TWT show a similar trend for all three methods, assymptotically approaching the wave speed of bubble free ice of 168 m $(\mu s)^{-1}$ (Figure 3). The velocities derived from the 25 MHz-CMP are systematically higher by $\sim$10 m $(\mu s)^{-1}$ than the core measurements. Although the 50 and 100 MHz-CMP differ from the core measurements by up to 10 m $(\mu s)^{-1}$ as well, their agreement is better as they approach the latter to within 5 m $(\mu s)^{-1}$ below 1.1 μs. The 200 MHz-CMP compares best with the core measurements, with maximum difference of 6 m $(\mu s)^{-1}$. However, its velocity gradient is systematically larger, the velocities being generally higher above 0.35 μs and smaller below. The velocities derived from the three different types of core measurements agree very well, with differences mainly in the upper 0.3 μs and below 1.1 μs.

To quantitatively estimate the differences of the seven data sets and to account for the different resolution of the methods it is useful to consider the rms differences of the velocity curves. As the DEP method has the highest accuracy and resolution, the filtered DEP velocitiy profile is used to define a standard velocity series $v_{\mathrm{int}}^{\mathrm{DEP}}$. The relative rms differences of the velocities $\sigma_{v_{\mathrm{int}}}$ are calculated by the equation

$$\sigma_{v_{\mathrm{int}}} = \sqrt{\frac{1}{N-1}\sum_{j=1}^{N}\left(\frac{v_{int,j} - v_{int,j}^{\mathrm{DEP}}}{v_{int,j}^{\mathrm{DEP}}}\right)^2}\,, \qquad (8)$$

where $v_{int,j}$ is the considered series of length N and $v_{int,j}^{\mathrm{DEP}}$ is the standard velocity series which is again resampled at the locations j of the considered series.

For the CMP velocities, the absolute rms differences vary between 7.8 and 1.8% for the 25 and 200 MHz-CMP, respectively (Table 2). The CMP rms differences show a trend to decrease with increasing frequency and number of data points. The relative rms differences between the averaged density based velocities and the standard velocities are 0.7 and 0.3% for the *Looyenga* [1965] and the *Kovacs et al.* [1995] mixture models, respectively.

Table 2. Root-mean-square differences of CMP and γ-absorption density data sets in relation to the standard DEP series

CMP/density data set	Number of data points	$\sigma_{v_{\text{int}}}$ %	σ_z %
25 MHz	6	7.8	5.7
50 MHz	13	3.0	2.2
100 MHz	14	5.1	3.7
200 MHz	22	1.8	1.4
Looyenga (1965)	1600	0.7	0.6
Kovacs and others (1995)	1600	0.3	0.1

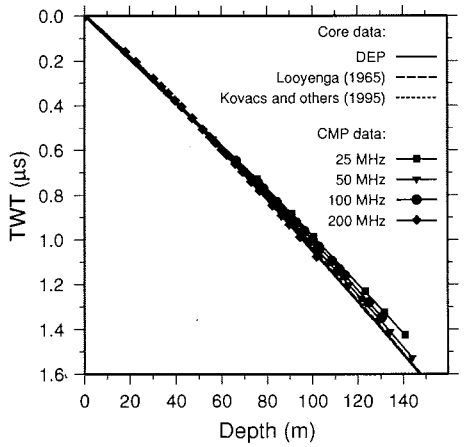

Figure 4. Two-way traveltime (TWT) vs depth calculated by integrating the velocity profiles.

Time to depth conversion

The TWT–depth relation is needed to convert the picked traveltimes of prominent reflectors detected in common-offset profiles to depth domain. As the TWT–depth relation is calculated by integrating the interval velocities, minor differences between the different profiles are smoothed out (Figure 4).

In analogy to Equation (8) we calculate the relative rms difference σ_z between the TWT–depth series of the different data sets and the standard TWT–depth series. For the definition of the standard depth series z^{DEP} as well as the calculation of σ_z we apply the same resampling and filtering as described above. The relative rms differences of the CMP TWT–depth functions are smaller than those of the relative rms velocity differences (Table 2). They decrease from 5.7% for the 25 MHz-CMP to 1.4% for the 200 MHz-CMP. Although the general trend is still that the rms difference decrease with increasing frequency, the 50 MHz CMP shows smaller differences than the one measured at 100 MHz. The rms differences calculated from the DEP and the *Looyenga* [1965] and *Kovacs et al.* [1995] mixture models are 0.6 and 0.1%, respectively.

Discussion

There could be several reasons for the observed discrepancies in the TWT–velocity and TWT–depth profiles from the different methods. In order to provide a quantitative uncertainty for the GPR measurements, individual errors arising from theoretical approximations

and measurement devices are estimated to explain the observed errors.

In general the CMP velocities appear to be higher than the velocities calculated from DEP and γ-density data. A systematic overestimation of velocities has also been noticed in former investigations [*Jezek and Roeloffs*, 1983; *Morey and Kovacs*, 1985]. Whereas instrument related timing errors are made responsible for deviations from laboratory measurements carried out by *Jezek and Roeloffs* [1983], *Morey and Kovacs* [1985] attribute observed differences in traveltimes to curved ray paths, resulting from the refraction of the propagating radar pulse at boundaries of a changing DC, which is not accounted for in the hyperbolic Equation (3). In our case, timing errors can be ruled out as the device and the data were checked by various means. If a curved ray path would be responsible, then a deviation of the same order should be observed for all CMPs. Especially the good agreement of the 200 MHz-CMP with the core based profiles refute this explanation.

When dipping layers are present, the observed reflections of a low velocity event cannot be distinguished from a high velocity event with horizontal layering without further information [*Yilmaz*, 1987]. To check whether the assumption of a horizontal subsurface geometry is justified in our case, prominent reflectors were picked from two common-offset GPR surveys carried out with the 200 MHz antennae, crossing at the location of B32. The detected reflectors are found to dip by some 4° relative to the surface around 1.1 μs and by less than 1° near 0.6 μs within 2 km of B32. As the CMP profiles were obtained approximately perpendicular to the gradient of the internal layers, dips of 4° and 1° cause the rms velocities used for NMO correction to be 0.25% and less than 0.1% higher than the true velocities, respectively [*Yilmaz*, 1987] (i.e. the interval velocities are slightly overestimated). These changes are smaller than the rms differences calculated above and only affect velocities below ~60 m. We therefore conclude that the slight dipping of the internal reflectors do not alter the TWT–depth function significantly.

The derivation of the hyperbolic Equation (3) presumed that the small-spread approximation is valid, i.e. that the offset is small compared to depth. However, this prerequisite is violated for all CMP analyses for the uppermost reflectors, and above 100 m for the 25 and 50 MHz-CMP, thus explaining the observed trend that differences between CMP and DEP velocities are larger for smaller depth.

Other contributions to the observed differences arise from the CMP surveys. Due to the decrease in resolution with increasing wavelength the best agreement with the DEP profile results from the fitting of 22 individual hyperbolae in the 200 MHz-CMP, whereas only 6 hyperbolae are available for the 25 MHz-CMP. Lateral variations of the physical properties in the upper few meters of the ice sheet could contribute to deviations, likewise might the simple separation of the borehole location B32 and the CMP center point by 100 m. However, the quantitative influence of lateral inhomogenities can only be investigated by time consuming multi-channel GPR survey geometries [*Fisher et al.*, 1992; *Greaves et al.*, 1996].

The differences in the various TWT–depth functions result directly from the time-to-depth and depth-to-time conversion of the interval velocities from the CMP and core measurements, respectively. Because of the smoothing effect of the velocity integration the rms differences decrease (Table 2). To determine the accuracy of the depth of a reflector observed in the time domain, it is important to consider the errors involved with the picking of reflector phases. Different phases of prominent reflectors can be separated in the radargram, making it possible to determine the time at which the first phase occurs to within one half-cycle. Investigations of the direct waves show that the transmitted radar pulse wavelets at all frequencies consist of more than eight half cycles, each of which is about $\lambda/2$ long. Most of the energy of the wavelets are located in the first four half cycles,

except for the 25 MHz pulse, where the main energy is distributed among six half cycles. During propagation, however, the transmitted wavelet is distorted due to several mechanisms, the most important being interferences at different, closely spaced thin layers [*Clough*, 1977]. In addition, especially at longer traveltimes, the energy decay due to geometric spreading and absorption is too large to be able to resolve the most energetic part of the wavelet. Considering these factors we conclude that the accuracy of the traveltime at which a reflector occurs can only be determined to about half the length of the energetic half-cycles of the wavelet. For the system used in this study, this means that the real TWT of an reflector detected with the 200, 100 and 50 MHz antennae is accurate to within $\sim \lambda$ (0.8, 1.7, 3.4 m), and $\sim \frac{3}{2}\lambda$ (10 m) for the 25 MHz antennae.

The TWT to depth conversion on the basis of CMP surveys yields additional errors between 1.4 an 5.7%. For a reflector at a depth of 100 m detected at 200 MHz, this corresponds to an error of 1.4 m because of the uncertainty of the 200 MHz-CMP, and 0.9 m due to the shape of the wavelet and the processes involved during reflections. For the 25 MHz measurements, these errors increase to 5.7 and 10.5 m, respectively. Applying the relation by *Kovacs et al.* [1995] to density profiles to calculate the TWT–depth relation produces a slightly better agreement with the DEP data than using the theoretical model by *Looyenga* [1965]. Although the high resolution DEP technique is the most direct and accurate way to determine the permittivity, the systematic nature of the measurement error implies that the error of a single data point of 1% remains valid for the whole TWT–depth profile [*Wilhelms*, 2000].

Conclusion

The uncertainty involved in the time to depth conversion accuracy of electromagnetic reflectors by state of the art methods has been determined to result in a minimum error of 1%. Maximum errors depend on the used method and range between 1% for DEP, 1–2% for density based mixture models, and between 1.5 and 6% for CMP surveys. In general it can be stated that the errors introduced by the time to depth conversion with a CMP analysis are of the same order as those related to the picking of reflection times.

The overall accuracy in depth of a reflector is determined by the wavelength and the shape of the wavelet of the transmitted pulse and the uncertainty of the method used for time–depth conversion. With the choice of an adequat high resolution of the GPR system, less than 4 m in our study, total errors range between 2 and 6% for depths around 100 m. However, errors could be as high as 12% when the wavelength is increased and the transmitted wavelet reaches a considerable fraction of the observation depth. This implies that higher frequencies should be used for the CMP surveys to resolve the velocity changes, most of which take place in the upper 60-80 m of the ice column. To get better insight into the processes coming along with electromagnetic reflections, it is necessary to carry out further investigations, e.g. by means of numerical calculations based on the measured complex DC. The comparison with real radargrams will provide the opportunity to derive more accurate estimations of the errors involved.

We conclude that the CMP method is suitable for estimating the depth of radar reflectors with sufficient accuracy. Compared to ice core measurements, it is a time saving technique, simple to be carried out, and does not require extensive logistics. CMP surveys are thus a useful tool to acquire region wide information of velocity distributions and time–depth relations, worth to become a standard application for glaciological GPR investigations.

Acknowledgments. We wish to thank Ian R. Joughin, Martin J. Siegert and one anonymous reviewer for their useful comments. The important contribution of the field parties during data acquisition is greatly acknowledged. The data would not have been acquired without the continuing maintenance of the radar system by Günter Stoof.

Preparation of this work was supported by the Deutsche Forschungsgemeinschaft grant Ni493/1 and two scholarships of the Studienstiftung des Deutschen Volkes. This work is a contribution to the "European Project for Ice Coring in Antarctica" (EPICA), a joint ESF (European Science Fonndation)/EC scientific programme, funded by the European Commission and by national contributions from Belgium, Denmark, France, Germany, Italy, the Netherlands, Norway, Sweden, Switzerland and the United Kingdom. This is EPICA publication no. 33.

References

Bogorodsky, V., C. Bentley, and P. Gudmandsen, *Radioglaciology*, D. Reidel Publishing Company, Dordrecht, Holland, 1985.

Clarke, T., and C. Bentley, High-resolution radar on Ice Stream B2, Antarctica: measurements of electromagnetic wave speed in firn and strain history from buried crevasses, *Ann. Glac.*, *20*, 153–159, 1994.

Clough, J. W., Radio echo sounding: reflections from internal layers in ice sheets, *J. Glaciol.*, *18*, 3–14, 1977.

Dix, C., Seismic velocities from surface measurements, *Geophysics*, *20*, 68–86, 1955.

Fisher, E., G. A. McMechan, and A. P. Annan, Acquisition and processing of wide-aperture ground-penetrating radar data, *Geophysics*, *57*, 495–504, 1992.

Fujita, S., H. Maeno, S. Uratsuka, T. Furukawa, S. Mae, Y. Fujii, and O. Watanabe, Nature of radio echo layering in the Antarctic ice sheet detected by a two-frequency experiment, *J. Geophys. Res.*, *104*, 13,013–13,024, 1999.

Garotta, R., and D. Michon, Continuous analysis of the velocity function and the move out corrections, *Geophysical Prospecting*, *15*, 584–597, 1967.

Greaves, R., J. Lesmes, D.P. Lee, and M. Toksöz, Velocity variations and water content estimated from multi-offset, ground-penetrating radar, *Geophysics*, *61*, 683–695, 1996.

Hempel, L., F. Thyssen, N. Gundestrup, H. B. Clausen, and H. Miller, A comparison of radio-echo sounding data and electrical conductivity of the GRIP ice core, *J. Glaciol.*, *46*, 369–374, 2000.

Jezek, K. C., and E. A. Roeloffs, Measurements of radar wave speeds in polar glacier using a down-hole radar target technique, *Cold Reg. Sci. Technol.*, *8*, 199–208, 1983.

Kovacs, A., A. Gow, and R. Morey, The in-situ dielectric constant of polar firn revisited, *Cold Regions Science and Technology*, *23*, 245–256, 1995.

Looyenga, H., Dielectric constant of heterogeneous mixtures, *Physica*, *31*, 401–406, 1965.

Moore, J., and J. Paren, New technique for dielectric logging of Antarctic ice cores., *Journal de Physique (Colloque C1)*, *48*, 155–160, 1987.

Morey, R. M., and A. Kovacs, Analysis of wide-angle reflection and refraction measurements, *CRREL Special Report*, *85-5*, 53–60, 1985.

Murray, T., G. W. Stuart, P. J. Miller, J. Woodward, A. M. Smith, P. R. Porter, and H. Jiskoot, Glacier surge propagation by thermal evolution at the bed, *J. Geophys. Res.*, *105*, 13,491–13,507, 2000.

Nereson, N. A., C. F. Raymond, R. W. Jacobel, and E. D. Waddington, The accumulation pattern across Siple Dome, West Antarctica, inferred from radar-detected internal layers, *J. Glaciol.*, *46*, 75–87, 2000.

Nixdorf, U., and F. Göktaş, Spatial depth distribution of the subglacial bed and internal layers in the ice around NGRIP, Greenland, derived with airborne RES, *J. Appl. Geophys.*, *47*, 175–182, 2001.

Oerter, H., F. Wilhelms, F. Jung-Rothenhäusler, F. Göktas, H. Miller, W. Graf, and S. Sommer, Accumulation rates in Dronning Maud Land as revealed by dielectrical-profiling measurements at shallow firn cores, *Ann. Glac.*, *30*, 27–34, 2000.

Richardson-Näslund, C., E. Aarholt, S.-E. Hamram, P. Holmlund, and E. Isaksson, Spatial distribution of snow in western Dronning Maud Land, East Antarctica, mapped by a ground-based snow radar, *J. Geophys. Res.*, *102*, 20,343–20,353, 1997.

Robin, G. d. Q., S. Evans, and J. T. Bailey, Interpretation of radio echo sounding in polar ice sheets, in *Philosophical Transactions of the*

Royal Society of London, vol. 146 of *A*, pp. 437–505, Royal Society of London, 1969.

Siegert, M. J., and R. Hodgkins, A stratigraphic link across 1100 km of the Antarctic ice sheet between the Vostok ice-core site and Titan Dome (near South Pole), *Geophys. Res. Letters*, *27*, 2133–2136, 2000.

Steinhage, D., U. Nixdorf, U. Meyer, and H. Miller, New maps of the ice thickness and subglacial topography in Dronning Maud Land, Antarctica, determined by means of airborne radio echo sounding, *Ann. Glac.*, *29*, 267–272, 1999.

Vaughan, D., H. Corr, C. Doake, and E. D. Waddington, Distortion of isochronous layers in ice revealed by ground-penetrating radar, *Nature*, *398*, 323–326, 1999.

Wilhelms, F., *Measurement of dielectric properties of polar ice cores (in German)*, vol. 367 of *Berichte zur Polarforschung*, Alfred-Wegener-Institut für Polar- und Meeresforschung, 2000.

Wilhelms, F., J. Kipfstuhl, H. Miller, K. Heinloth, and J. Firestone, Precise dielectric profiling of ice cores: a new device with improved guarding and its theory, *J. Glaciol.*, *44*, 171–174, 1998.

Yilmaz, O., *Seismic data processing*, vol. 2 of *Investig. Geophys.*, Society of Exploration Geophysicist, 1987.

Olaf Eisen, Uwe Nixdorf, Frank Wilhelms, Heinrich Miller, Alfred-Wegener-Institut für Polar- und Meeresforschung, Postfach 120161, 27515 Bremerhaven, Germany. (e-mail: oeisen@awi-bremerhaven.de)

PAPER II

PAPER II is reprinted from the Annals of Glaciology with permission of the International Glaciological Society.

Annals of Glaciology 37, 6 pp., in press, 2003. © *IGS 2003*

Identifying isochrones in GPR profiles from DEP-based forward modeling

Olaf Eisen, Frank Wilhelms, Uwe Nixdorf, and Heinrich Miller

Alfred-Wegener-Institut fiir Polar- und Meeresforschnng Bremerhaven, Bremerhaven, Germany

Abstract. Isochronic continuous horizons between 20 and 90 m depth in a ground penetrating radar (GPR) profile, recorded in Dronning Maud Land, Antarctica, are identified by comparison of synthetic and measured single radar traces. The measured radargram is derived from a stacked GPR profile, the synthetic radargram is computed by convolution of the complex reflection coefficient profile, based on dielectric profiling (DEP) data of a 150 m ice core, with a depth invariant wavelet. It reproduces prominent reflections of the measured radargram to a considerable degree. Analysing matching peaks in both radargrams enables us to identify isochronic reflections and transfer individual volcanic event datings to the GPR profile. Reflections are primarily caused by changes in permittivity, changes in conductivity are of minor importance. However, several peaks in permittivity and conductivity show a good correlation and indicate that some reflections are related to acidic layers. The results demonstrate the possibility to reproduce radargrams from ice core property profiles, a necessary step for the interpretation of remotely sensed radar data, and the general significance of connecting ice core and radar data for correct interpretations. Problems related to forward modeling, data gaps, origin of permittivity peaks, and GPR profiles used for comparison, are discussed.

Introduction

The European Project for Ice Coring in Antarctica (EPICA) aims at retrieving two deep ice cores in different regions of the Antarctic ice sheet. Drilling at Dome Concordia is performed since 1996, the second deep drilling operation started in 2001 at the new Kohnen station in Dronning Maud Land (DML), near the site DML05. Variations in the spatial distribution of precipitation and ice sheet dynamics make it necessary to use additional information for accurate interpretation and extension of ice core data to neighboring regions. Spatial accumulation rates can be obtained from snow pits, shallow ice cores, and spaceborne remote sensing [*Sommer et al.*, 2000; *Karlöf et al.*, 2000; *Wahr et al.*, 2000; *Zwally et al.*, 2002]. The interpretation of the internal ice sheet structure in terms of accumulation rates can be accomplished by ground penetrating radar (GPR) surveys [*Richardson-Näslund et al.*, 1997; *Nereson et al.*, 2000; *Siegert and Hodgkins*. 2000; *Kanagaratnam et al.*, 2001].

Electromagnetic (EM) waves penetrating the ice are partially reflected at boundaries where the complex dielectric constant changes, mainly caused by variations in ice density and chemical composition. Assuming that a continuous internal reflection horizon (IRH) corresponds to an isochronous layer, the spatial variation of layer depth provides information on variations in the accumulation rate and changes due to ice sheet dynamics.

Dating of IRHs is achieved by converting GPR profiles from traveltime to depth domain, using EM velocity–depth relations [*Jezek and Roeloffs*, 1983; *Clarke and Bentley*, 1994; *Richardson-Näslund et al.*, 1997; *Hempel et al.*, 2000; *Eisen et al.*, 2002], and transfer age–depth relations, usually obtained from snow pits or ice cores [*Oerter et al.*, 1999; *Sommer et al.*, 2000], to prominent IRHs. Other studies demonstrated the direct connection between volcanic events and IRHs [e.g. *Millar*, 1981; *Bogorodsky et al.*, 1985; *Siegert*, 1999; *Hempel et al.*, 2000], but so far a direct comparison between synthetic radargrams based on ice core data and

measured radargrams is still pending [*Moore*, 1988; *Miners et al.*, 1997].

In this study we demonstrate the possibility to reproduce prominent IRHs in a GPR radargram by forward modeling, identify most as isochrones, some of which are related to acidic signals, like volcanic eruptions, and transfer the dating to continuous horizons in a GPR profile. The data were obtained during several EPICA pre-site surveys in DML. In 1998/99, numerous GPR profiles were recorded, connecting the locations of ice cores drilled in earlier seasons. High resolution dielectric profiling (DEP) along the ice core B32, retrieved at DML05 in 1997/98 [*Oerter et al.*, 2000], forms the basis for calculating synthetic radargrams with a general frequency domain convolution using a depth invariant wavelet.

GPR Survey Analysis

Common-offset GPR measurements were performed with a commercial 200 MHz monopulse bistatic RAMAC system (Malå Geoscience, Sweden). The antennae were mounted on a sled and pulled by a skidoo at an average speed of 8 km h^{-1}, passing the borehole location B32 in a distance of a few decimeters; a distance meter trigged the transmitter pulse at an interval of 1 m. Each trace consists of 8 vertically stacked pulse recordings of a 1500 ns two-way traveltime (TWT) window containing 2400 samples.

Tracking of coherent patterns in adjacent traces makes it possible to identify prominent reflectors in processed GPR profiles (Figure 1). Processing includes 5-fold horizontal stacking, bandpass filtering, and automatic gain control (AGC). Conversion from TWT to depth domain is achieved by applying a velocity-depth distribution derived from common-midpoint measurements (CMP) [*Eisen et al.*, 2002]. In the resulting profile, numerous continuous prominent IRHs can be identified below 20 m depth, each between 1.5 and 3 m wide. They will be referred to later when comparing GPR and synthetic radargrams.

Due to the relatively low signal-to-noise ratio (SNR) and lateral inhomogeneity of the firn pack, it is difficult to locate the arrival time of IRHs exactly when considering a single GPR trace for comparison with a synthetic radargram. To increase the SNR of the GPR data for further analysis, and to minimise the influence of reflections from obstacles at the surface, e.g. a weather station and metal stakes, we create a single trace radargram, S_{GPR}, used for later comparison, by stacking all traces from eleven different GPR profiles located within a radius of 50 m of B32. Before stacking, the traces are shifted to the primary signal of the direct air wave, resampled at a sample rate of 0.5 ns. After stacking and dewowing, a 100 ns AGC filter is applied to the trace to correct for device related DC components, geometric spreading, absorption, etc.

Forward Modeling of Radargrams

The forward modeling of impulse measurements generally considers the distribution of reflection coefficients with depth to be the impulse response function of the subsurface. The convolution of the transmitted signal with the impulse response function results in the recorded trace, as described in the following section.

Ice core DEP data

The complex relative dielectrical constant can be written as

$$\epsilon = \epsilon' - i\epsilon'' = \epsilon' - i\frac{\sigma}{\epsilon_0 \omega} = |\epsilon| e^{-i\delta}, \qquad (1)$$

where the real part ϵ' is the ordinary relative permittivity of the medium. The imaginary part ϵ'' is the dielectric loss factor and can be expressed as a function of conductivity σ, angular frequency ω, and the permittivity of vacuum ϵ_0. The last expression defines the loss tangent, $\tan\delta = \epsilon''/\epsilon'$.

Along an ice core, ϵ can be determined by means of DEP [*Moore and Paren*, 1987]. An improved DEP device developed by *Wilhelms et al.* [1998], and further refined by *Wilhelms*

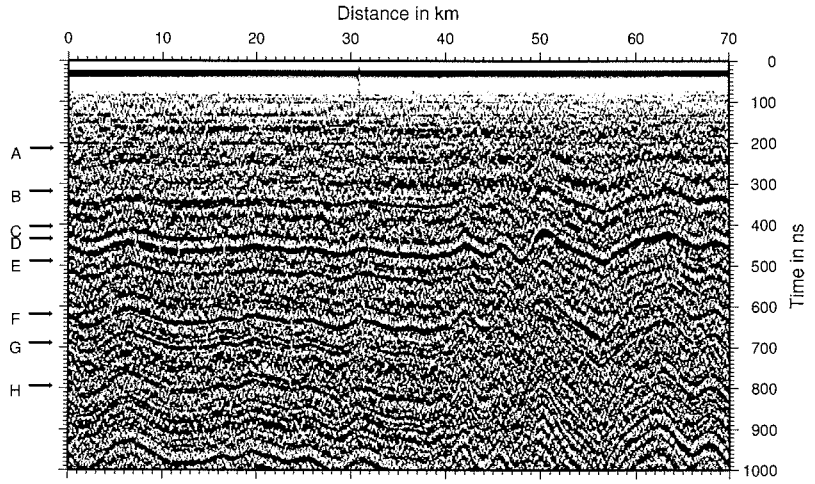

Figure 1. Example for a filtered, stacked, and gain corrected GPR profile, recorded with unshielded 200 MHz antennae. The profile runs from the drill site B32 at DML05 to DML15, traces were recorded every meter. Dominant horizons are labelled A–H and indicated by arrows, depth is in respect to the 1998 surface. The vertical line in the upper part near km 32 is caused by a hardware failure of the system.

[2000], essentially a calibrated guarded scanning capacitor, allows the simultaneous measurement of both components of ϵ. This device was used at a frequency of 250 kHz to determine ϵ along the ice core B32 in $\Delta z = 5$ mm increments with a systematic accuracy of about 1% and a statistical error of ~0.1% for each component, and an accuracy of 1 cm in depth (Figure 2). The depth error results from the positioning of the 1 m long core sections in the measuring bench.

Several schemes to reject sections with poor core quality, and thus false DEP data, were investigated. The best compromise between least rejection and least disturbed convolution signals are obtained by calculating running mean and standard deviation within a 2.5 m window along the core. DEP values that show a permittivity which is more than one standard deviation below the window mean are rejected, as the lower permittivity values are most likely caused by cracks in the ice.

Following this procedure, about 3.5% of the DEP data with an average section length of 2 cm had to be removed in the upper 100 m of the core. In total, 4.5% of the DEP data is missing.

The complex reflection coefficient

The complex reflection coefficient at an interface of two mediae with different dielectrical properties is determined by their complex impedance contrast. The reflection coefficient of two adjacent layers with complex dielectric constants ϵ_k and ϵ_{k+1} measured at depths $k\Delta z$ and $(k+1)\Delta z$, respectively, is given by

$$R_{k+\frac{1}{2}} = R'_{k+\frac{1}{2}} + iR''_{k+\frac{1}{2}} = \frac{\sqrt{\epsilon_k} - \sqrt{\epsilon_{k+1}}}{\sqrt{\epsilon_k} + \sqrt{\epsilon_{k+1}}}, \quad (2)$$

which can be separated and rearranged to obtain $R'_{k+\frac{1}{2}}$ and $R''_{k+\frac{1}{2}}$ as a function of $|\epsilon_k|$, $|\epsilon_{k+1}|$, δ_k and δ_{k+1}. The index $k+\frac{1}{2}$ means that the corresponding depth value for R is the mean depth of both data points, i.e. $(k+\frac{1}{2})\Delta z$.

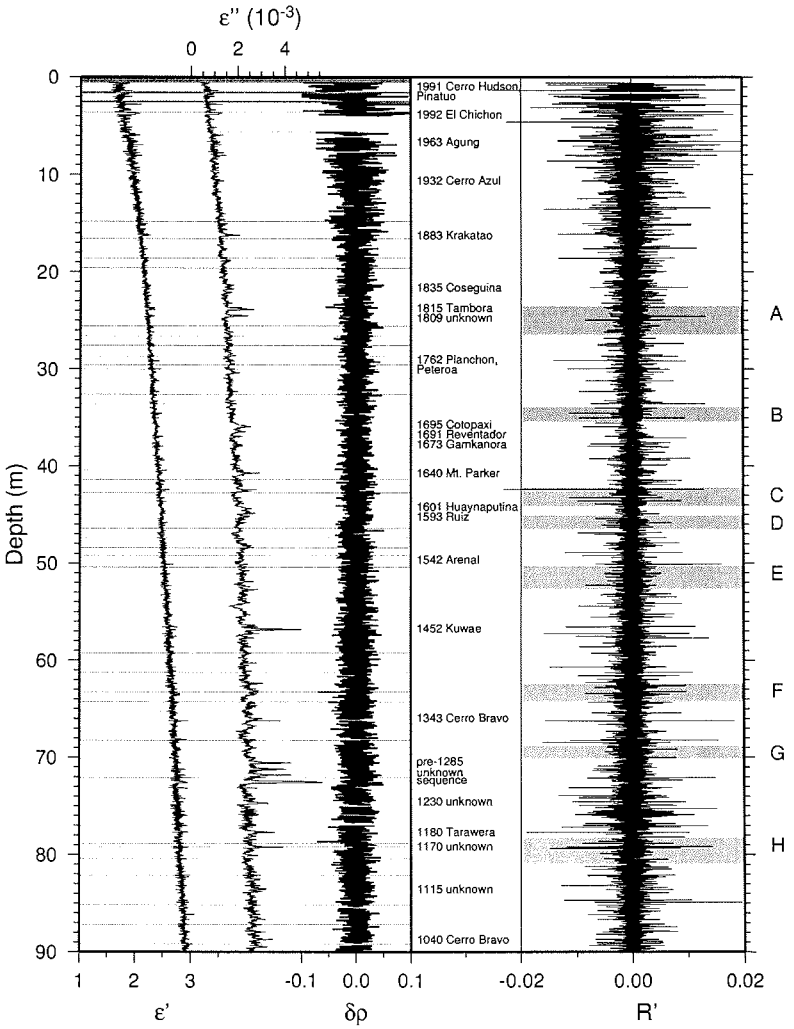

Figure 2. Depth distribution of the measured ordinary relative permittivity ϵ', dielectric loss factor ϵ'', scaled to 200 MHz, density variation $\delta\rho$, the real part R' of the complex reflection coefficient, and name and date of identified volcanic events of the ice core B32. The density variation is calculated from γ-absorption measurements, corrected for core breaks, in respect to the boxcar filtered mean density of a 5 m window. The wide grey horizontal bars labelled A–H on the right indicate the depth and vertical extent of the most prominent reflection horizons in the GPR profile (Figure 1) near B32, corrected to the 1998 surface. The narrow grey horizontal bars indicate gaps in the DEP data record.

Several tests show that gaps larger than several Δz produce too low reflection coefficients when using a linear interpolation, and too large reflection coefficients when applying different spline interpolation schemes. To avoid artificial values, the DEP data is linearly interpolated in gaps that are $\sim 3\Delta z$ in length or smaller, and R is calculated from Equation (2). If the gap length exceeds this limit, R is set to 0 (Figure 2). We consider this to be a more accurate way of treating missing DEP data than to interpolate ϵ on an equidistant grid before calculating the reflection coefficient, as the change in ϵ is more important than the actual value. Support for this procedure comes from test runs with downsampled DEP data, as with a new sample interval of $\sim 5\Delta z$ significant changes in the reflection characteristics are already evident.

Analogous to the TWT of a reflected radar pulse in ice, a propagation time for each data point of the $R(\Delta z)$ series can be calculated from the in-situ EM wave speed, $c = c_0/\sqrt{\epsilon'}$, with c_0 being the wave speed in vacuum. The resulting non-equidistant series is then projected onto an equidistant grid by means of a linear interpolation and a time increment $\Delta t = \Delta z/c_{ice} = 29.7$ ps, yielding the series $R(\Delta t)$ (Δt is the time necessary for an EM wave to propagate the DEP sampling distance of 5 mm in ice with $c_{ice} = 1.68 \times 10^8$ ms^{-1} [*Bogorodsky et al.*, 1985]).

Radar wavelets

Numerous authors emphasise the crucial role of the transmitted radar wavelet for forward modeling of radargrams and GPR processing [*Moore*, 1988; *Arcone et al.*, 1995; *Hildebrand*, 1996]. We investigate several wavelets from raw GPR data, among which are the direct air wave, reflections from the ice shelf–water boundary, and several internal reflections. Although the EM reflections from the ice shelf–sea water boundary represent a close image of the original reflected pulsed, this wavelet only partly reproduces reflections in the upper 30 m of the ice using DEP data. Reasons are most

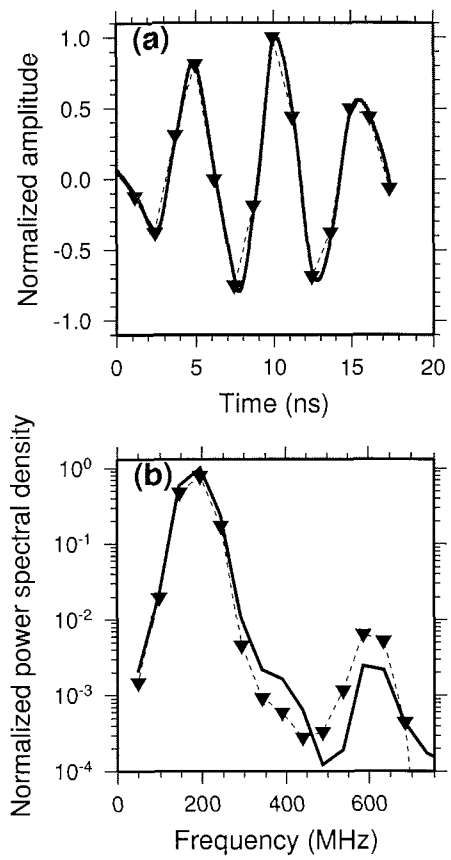

Figure 3. (a) Time domain signals and (b) power spectrum of the raw data wavelet (thin dashed line with triangles) determined from an internal reflection, and the interpolated resampled wavelet used for the convolution (thick line).

likely the different physical in-situ properties in the upper layers of the ice shelf in comparison to the site DML05 on the polar plateau. The wavelet was recorded near Neumayer station, with refrozen meltwater at the surface and solid ice underneath. Thus, absorption, dispersion, phase shifts etc. lead to a different wavelet shape, and thus to different reflections. Best results are obtained with a wavelet determined from a strong internal reflection recorded during a CMP survey near DML05, which is resampled using an Akima spline interpolation at 2048 equidistant points and a time increment Δt as above (Figure 3). This results in the wavelet series $W(\Delta t)$ we use for further calculations.

Frequency domain convolution

The convolution of the wavelet series $W(\Delta t)$ with the reflection coefficient series $R(\Delta t)$, i.e. $S_{DEP} = W * R$, is carried out in the frequency domain by multiplying their Fast Fourier Transforms. The resulting synthetic DEP radargram $S_{DEP}(\Delta t)$ is transformed to depth by applying the inverse TWT–depth conversion introduced above.

Results

Isochrones are layers of equal age that obtained a similar characteristic at the surface on a regional scale, which is sustained during vertical advection and deformation. The accurate dating of GPR profiles requires the identification of isochronic IRHs, which can best be achieved by identifying matching peaks in the measured GPR and synthetic DEP radargrams. If the peaks are related to chemical origin, the corresponding IRHs are isochrones, and, in the case of volcanic events, the dating can be transferred to the GPR profile. As firn age is monotonically increasing with deph, adjacent layers which are parallel to isochronic IRHs have to be isochrones as well. In the following we will carry out this procedure for the prominent IRHs selected in Figure 1.

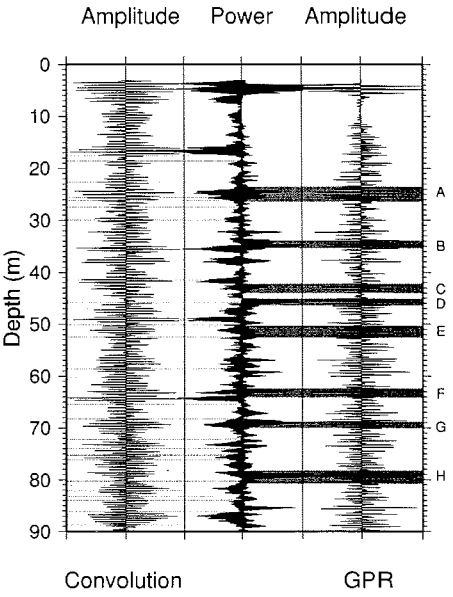

Figure 4. Variable amplitude wiggle plot of the synthetic DEP radargram S_{DEP} (left) and the measured gain corrected GPR radargram S_{GPR} (right). In the middle, the squared envelopes of each radargram are shown, with the power of S_{DEP} increasing to the left and S_{GPR} increasing to the right. The GPR signal is corrected to the 1998 surface, the first 3 m have been muted because of the influence of the direct and ground wave. A 10 cm wide mean boxcar filter has been applied to the envelopes to increase clarity. Wide grey bars in the right half labelled A–H indicate prominent reflection horizons in the GPR profile (Figure 1), narrow grey bars in the left half indicate gaps in the DEP data (Figure 2).

DEP vs. GPR radargram

For the direct comparison of both radargrams we use their squared envelopes, which are proportional to energy, calculated from the single trace radargrams. Due to the influence of the direct air and ground wave as well as

antenna ringing, signals with a TWT < 50 ns ($\sim$ 10 m) are neglected in the following comparison.

Most prominent IRHs in the GPR profile (events A-H, Figure 1) are visible in S_{GPR} as strong peaks (Figure 4). Some, however, have rather small amplitudes (e. g. event E), but can nevertheless be clearly identified as continuous signals in the GPR profile.

In general, the power envelope of the synthetic trace S_{DEP} shows a good agreement in numerous incidents with the power envelope of S_{GPR}, enabling the identification of distinct reflections. However, some outliers are also present on either side. Matching partners of comparable size to the GPR envelope are visible in the DEP envelope for events A, B, C, F, and G. A very good agreement, even in phase structure, exists for events A, F, and G. Events B and E have S_{DEP} envelope peaks of only about half the width of the S_{GPR} signal, and their maxima are shifted by 0.5 and -1.0 m, respectively. For events C and F, the directly matching envelope peak is of same size, but while event C is preceded by a stronger signal which is not visible in S_{GPR}, event F is followed by one. A direct partner in S_{DEP} is missing for event D, and the peak in S_{DEP} is smaller in size and with a slightly shifted maximum for event H, but still comparable in phase. The most obvious outliers in S_{DEP} occur at 16.5, 49, and 64 m. We now discuss probable reasons for these differences.

Qualitative error analysis

Numerous factors affect the shape of the synthetic and the recorded radargrams. The most obvious problems are missing DEP data, strongly altering interference patterns of reflected wave trains, and the presence of noise in the GPR profiles.

Comparison studies with single GPR traces or small ensembles of stacked traces were only partly successful. The GPR processing sequence described above makes use of coherent positions of reflecting horizons with depth within a radius of 50 m around B32, i.e. time shifts during the recording due to surface of reflector roughness are smaller than half a wavelength (0.5 m for $c = 2.0 \times 10^8$ ms^{-1}). Although stacking of more than 500 traces significantly increases the SNR and emphasises dominant horizons, weaker signals might be destroyed.

The original DEP data, on the other hand, represents a point measurement, which therefore has a low SNR, but a high vertical resolution. Lateral inhomogeneities are present, especially in the upper part of the firn, where sastrugis are still distinguishable and might lead to a different reflectivity over one Fresnel zone than calculated from the DEP data. Moreover, parts of the data are missing, and cannot be interpolated easily without introducing artificial reflection properties. Gaps of a few centimeters in length might already result in the loss of considerable information on reflectivity. For example, four gaps with a total length of 8 cm occur within event D. Three of these gaps occur at points where ϵ seems to change significantly, suggesting that the strong peak of S_{GPR} at 45.5 m lacks a matching peak in S_{DEP} because of wrong values for R. Likewise, event H is interrupted in the DEP data by five gaps.

An additional cause for differences of both radargrams comes along with the convolution scheme. In general, the propagating wave changes shape due to dispersion effects, and a complex reflection coefficient causes phase shifts at each layer boundary. The use of a constant wavelet neglects both processes. Sensitivity runs with different wavelets indicate that the reflection characteristics for longer traveltimes depend on the wavelet choice, e.g. with a different signal the single DEP reflection at 86 m is strongly reduced in magnitude and becomes a multi peak signal. Moreover, interferences due to multiple reflections are not accounted for by a simple convolution. This could be the reason for the sharp peaks in S_{DEP} at 49 and 64 m, which do not have any peak in S_{GPR}. The broad peak between 16.0 and 17.5 m, on the other hand is matched by two much smaller and

sharper GPR peaks, and might be the result of constructive interference caused by missing reflectivity and multiple reflections, or negative interference in the GPR because of pronounced lateral inhomogeneities at this depth.

The AGC applied to the GPR trace basically compensates for energy losses due to geometric spreading. As pointed out by *Hildebrand* [1996], absorption and reflection losses as well as focusing are of minor importance in the upper part of the considered depth range, and are therefore no major factors for discrepancies. At larger traveltimes, however, the reflected GPR signal is close to the noise level, unavoidably decreasing the SNR, and thus resulting in larger differences in magnitude of matching peaks.

Physical origin of reflections

To reveal the physical origin of the observed matching synthetic reflections, we perform two sensitivity studies. For the calculation of the synthetic radargram S^I_{DEP} of the first study, ϵ'' is smoothed with a 20 m boxcar mean filter, ϵ' is left unchanged. For the second study, resulting in S^{II}_{DEP}, selected individual peaks in ϵ', that show a correlation with conductivity signals at same depths, are smoothed and ϵ'' is left unchanged.

The synthetic radargram S^I_{DEP} is quasi identical to the original S_{DEP}. The second study demonstrates that amplitudes of reflections in S^{II}_{DEP} are 1–2 orders of magnitude smaller than prominent peaks in S_{DEP} at the same depth. Moreover, because of the increased variability of the conductivity record, the position of reflections in S^{II}_{DEP} show a less clear agreement with S_{GPR}, i.e. they cannot explain the observed matching IRHs of S_{DEP} and S_{GPR}. These results confirm earlier findings [*Moore*, 1988; *Hildebrand*, 1996; *Miners et al.*, 1997] that the reflection coefficient is dominated by changes in permittivity and that conductivity changes are negligible. As we relate the origin of reflections to changes in permittivity coinciding with acidic layers, two questions arise: what is the cause of the correlation between chemical impurities and permittivity; do acidic layers affect the permittivity of the firn?

We rule out measurement artifacts related to the relaxation frequency of ice, as the DEP processing scheme has been extensively tested in this respect [*Wilhelms*, 2000]. In some cases, e. g. the Coseguina (1835, 21.7 m) and Tambora (1815, 23.8 m) events, the γ-absorption density record shows distinct peaks in density as well. In the case of the adjacent unknown eruption (1809, 24.5 m), a comparable peak in density is missing (Figure 2). The DEP-based density at the same depth, calculated with the complex mixing model [*Wilhelms*, 2000], i. e. corrected for dielectrical mixing of density and conductivity of the complex ϵ of firn, shows the same pattern. This indicates that the correlations between acidic peaks in conductivity, permittivity, and density is not systematic, but that different mechanisms are present, as pointed out by *Fujita et al.* [2000].

The simplest explicative process is of meteorological origin, e. g. accumulation coming along with unusual circulation patterns, increasing chemical impurities and changing snow properties simultaneously. Nevertheless, complex dielectrical mixing between the air and snow phase, changes in the firn lattice, or protonic defects, related to chemical impurities, might play a role at different frequencies, requiring further investigations on the microphysical level.

Identifying isochrones

The ice core B32 has been dated by counting annual layers in various chemical records [*Sommer et al.*, 2000], and volcanic events have been identified by *Göktaş* [2002] by a combination of annual layer counting, nss-sulphate concentrations, and identified H_2SO_4 depositions (Figure 2).

Having related the physical origin of matching peaks of S_{GPR} and S_{DEP} to permittivity peaks in the ϵ–depth distributions (Figure 2) enables us to connect certain chemical events with dominant signals in the DEP radargram.

Because of the comparable structure of several permittivity and conductivity peaks, we have to assume that these permittivity peaks are related to volcanic eruptions or other chemical events, with the consequence that the corresponding IRHs are isochrones. The ice core dating can then be transferred via several matching peaks to the GPR radargram and further to the GPR profile. It has to be kept in mind that the strongest peak of an IRH observed in the radargram is slightly shifted to larger traveltimes, or depths, as the wavelet maximum is delayed from the first arrival by ~ 10 ns, corresponding to about 2 m.

Of the set of prominent IRHs we selected for our analysis, the double peak of event A is coincident with the Tambora and one unknown eruption in 1815 and 1809, respectively. Events C and F coincide with strong peaks in ϵ'', which result from above normal values in several chemical species (dated to 1620 and 1375, respectively), but which make it difficult to attribute these signals solely to volcanic eruptions [H. Oerter, personal communication, 2002]. Although for event H the matching peak is not of as good a quality as at shallower depths, it is striking that two eruptions, Trawera in 1180 and one unknown in 1170, are dominant at the same depth. Event D is coincident with the Ruiz eruption (1593), but as a corresponding peak in S_{DEP} is missing, the origin of the IRH is unclear.

To summarise, six out of the eight strongest IRHs evident from the GPR profile show matching peaks in GPR- and DEP-based radargrams, all of which are caused by peaks in permittivity. Four of these coincide with signals in the conductivity of chemical origin, with a very good correlation to permittivity, two of which are attributed to volcanic events. This evidence strongly suggests that these four events are isochrones. As all dominant observed continuous IRH in the considered depth range are parallel to adjacent identified isochrones, they have to be of isochronous origin as well.

Conclusion

Based on a simple convolution scheme we are able to calculate a synthetic radargram from high resolution DEP ice core data, which reproduces dominant features of a measured radargram to a considerable degree. In four cases, the ice core dating from single chemical events can be directly transferred to continuous IRHs in common-offset GPR profiles, via matching dominant peaks in the radargrams. The dated horizons provide an independent means to synchronise ice cores from different locations, and can be used to determine the regional and temporal distribution of the accumulation rates.

All IRHs are caused by changes in the permittivity. However, major IRHs in the depth range between 20 and 90 m are associated with volcanic eruptions or distinct chemical events of other origin, that seem to cause changes in the chemical as well as physical properties.

Discrepancies between the synthetic and real radargram are associated with gaps in the DEP data, the presence of noise in the GPR data, and lacking consideration of important physical phenomenon during wave propagation by the convolution scheme. To overcome data gaps, detailed studies on the random structure on the DEP profiles on a regional scale, and their influence on EM reflections are required to develop interpolation procedures that successfully reproduce lacking data without introducing artificial EM reflections.

Instead of developing more sophisticated convolution schemes, we suggest to use finite-difference forward modeling for calculating synthetic radargrams, as the simulation of the propagation and reflection processes of the EM waves, e.g. multiple reflections, phase shifts, and absorption, are implicitly accounted for. Currently, work is in progress to calculate finite-difference–based radargrams from the DEP data used for this study.

Acknowledgments. We acknowledge the important contribution of the field parties during data acquisition. The data would not have been ac-

quired without the continuing maintenance of the radar system by Günter Stoof. Preparation of this work was supported by the Deutsche Forschungsgemeinschaft grant Ni493/1 and two scholarships of the Studienstiftung des Deutschen Volkes. The final manuscript profited from the valuable comments of John Moore. The contribution of Nobuhiko Azuma (Scientific Editor) and one anonymous reviewer is greatly acknowledged. This work is a contribution to the "European Project for Ice Coring in Antarctica" (EPICA), a joint ESF (European Science Foundation)/EC scientific programme, funded by the European Commission and by national contributions from Belgium, Denmark, France, Germany, Italy, the Netherlands, Norway, Sweden, Switzerland and the United Kingdom. This is EPICA publication no. 54.

References

Arcone, S., D. Lawson, and A. Delaney, Short-pulse wavelet recovery and resolution of dielectric contrasts within englacial and basal ice of Matanuska Glacier, Alaska, U.S.A., *J. Glaciol.*, *41*, 68–86, 1995.

Bogorodsky, V., C. Bentley, and P. Gudmandsen, *Radioglaciology*, D. Reidel Publishing Company, Dordrecht, Holland, 1985.

Clarke, T., and C. Bentley, High-resolution radar on Ice Stream B2, Antarctica: measurements of electromagnetic wave speed in firn and strain history from buried crevasses, *Ann. Glac.*, *20*, 153–159, 1994.

Eisen, O., U. Nixdorf, F. Wilhelms, and H. Miller, Electromagnetic wave speed in polar ice: Validation of the CMP technique with high resolution DEP and γ-density measurements, *Ann. Glac.*, *34*, 150–156, 2002.

Fujita, S., T. Matsuoka, T. Ishida, K. Matsuoka, and S. Mae, A summary of the complex dielectirc permittivity of ice in the megahertz range and its application for radar sounding of polar ice sheets, in *The Physics of Ice Core Records*, edited by T. Hondoh, 1 ed., pp. 185–212, Hokkaido University Press, 2000.

Göktaş, F., *Characterisation of glacio-chemical and glacio-meteorological parameters of Amundsenisen, Dronning Maud Land, Antarctica*, vol. 425 of *Berichte zur Polarforschung*, Alfred-Wegener-Institut für Polar- und Meeresforschung, 2002.

Hempel, L., F. Thyssen, N. Gundestrup, H. B. Clausen, and H. Miller, A comparison of radio-echo sounding data and electrical conductivity of the GRIP ice core, *J. Glaciol.*, *46*, 369–374, 2000.

Hildebrand, A., Untersuchung der Laufzeit- und Amplitudenverhalten elektromagnetischer Impulse bei glaziologischen Radarmessungen, Ph.D. thesis, Westfälische Wilhelmsuniversität Münster, 1996.

Jezek, K. C., and E. A. Roeloffs, Measurements of radar wave speeds in polar glacier using a down-hole radar target technique, *Cold Reg. Sci. Technol.*, *8*, 199–208, 1983.

Kanagaratnam, P., S. Gogineni, N. Gundstrup, and L. Larsen, High-resolution radar mapping of internal layers at the North Greenland Ice Core Project, *J. Geophys. Res.*, *106*, 33,799–33,812, 2001.

Karlöf, L., et al., A 1500 years record of accumulation at Amundsenisen western Dronning Maud Land, Antarctica, derived from electrical and radioactive measurements on a 120 m ice core, *J. Geophys. Res.*, *105*, 12,471–12,483, 2000.

Millar, D. H. H., Radio echo layering in polar ice sheets and past volcanic activity, *Nature*, *292*, 441–443, 1981.

Miners, W., A. Hildebrand, S. Gerland, N. Blindow, D. Steinhage, and E. Wolff, Forward Modelling of the Internal Layers in Radio Echo Sounding Using Electrical and Density Measurements from Ice Cores, *J. Phys. Chem. B*, *101*, 6201–6204, 1997.

Moore, J., Dielectric variability of a 130 m Antarctic ice core: implications for radar sounding, *Ann. Glac.*, *11*, 95–99, 1988.

Moore, J., and J. Paren, New technique for dielectric logging of Antarctic ice cores., *Journal de Physique (Colloque C1)*, *48*, 155–160, 1987.

Nereson, N. A., C. F. Raymond, R. W. Jacobel, and E. D. Waddington, The accumulation pattern across Siple Dome, West Antarctica, inferred from radar-detected internal layers, *J. Glaciol.*, *46*, 75–87, 2000.

Oerter, H., W. Graf, F. Wilhelms, A. Minikin, and H. Miller, Accumulation studies on Amundsenisen, Dronning Maud Land, Antarctica, by

means of Tritium, dielectric profiling and stable-isotope measurements: first results from the 1995–96 and 1996–97 field seasons, *Ann. Glac.*, *29*, 1–9, 1999.

Oerter, H., F. Wilhelms, F. Jung-Rothenhäusler, F. Göktas, H. Miller, W. Graf, and S. Sommer, Accumulation rates in Dronning Maud Land as revealed by dielectrical-profiling measurements at shallow firn cores, *Ann. Glac.*, *30*, 27–34, 2000.

Richardson-Näslund, C., E. Aarholt, S.-E. Hamran, P. Holmlund, and E. Isaksson, Spatial distribution of snow in western Dronning Maud Land, East Antarctica, mapped by a ground-based snow radar, *J. Geophys. Res.*, *102*, 20,343–20,353, 1997.

Siegert, M., On the origin, nature and uses of Antarctic ice-sheet radio-echo layering, *Progress in Physical Geography*, *23*, 159–179, 1999.

Siegert, M. J., and R. Hodgkins, A stratigraphic link across 1100 km of the Antarctic ice sheet between the Vostok ice-core site and Titan Dome (near South Pole), *Geophys. Res. Letters*, *27*, 2133–2136, 2000.

Sommer, S., et al., Glacio-chemical study covering the past 2 kyr on three ice cores from Dronning Maud Land, Antarctica 1. Annually resolved accumulation rates, *J. Geophys. Res.*, *105*, 29,411–29,421, 2000.

Wahr, J., D. Wingham, and C. Bentley, A method of combining ICESat and GRACE satellite data to constrain Antarctic mass balance, *J. Geophys. Res.*, *105*, 16,279–16,294, 2000.

Wilhelms, F., *Measurement of dielectric properties of polar ice cores (in German)*, vol. 367 of *Berichte zur Polarforschung*, Alfred-Wegener-Institut für Polar- und Meeresforschung, 2000.

Wilhelms, F., J. Kipfstuhl, H. Miller, K. Heinloth, and J. Firestone, Precise dielectric profiling of ice cores: a new device with improved guarding and its theory, *J. Glaciol.*, *44*, 171–174, 1998.

Zwally, H., et al., ICESat's laser measurements of polar ice, atmosphere, ocean, and land, *J. Geodynamics*, *34*, 405–445, 2002.

Olaf Eisen, Frank Wilhelms, Uwe Nixdorf, Heinrich Miller, Alfred-Wegener-Institut für Polar- und Meeresforschung, Postfach 120161, 27515 Bremerhaven, Germany. (e-mail: oeisen@awi-bremerhaven.de)

PAPER III

Geophysical Research Letters 30(5), 22-1-22-4, 2003. © *AGU 2003*

Revealing the nature of radar reflections in ice: DEP-based FDTD forward modeling

Olaf Eisen, Frank Wilhelms, Uwe Nixdorf, and Heinrich Miller

Alfred-Wegener-Institut für Polar- und Meeresforschung Bremerhaven, Bremerhaven, Germany

Abstract. Successful simulation of ground penetrating radar (GPR) traces in polar ice is achieved by numerical finite-difference time-domain (FDTD) forward modeling. Properties of the modeled medium are taken from high resolution dielectric profiling (DEP) of the upper 100 m of an ice core from Dronning Maud Land, Antarctica. The GPR reference trace is calculated from stacking of a normal moveout corrected common-midpoint survey, carried out near the borehole location. The excellent agreement of synthetic and GPR-based results demonstrates the capability of FDTD models to reproduce radargrams from ice core properties for interpretation of radio echo sounding data, and emphasizes the exploitation of radar data for improved interpretations of glaciological climate proxys. In addition to presenting modeling results, we perform sensitivity experiments to investigate the nature and origin of radar reflection in ice, discuss reasons for the failure of modeling studies in the past, and indicate new approaches.

Introduction

Radio echo sounding has become a standard tool for glaciological applications to determine ice thickness, internal structure, basal properties, accumulation rates, and ice dynamics [*Robin et al.*, 1969; *Oswald and Robin*, 1973; *Hempel and Thyssen*, 1992; *Arcone et al.*, 1995; *Corr et al.*, 2002, among others]. The basic processes are reasonably well understood, i.e. partial reflection of the propagating electromagnetic (EM) waves at dielectric discontinuities. Most applications related to internal structures, however, still depend on assumptions and require further information to enable unambiguous data interpretations.

Several studies have demonstrated the importance of density in the upper part of the ice sheet and the connection of volcanic events with deeper internal reflection horizons [e.g. *Millar*, 1981; *Bogorodsky et al.*, 1985; *Siegert*, 1999; *Hempel et al.*, 2000]. However, calculation of corresponding synthetic radargrams, based on density and conductivity profiles, only had very limited success [*Miners et al.*, 1997]. Although utilization of the complex dielectric constant from dielectric profiling (DEP) in recent studies has partly advanced the agreement between synthetic and measured radargrams [*Kohler et al.*, 2003; *Eisen et al.*, 2003], further improvements are still necessary.

This study demonstrates that problems related to the limited representation of wave phenomena in earlier models (for detailed summaries see *Miners* [1998]; *Hildebrand* [1996]) and large lateral inhomogeneities of physical and chemical properties of ice [L. Karlöf, Norwegian Polar Institute, personal communication, 2002] can be overcome by adopting established numerical modeling and radar processing techniques from other fields. We present a successful reproduction of measured ground penetrating radar (GPR) data by a finite-difference time-domain (FDTD) modeling approach based on ice core DEP data. The successful comparison of the modeled radargram with processed radar data validates the underlying modeling approach and facilitates sensitivity studies to proof the power of FDTD modeling as a tool for physical-chemical studies on the nature of radar reflections in ice.

DEP

Modeling of EM wave propagation requires knowledge of the physical structure of the me-

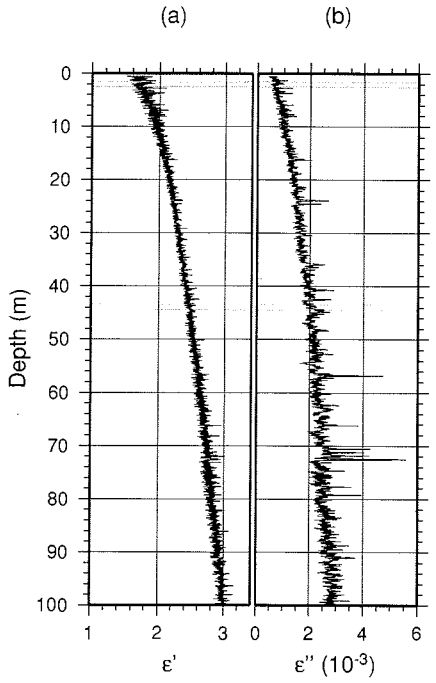

Figure 1. Dielectric properties of ice core B32 as a function of depth. (a) Ordinary relative permittivity ε'; (b) dielectric loss factor ε'', measured at 250 kHz and scaled to 200 MHz. The underlain gray narrow horizontal bars indicated gaps in the DEP data record.

dium of interest. The most accurate prescription of medium properties is provided by the vertical distribution of the dielectric constant ε from DEP measurements along ice cores [*Moore and Paren*, 1987].

The improved DEP device developed by *Wilhelms et al.* [1998], and further refined by *Wilhelms* [2000], allows the simultaneous measurement of both components of $\varepsilon = \varepsilon' - i\varepsilon'' = \varepsilon' - i\sigma(\varepsilon_0\omega)^{-1}$, where the real part ε' is the ordinary relative permittivity of the medium; the imaginary part ε'' is the dielectric loss factor. The latter can be expressed as a function of conductivity σ; angular frequency ω; and permittivity of vacuum ε_0.

The ice core B32 was retrieved in 1997/98 during the EPICA pre-site survey in Dronning Maud Land, Antarctica [*Oerter et al.*, 2000], and profiled at a frequency of 250 kHz in $\Delta z =$ 5 mm increments (Figure 1). Each component has a systematic accuracy of about 1% and a statistical error of 0.1%. Sections with peaks of low ε', caused by cracks in parts of poor core quality, were removed in both ε-components, if the actual value differed from the 2.5 m running mean by more than one standard deviation of the same window. In total, 4.5% of the final ε–depth series were missing or had to be rejected.

FDTD Modeling

Advantages of the FDTD technique are the implicit inclusion of EM wave phenomena occuring during propagation, like multiple reflections, interferences, absorption, geometrical spreading, ray focusing, phase shifts, etc. Our numerical model is based on a FDTD set of Maxwell's curl equations [*Yee*, 1966], implemented on a staggered grid with absorbing boundary conditions. (*Taflove* [1995] provides extensive discussions on physical interpretations, implementation approaches, and other applications.) Results of this study are obtained with a 2D version of the model, with the transmitter (TX) being represented by an infinite electric line source perpendicular to the (x, z) model space (E_y-polarized source sig-

nal), thereby decoupling the transversal electric (TE) and magnetic modes (TM) [*Hohmann*, 1988]. Duration and shape of the source wavelet are determined from the air wave of the 200 MHz common-midpoint (CMP) radargram described below, interpolated onto equidistant time increments Δt using an Akima spline (details on the wavelet can be found in *Eisen et al.* [2003]). The DEP data are linearly interpolated onto the cartesian space grid, assuming lateral homogeneity in ice and air, with $\varepsilon_{air} = 1$ and $\sigma_{air} = 0$.

The parallelized model was implemented on a NEC SX-6 supercomputer at the Deutsches Klimarechenzentrum (DKRZ, Hamburg, Germany). Model dimensions for all runs are 10 m in horizontal direction ($x \in [-5\text{ m}, 5\text{ m}]$), and 120 m in vertical direction ($z \in [-20\text{ m}, 100\text{ m}]$), with an isotropic space increment $\Delta = 0.01$ m and a time increment $\Delta t = 0.01$ ns, thus providing high resolution of the source pulse, satisfying the stability criterion, and reducing numerical dispersion [*Taflove*, 1995]. Further decreasing space and time increments for testing purposes did hardly change results, confirming that numerical diffusion can be neglected at this frequency and level of DEP resolution. The TX is positioned at $(x, z) = (-0.25\text{ m}, -0.05\text{ m})$, the receiver (RX) at $(x, z) = (0.25\text{ m}, -0.05\text{ m})$, representing the survey geometry of the first CMP trace. Simulation of 1000 ns of wave propagation with this parameter set resulted in the synthetic radargram S_{FD}. The computation took less than 1 h, required 1.5 GBytes RAM memory, and 7 h of CPU time at 3.7 GFlops on 8 dedicated CPUs.

Radar Reference Data

Comparisons of modeled radargrams with measured radar data require suitable reference traces. These can either be derived from single point, common-offset or CMP radar surveys. Whereas the first two survey setups are carried out at a fixed TX–RX distance, stationary in the first case and moving across the surface in the second, the CMP recording technique, adapted from seismic data acquisition, provides multifold coverage at several nonzero-offsets, thereby improving SNR and yielding subsurface velocity information [*Garotta and Michon*, 1967; *Yilmaz*, 1987].

The CMP survey was recorded ~100 m south of the borehole B32 in 1998/99 with a commercial RAMAC GPR device (Malå Geoscience, Sweden), operated with two unshielded 200 MHz dipole antennae. Starting with a minimal TX–RX offset of 1.0 m, 139 traces were recorded at 0.5 m offset increments, applying 512-fold vertical stacking to each trace. The CMP-based velocity model [*Eisen et al.*, 2002] is used to apply a normal moveout (NMO) correction to each trace. Subsequent stacking of all NMO corrected traces results in one single reference trace, S_{CMP}, used for validation of S_{FD}.

Synthetic vs. Reference Trace

Before carrying out the comparison of modeled and measured radargrams three problems need to be considered: first, a separation between drilling location and CMP survey of some 100 m; second, one year of accumulation between ice core retrieval and GPR survey; and third, simulation of a 3D wave propagation process with a 2D model. These differences are partly taken care of by linearly correcting the CMP two-way traveltime (TWT) to the 1998 surface–depth structure at the borehole and applying a 200 ns automatic gain control filter to both traces, also correcting for antenna gain and system properties. The comparison is limited to the interval 100–1000 ns TWT, both to avoid interference of the air and ground wave with internal reflection hyperbolae in the CMP data, and to reduce the influence of bad core data at greater depth.

Comparing both radargrams indicates similarities, but also demonstrates their different origin (Figure 2). Whereas most signals in S_{CMP} are distinct events, fewer reflections in S_{FD} clearly rise above background noise. This is, however, not surprising, as a noise-reducing

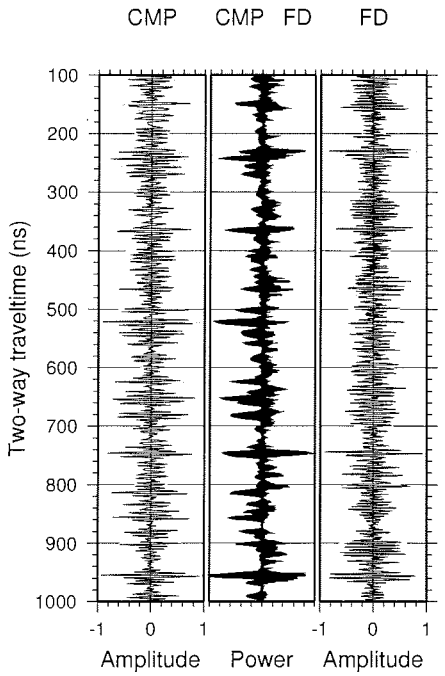

Figure 2. Comparison of CMP and FD trace amplitude and power as a function of two-way traveltime (TWT). The left panel shows the gain corrected CMP-based trace S_{CMP} in wiggle format, underlain by the trace envelope (displayed in positive and negative axis directions). The right panel shows the corresponding FD-based trace S_{FD}. The middle panel shows the power of both traces, calculated from the squared envelopes, with the power of S_{CMP} increasing to the left, and S_{FD} increasing to the right. All displays are normalized to the maximum magnitude in the interval 100–1000 ns.

processing step similar to CMP stacking is missing for the modeled trace, i.e. the noise inherent to the DEP data is still present in S_{FD}, with little numerical diffusion added, resulting in a lower SNR than for S_{CMP}.

Although consideration of the power distribution instead of amplitude–phase relations of return signals comes along with a loss of phase information, it results in a more robust quantity for comparison and applications like tracking of internal reflection horizons, as strong reflections are emphasized by reduced noise level. The distributions of major reflections show an excellent agreement. Numerous peaks occur in both power radargrams, several of which are of comparable magnitude, the most obvious ones at 220, 360, 740 and 950 ns TWT. Despite the lower SNR for S_{FD}, several events show good agreement with S_{CMP} not only in their onset and magnitude, like the reflections at 340 ns, but also in the phase structure, e.g. events at 740 and 950 ns. In some cases the reflection pattern is comparable, but the magnitudes differ, like the double peaks around 240 ns in either radargram with reversed order of reflection strength, or the 500–520 ns sequence.

Different schemes were applied for evaluating and correcting the DEP data set. The results emphasize that the ε–depth distribution is the most important factor for reproducing survey radar data. Missing or wrong DEP data sections have more severe influence on the synthetic trace than slightly different source wavelets, numerical approximations, or model geometry. In particular, agreement of the phase structure of reflections originating from only partly consolidated firn cannot be expected in general, as the lateral dielectric variations of small scale features like sastrugis occur within the first Fresnel zone, implying interference of the reflected elementary wave trains. A lateral homogeneous ε-distribution does not reproduce these variations.

An objective measure of the agreement of traces is important for comparing different modeling approaches or judging sensitivity studies.

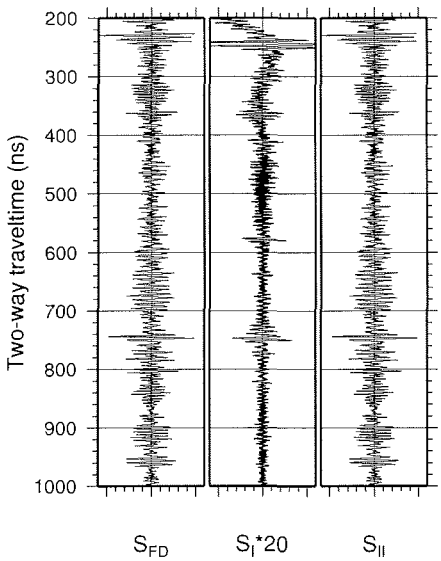

Figure 3. Comparison of the original FD-trace S_{FD} with the two results of the sensitivity studies. Note that the amplitude of S_I is multiplied by a factor of 20.

One example is the correlation coefficient of trace power distributions, which results as 0.43. The correlation coefficients of trace amplitudes is less suitable for evaluating the agreement, indicated by the low value of 0.13, as small differences in timing of phase shifts of single events can completely destroy the correlation.

Sensitivity Studies

The good agreement between modeled and measured radargrams validates the modeling approach and enables the numerical investigation of the physical origin of reflections. To this end we perform two sensitivity experiments. We calculate a synthetic radargram, S_I, from a smoothed distribution of ε', filtered with a 20 m boxcar running mean, and unchanged ε''. The opposite filtering is carried out for a second experiment, i.e. only ε'' is filtered, resulting in S_{II}. Whereas the amplitudes and phases of reflections in S_I are quite different from those of the original synthetic radargram S_{FD}, S_{II} is very similar (Figure 3).

This has several implications. The second study demonstrates that the reflection structures of S_{FD}, and because of their good agreement also of S_{CMP}, are almost solely determined by permittivity. Reflections caused by changes in conductivity are 1–2 orders of magnitude smaller than those caused by variations in permittivity in the considered depth range, as seen from S_I. Moreover, changes in conductivity are also too small to have a considerable influence on the phase structure of reflection signals.

The results confirm earlier findings [*Moore*, 1988; *Hildebrand*, 1996; *Miners*, 1998] that the reflection coefficient in the upper hundreds of meters is dominated by changes in permittivity and that conductivity changes are negligible. An interesting feature is the occurrence of three distinct reflections in S_I at the same depth as in S_{II}, that also show comparable amplitude ratios (at 240, 360 and 740 ns TWT). This implies that the change in permittivity of the ice core record, responsible for the reflections in S_{II} and S_{FD}, is accompanied by a change in conductivity, or vice versa. Possible explanations are: dielectric mixing of the complex ε of the air–snow mixture according to the general cubical power law proposed by *Landau and Lifschitz* [1982] in the 1940s, and investigated by means of DEP by *Wilhelms* [2000]; direct influence of chemical impurities on the permittivity [*Fujita et al.*, 2000]; or a common formation process, as found in other radar data [*Eisen et al.*, 2003].

Summary

This study demonstrates that successful modeling of GPR data in polar ice can be achieved by means of the DEP-based FDTD technique. Problems of other approaches, like lacking consideration of important physical processes in convolution models or utilization of a density-based permittivity, are overcome by their im-

plicit inclusion in the governing equations and provision of an accurate picture of the complex physical properties of the subsurface by high resolution in-situ DEP data, respectively.

Lateral inhomogeneities of the medium and gaps in the DEP data are likely the main reasons for remaining discrepancies. On the GPR side, reduction of noise can be achieved by analysis of CMP surveys. For modeling, improved solutions with lower noise level could be obtained by either stacking ice core profiles from neighboring cores or simulating CMP-like survey setups with subsequent processing, unfortunately requiring a huge amount of computer time and memory. Apart from limitations set by the inhomogeneous nature of the ice pack, exact matching of measured and synthetic radargrams requires model extension to 3D and accurate representation of antennae and system properties.

Nevertheless, the present success already encourages the study of electromagnetic reflection phenomena in deeper parts of the ice sheets by forward modeling, the most important ones being the transition from permittivity to conductivity dominated reflections and the influence of ice fabric on signal properties. The new EPICA ice core from Dronning Maud Land, in conjunction with airborne radar data, provides a promising data set to achieve these goals in the near future.

Acknowledgments. The original version of the FDTD model was developed by Volker Mayer and Jupp Sandmeier as a module for the commercial GPR analysis PC software Reflex (Sandmeier Software, Karlsruhe, Germany). They gave helpful advice for decoupling the module from the PC software for our special purposes. Debugging and optimization greatly profited from support by Stephan Frickenhaus, AWI computing centre, and Klaus Ketelsen, DKRZ. The paper benefited from the comments by Jack Kohler and Richard Hindmarsh (reviewers), the contribution from James Famiglietti (scientific editor) is greatly acknowledged. Preparation of this work was supported by the Deutsche Forschungsgemeinschaft grant Ni493/1 and two scholarships of the Studienstiftung des Deutschen Volkes. This work is a contribution to the "European Project for Ice Coring in Antarctica" (EPICA), a joint ESF (European Science Foundation)/EC scientific programme, funded by the European Commission and by national contributions from Belgium, Denmark, France, Germany, Italy, the Netherlands, Norway, Sweden, Switzerland and the United Kingdom. This is EPICA publication no. 55.

References

Arcone, S., D. Lawson, and A. Delaney, Short-pulse wavelet recovery and resolution of dielectric contrasts within englacial and basal ice of Matanuska Glacier, Alaska, U.S.A., *J. Glaciol.*, *41*, 68–86, 1995.

Bogorodsky, V., C. Bentley, and P. Gudmandsen, *Radioglaciology*, D. Reidel Publishing Company, Dordrecht, Holland, 1985.

Corr, H. F. J., A. Jenkins, K. W. Nicholls, and C. S. M. Doake, Precise measurement of changes in ice-shelf thickness by phase-sensitive radar to determine basal melt rates, *Geophys. Res. Letters*, *29*, 73-1–74-4, 2002.

Eisen, O., U. Nixdorf, F. Wilhelms, and H. Miller, Electromagnetic wave speed in polar ice: Validation of the CMP technique with high resolution DEP and γ-density measurements, *Ann. Glac.*, *34*, 150–156, 2002.

Eisen, O., F. Wilhelms, U. Nixdorf, and H. Miller, Identifying isochrones in GPR profiles from DEP-based forward modelling, *Ann. Glac.*, *37, -in press-*, 2003.

Fujita, S., T. Matsuoka, T. Ishida, K. Matsuoka, and S. Mae, A summary of the complex dielectirc permittivity of ice in the megahertz range and its application for radar sounding of polar ice sheets, in *The Physics of Ice Core Records*, edited by T. Hondoh, 1 ed., pp. 185–212, Hokkaido University Press, 2000.

Garotta, R., and D. Michon, Continuous analysis of the velocity function and the move out corrections, *Geophysical Prospecting*, *15*, 584–597, 1967.

Hempel, L., and F. Thyssen, Deep Radio Echo Soundings in the vicinity of GRIP and GISP2

Drill Sites, Greenland, *Polarforschung*, *62*, 11–16, 1992.

Hempel, L., F. Thyssen, N. Gundestrup, H. B. Clausen, and H. Miller, A comparison of radio-echo sounding data and electrical conductivity of the GRIP ice core, *J. Glaciol.*, *46*, 369–374, 2000.

Hildebrand, A., Untersuchung der Laufzeit- und Amplitudenverhalten elektromagnetischer Impulse bei glaziologischen Radarmessungen, Ph.D. thesis, Westfälische Wilhelmsuniversität Münster, 1996.

Hohmann, G. W., Numerical modeling for electromagnetic methods of geophysics, in *Electromagnetic methods in applied geophysics*, edited by M. N. Nabighian, vol. 1 of *Geophysical monograph series*, pp. 313–364, Soc. of Expl. Geophys., 1988.

Kohler, J., J. C. Moore, and E. Isaksson, Comparison of modelled and observed responses of a glacier snowpack to ground-penetrating radar, *Ann. Glac., 37, -in press-*, 2003.

Landau, L. D., and E. M. Lifschitz, *Elektrodynamik der Kontinua*, no. VIII in Lehrbuch der theoretischen Physik, Akademie-Verlag, Berlin, 1982.

Millar, D. H. H., Radio echo layering in polar ice sheets and past volcanic activity, *Nature*, *292*, 441–443, 1981.

Miners, W., A. Hildebrand, S. Gerland, N. Blindow, D. Steinhage, and E. Wolff, Forward Modelling of the Internal Layers in Radio Echo Sounding Using Electrical and Density Measurements from Ice Cores, *J. Phys. Chem. B*, *101*, 6201–6204, 1997.

Miners, W. D., Electromagnetic reflections inside ice sheets, Ph.D. thesis, Open University, 1998.

Moore, J., Dielectric variability of a 130 m Antarctic ice core: implications for radar sounding, *Ann. Glac.*, *11*, 95–99, 1988.

Moore, J., and J. Paren, New technique for dielectric logging of Antarctic ice cores., *Journal de Physique (Colloque C1)*, *48*, 155–160, 1987.

Oerter, H., F. Wilhelms, F. Jung-Rothenhäusler, F. Göktas, H. Miller, W. Graf, and S. Sommer, Accumulation rates in Dronning Maud Land as revealed by dielectrical-profiling measurements at shallow firn cores, *Ann. Glac.*, *30*, 27–34, 2000.

Oswald, G. K. A., and G. d. Q. Robin, Lakes beneath the Antarctic ice sheet, *Nature*, *245*, 251–254, 1973.

Robin, G. d. Q., S. Evans, and J. T. Bailey, Interpretation of radio echo sounding in polar ice sheets, in *Philosophical Transactions of the Royal Society of London*, vol. 146 of *A*, pp. 437–505, Royal Society of London, 1969.

Siegert, M., On the origin, nature and uses of Antarctic ice-sheet radio-echo layering, *Progress in Physical Geography*, *23*, 159–179, 1999.

Taflove, A., *Computational Electrodynamics: The Finite-Difference Time-Domain Method*, Artech House, Boston, 1995.

Wilhelms, F., *Measurement of dielectric properties of polar ice cores (in German)*, vol. 367 of *Berichte zur Polarforschung*, Alfred-Wegener-Institut für Polar- und Meeresforschung, 2000.

Wilhelms, F., J. Kipfstuhl, H. Miller, K. Heinloth, and J. Firestone, Precise dielectric profiling of ice cores: a new device with improved guarding and its theory, *J. Glaciol.*, *44*, 171–174, 1998.

Yee, K. S., Numerical solution of initial boundary value problems involving Maxwell's equations in isotropic media, *IEEE Transactions on Antennas and Propagation*, *14*, 302–307, 1966.

Yilmaz, O., *Seismic data processing*, vol. 2 of *Investig. Geophys.*, Society of Exploration Geophysicist, 1987.

Olaf Eisen, Frank Wilhelms, Uwe Nixdorf, Heinrich Miller, Alfred-Wegener-Institut für Polar- und Meeresforschung, Postfach 120161, 27515 Bremerhaven, Germany. (e-mail: oeisen@awi-bremerhaven.de)

PAPER IV

PAPER IV is the reprint of an article published in Tellus B: complete citation information of the final version of the paper, as published in the print edition of Tellus B, is available on the Blackwell Synergy online delivery service, accessible via the journal's website at
http:www.blackwellpublishing.com/journals/TEB
or
http:www.blackwell-synergy.com

Tellus 55B, 1007–1017, 2003. © *Blackwell Munksgaard 2003*

Alpine Ice Cores and Ground Penetrating Radar: Combined Investigations for Glaciological and Climatic Interpretations of a Cold Alpine Ice Body

Olaf Eisen[1], Uwe Nixdorf[1], Lothar Keck[2], and Dietmar Wagenbach[2]

[1] Alfred-Wegener-Institut für Polar- und Meeresforschung Bremerhaven, Bremerhaven, Germany
[2] Institut für Umweltphysik, Universität Heidelberg, Heidelberg, Germany

Abstract. Accurate interpretation of ice cores as climate archives requires detailed knowledge about their past and present geophysical environment. Different techniques facilitate the determination and reconstruction of glaciological settings surrounding the drilling location. During the ALPCLIM project, two ice cores containing long-term climate information were retrieved from Colle Gnifetti, Swiss-Italian Alps. Here, we investigate the potential of ground penetrating radar (GPR) surveys, in conjuction with ice core data, to obtain information about the internal structure of the cold alpine ice body to improve climatic interpretations. Several drill sites are connected by GPR profiles, running parallel and perpendicular to the flow line, thus yielding a 3D picture of the subsurface and enabling the tracking of internal reflection horizons between the locations. As the observed reflections are of isochronic origin, they permit the transfer of age–depth relations between the ice cores. The accuracy of the GPR results is estimated by comparison of transferred time scales with original core datings, independent information from an older ice core, and, based on glaciological surface data, findings from flow modeling. Our study demonstrates that GPR data is a mandatory tool for alpine ice core studies, as they allow to map major transitions in physical-chemical properties, transfer age–depth relations between sites, complement ambiguous peaks in core records for interpretation, and establish a detailed picture of the flow regime surrounding the climate archive.

1. Introduction

Ice cores from mid-latitude cold glaciers may provide unique records of environmental and climate changes which are important to supplement respective paleo-information commonly retrieved from polar drill sites [*Wagenbach*, 1989]. However, alpine ice core data are much more difficult to interpret in terms of their underlying atmospheric signals than their polar counterparts. Among others, respective shortcomings are basically due to the small areal extent of cold mountain glaciers, i.e. some 100 m or so. This leads to significant changes of the glaciological boundary conditions (i.e. glacier thickness, surface and bedrock topography, firn/ice transition depth and net snow accumulation rate) [*Vincent et al.*, 1997].

In Alpine ice core studies, apart from very exceptional dome drill positions, upstream effects have to be considered carefully to ensure reliable extraction of the net atmospheric change from the isotopic (δ^{18}O, δD) and chemical (aerosol related species, entrapped trace gases) ice core records [*Wagenbach*, 1994]. Inflow of material deposited upstream of the borehole may thus systematically affect the vertical temperature distribution, flow model based dating, the enclosure of trace gases, and, most important, the impurity and isotope depth profile [*Preunkert et al.*, 2000]. Evaluation of such upstream effects needs extensive work including establishment of back trajectories from ice flow modeling along with secondary ice core investigations in the relevant catchment area of the main drill position.

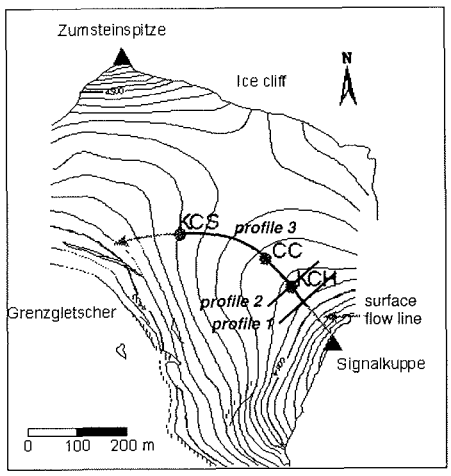

Figure 1. Surface topography of southern Colle Gnifetti flank showing the location of deep ice core positions and GPR profiles 1–3. Contour lines refer to 10 m altitude steps.

In this context, ground penetrating radar (GPR) provides a powerful tool to map the glacier thickness distribution needed for ice flow modeling. As a matter of principle, GPR may be used as well to establish the stratigraphy of internal radar reflection horizons [*Bogorodsky et al.*, 1985], which are expected in favourable cases to indicate isochronic layers. Such GPR based mapping of englacial isochrones may allow to depict the spatial accumulation and vertical strain rates distribution on a quasi-continuous scale. This feature would greatly help to verify the flow regime, encountered upstream effects, and the matching of ice core chronologies obtained in the drill site area of interest. Whereas GPR sounding of glacier thickness is routinely deployed at polar and alpine sites, continuous internal radar reflector mapping has been accomplished so far only on polar and subpolar ice sheets by large scale tracking of (presumably) acidic volcano horizons [e.g. *Millar*, 1981; *Siegert*, 1999; *Hempel et al.*, 2000].

Here we present a GPR study on a cold Alpine glacier saddle (Colle Gnifetti, Swiss-Italian Alps) aimed at prospecting the potential to track englacial reflectors over the relevant drill site area. Colle Gnifetti, which constitutes the key site for long term ice core records from the Alps, has been investigated through several glaciological and ice core drilling projects [*Döscher et al.*, 1995]. Hence, basic information on glacier flow, age–depth relation and vertical distribution of physical and chemical properties has been partially available. With respect to the latter feature almost all mountain drill sites significantly differ from polar ones through the much larger depth fraction made up by porous firn, the prominent occurrence of melt layers (i.e. higher density variability) and the much higher and more variable impurity content. Thus, the study focuses also on some experimental evidence to what extent the interaction of GPR pulses with that alpine feature may provide useful englacial reflection signals.

2. Glaciological and Glacio-Chemical Settings

The Colle Gnifetti forms a small glacier saddle within the summit range of Monte Rosa (Swiss-Italian Alps) where it provides at 4450–4560 m a.s.l. the uppermost accumulation area of Grenzgletscher. Due to a very exposed position, wind erosion controls its net annual snow accumulation which therefore reflects only by some 10% the mean precipitation rate [*Alean et al.*, 1983]. Almost all ice core activities took place in the southern part of the saddle which provides a relatively low annual snow accumulation. Approximately along a common surface flow line of this area, three cores were drilled to bedrock (Figure 1).

In this area, detailed surface velocity and accumulation rate data were obtained from multi-year geodetic observations of a stake array and additional shallow ice core drillings, respectively [*Keck*, 2001; *Lüthi*, 2000]. As shown in Figure 1, the present GPR study was mainly dedicated to the area associated with the three

deep drillings. The typical glaciological parameters encountered in the GPR mapped area are summarised in Table 1.

Ice core chronologies deployed in this study were established by annual layer counting from major ions stratigraphy, which was backed up by absolute time horizons from extreme Saharan dust deposits (1977, 1936, 1902 [*Armbruster*, 2000]) and thermo-nuclear bomb tests (1963). As is the case for all alpine drill sites exposed to strong wind scouring and thus low and irregular snow deposition, dating by annual layer counting and preservation of stratigraphical horizons remains ambiguous at Colle Gnifetti. Furthermore, dating uncertainty increases dramatically with depth due to annual layer thinning and the associated non-linear age–depth relationship.

The chemical composition of Colle Gnifetti ice body may be characterised as follows:

There are highly variable mineral dust levels with a background around 0.55 mg kg^{-1} strongly enhanced on a multi-annual time scale by Saharan dust layers to some 10 mg kg^{-1} [*Wagenbach et al.*, 1996]. Significant inputs of acidity aerosol components (sulphate, nitrate) mainly occurred since 1950 corresponding to about 20 to 40 m depth in the addressed area. During that period mostly annual peaks are seen, exceeding the background of around 140 μg kg^{-1} and 180 μg kg^{-1} for sulphate and nitrate, respectively, by up to a factor of 20 [*Maupetit et al.*, 1995].

In view of strong acidic horizons known to produce GPR reflections, Colle Gnifetti displays high frequency acidic spikes roughly on an annual time scale during the industrial era [*Preunkert et al.*, 2001]. This pattern is, however, strongly disturbed by the distinct but irregular inputs of alkaline dust and the preferential erosion of relatively clean snow of the winter half year. Thus, the chemical stratigraphy of potential acidic layers in the industrial era displays a rather erratic structure with distinct peaks emerging in sub-seasonal to multi-annual sequences.

From the continuous chemical depth profiles available from all three ice cores, we used the following parameters to contrast the chemical stratigraphy with the GPR based reflector pattern:

> Ca^{2+} serving as proxy for the total mineral dust content as controlling the insoluble particulate matter and melt water alkalinity of the ice matrix.
>
> The positive values of the ion balance reduced to (SO_4^{2-}+NO_3^-−Ca^{2+}−NH_4^+) to illustrate the variability of apparent meltwater acidity. Note that negative numbers of this parameter are redundant since they virtually reproduce the pattern of the calcium concentration.

3. The GPR-Method

Ice core records and GPR data provide mutual information on glacial subsurface structure and composition. Whereas ice cores yield vertical profiles of physical features (density, crystal fabric properties, etc.) and chemical impurities in a one-dimensional resolution on a centi- to decimeter depth scale, analyses of GPR data result in two-dimensional pictures of the subsurface structure of the ice body. Although horizontal and vertical changes on the order of meters can be extracted from GPR data, it is in general not possible to unambiguously identify the causes of the obtained structures by this method. The combination of ice core records and GPR data may thus help to extrapolate ice core information along GPR profiles, resulting in a two-dimensional picture of the physical and chemical properties of the subsurfaces, which is limited, however, by the lateral coherency of the observed signal and the depth resolution of the GPR data.

To determine the internal structure of a glacier, tracking of continuous internal reflectors is required. In general, an electromagnetic (EM) pulse is transmitted at the surface and the propagating wave is partially reflected

Table 1. Basic glaciological parameters observed along a flow line at Colle Gnifetti.

characteristic	description & reference
snow zone characterisation	cold infiltration-recrystallisation zone, associated with occasional melt-layer formation at a downslope decreasing rate [after *Shumskii*, 1964]
englacial temperature	18 m firn temperature $-14,3$°C [*Suter*, 2002] basal temperature $-12,3$°C [*Haeberli and Funk*, 1991]
glacier thickness	systematically decreasing from about 140 m in the lower to ~50 m in the upper area [this study; *Haeberli and Funk*, 1991; *Lüthi*, 2000]
annual snow accumulation	systematically decreasing from around 60 cm water equivalent (WE) at KCS borehole to 20 cm WE at the upper KCH positions [*Keck*, 2001]
horizontal surface velocity	systematically decreasing from 2 ma^{-1} in the lower area to less than 1 ma^{-1} in the upper area [*Lüthi*, 2000]
firn–ice transition depth	around 45 m and 36 m at the KCS and KCH borehole position, respectively [*Keck*, 2001]

at discontinuities of the dielectric properties of a medium, i.e. permittivity and conductivity [*Robin et al.*, 1969; *Bogorodsky et al.*, 1985], and the reflected signals are recorded at the surface as a function of two-way traveltime (TWT). The resulting picture of the subsurface is referred to as the time domain radargram.

In a cold alpine ice body, discontinuities of the dielectric constant are expected to be mainly related to ice layers (i.e. rapid changes of density within the firn), but also outstanding impurity horizons have to be considered (e.g. acidic spikes). The processes forming the EM reflector take place at the glaciers surface at approximately the same time. Interaction of surface accumulation and flow field determine the submergence rate of an isochronic surface. It is therefore reasonable to assume that internal reflectors are isochrones.

Two types of measurement are common in GPR data acquisition: common-offset (CO) and common-midpoint (CMP) surveys. For CO surveys, transmitter (TX) and receiver (RX) are kept at a fixed distance and moved across the surface. For the CMP recording technique, the distance between TX and RX is symmetrically increased relative to the stationary center point, basically yielding information about the velocity–depth profile. This method is a standard tool in seismic data acquisition [*Garotta and Michon*, 1967; *Yilmaz*, 1987], and has also been applied successfully in modified versions to glaciological GPR surveys [*Gudmandsen*, 1971; *Hempel et al.*, 2000; *Murray et al.*, 2000].

3.1. Data Acquisition

Radar measurements were performed with a commercial RAMAC GPR set of the Swedish company Malå Geoscience, a monopulse bistatic radar system that can be operated with antennae of different frequencies. CO measurements were carried out with shielded 250 MHz antennae, which are permanently mounted in a sled box at a fixed distance of 36 cm. The common-midpoint survey was carried out with

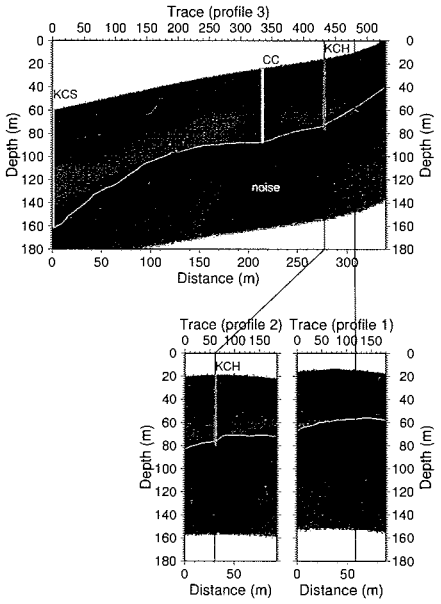

Figure 2. Surface and bedrock topography (light grey) in meters below 4500 m a.s.l. along profiles 1–3. Location and extent of the KCS, CC, and KCH boreholes are shown as vertical bars, crossover points of profiles are shown as thin black lines. The bedrock depths were determined by strongly enlarging the processed data and applying a colour amplitude scaling. The grayscale indicates the trace envelope, i.e. signal magnitude, instead of the trace amplitude. The noise centered at 220 m upslope of KCS (approximately near CC) probably results from scattered metal remains buried underneath the surface, their fan-like structure is due to migration processing.

a pair of unshielded antennae operating at a center frequency of 100 MHz. For either system setup the TX and RX are connected with the central processing unit via light conducting cables, thus avoiding noise from ohmic conductors. The processing unit was operated by a Husky FC PX5 personal computer, using the GPR system software.

Three CO profiles were measured along the three profile lines 1–3 (Figure 1), which were already marked with geodetic stakes. The transmitter was triggered by a distance wheel, mounted at the rear of the sled box, and set to a trigger interval of 0.5 m. Trace length was 1.5 μs with 2048 samples per trace. To increase the signal-to-noise ratio 32-fold vertical stacking was applied for each stored trace.

For the CMP survey, the KCH borehole was chosen as the center point, and TX–RX offset was increased along profile 2, perpendicular to the flow line. Traces were recorded in a 1.5 μs time window with 2048 samples and 256-fold vertical stacking, manually triggered in 1 m increments in the interval 1 to 100 m.

3.2. Post-recording processing

Processing was performed using Paradigm Geophysical FOCUS version 4.2 software. Standard post-recording processing features for CMP and CO radio-echo sounding data include filtering and gain correction. CMP data are then analyzed in the time domain, resulting in a TWT–depth model. The major processing steps for CO surveys are migration and TWT–depth conversion, each requiring a profile of propagation velocity.

In the present study it was not feasable to apply post-recording horizontal stacking of neighbouring traces, usually used to decrease noise, because of the steep internal and bottom features. Although stacking was successful in the upper few meters, the coherency of internal reflectors at greater depth decreased, thus making it more difficult to track continuous internal reflections. For further processing, the data were therefore only bandpass filtered, and the recording position (accurate to $\sim$1%) assigned to each trace. Based on the comparison of TWT–depth profiles derived from the CMP survey and ice core data, discussed below, migration of the CO profiles and conversion to depth domain was carried out using the TWT–depth model determined from the ice core density profiles. The same CO processing sequence

was applied to all three CO profiles, resulting in a picture of the subsurface and bedrock structure (Figure 2).

4. GPR and Ice Cores

An essential aim of our study is to investigate the possibility to transfer age–depth relations from one ice core to another using GPR data by analysing the structure of internal reflections. Before linking radargrams to ice core records, we perform two comparisons to estimate errors of either data set and to limit the effect of ambiguities arising in the traveltime versus depth profiles and ice thickness results.

4.1. Traveltime–depth profiles

Apart from CMP surveys, EM propagation velocities can also be derived from ice core records, e.g. dielectric profiling (DEP) [*Moore and Paren*, 1987; *Wilhelms*, 2000] or density [*Looyenga*, 1965; *Robin et al.*, 1969]. Using the KCS and KCH density profiles, we apply the *Looyenga* [1965] mixture model for calculating two interval velocity–depth profiles. The CMP velocity model at KCH is based on the analysis of five internal and one bottom reflector.

Interval velocities are systematically higher for the CMP than for the density derived profile (Figure 3 (a)). This leads to ~10% larger depth of the CMP model for the same TWT compared to the density based model (Figure 3 (b)). Reasons for the systematic differences of both data sets are investigated in the discussion. As wave speed profiles derived from different physical properties of ice cores are more consistent than those based on CMP surveys [*Eisen et al.*, 2002], we use the TWT–depth relations from KCS and KCH for migration and conversion of the radargrams to the depth domain.

4.2. Bedrock topography

In theory, the depth of a perfect plane reflector should be identifiable within a quarter of the wavelengths, i.e. 0.2 m and 0.4 m for the 250 MHz and 100 MHz antennae, respectively. However, the rough nature of the bed, a non-planar curvature, and uncertainties in the velocity–depth distribution decrease the accuracy with which the bed topography can be determined. The bedrock topography can be extracted from high resolution CO profiles (Figure 2), and for KCH also from the CMP data (Figure 3). Especially in those parts of the CO profiles with steep bedrock topography the bed reflection is brouille, and can only be determined with an accuracy of approximately ± 5 m. In the other parts it is clearly identifiable to within 2 m. Ice thickness derived from CO data is 102 m ± 5 m at KCS, and 58 m ± 5 m at KCH (Table 2). The depths at the crossing points of surveys are within 4 m of each other. The ice thickness derived from the CMP measurements at KCH is 60 m ± 2 m.

Additional information on ice thickness is available from earlier GPR surveys [*Wagner*, 1996; *Lüthi*, 2000] and borehole depths. Drilling was stopped when the amount of debris in the retrieved ice core increased, indicating that the basal layer was reached. Logged depths at KCS and KCH in 1995 are 101 and 61 m, respectively [*Lüthi*, 2000]. Based on this data and flow modeling for conversion to the 2000 surface, the KCS and KCH borehole bottoms should be located at depths of 101.3 and 61.7 m, respectively (Table 2).

4.3. Internal structure and ice core profiles

A straight forward apportionment of individual internal reflectors to outstanding physical or chemical events seen in the ice cores is not feasible. This may have been expected in view of the uncertainty in the individual absolute depth scales but also in view of the relatively high frequency with which the potentially radar active features like acid spikes, melt layers etc. occur in alpine ice cores. Nevertheless, the matching of ice core records via GPR profiles can be achieved.

The drilling locations KCH and KCS are connected via GPR profile 3 (Figure 4). To

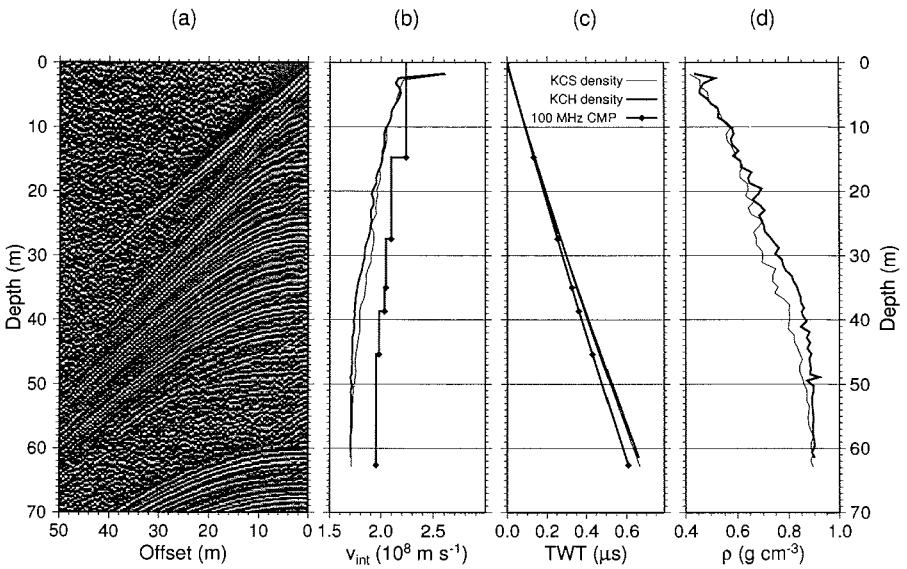

Figure 3. Comparison of ice core density and common-midpoint (CMP) based profiles at KCH drill site position: (a) 100 MHz CMP radargram; (b) depth profile of interval velocity v_{int}; (c) depth profile of two-way traveltime; (d) depth profile of smoothed density ρ.

Table 2. Comparison of ice core and GPR based data on ice thicknesses at Colle Gnifetti.

Data Set	KCS	KCH	$X_{1,3}$	Remarks
Borehole Data and Flow Modeling				
core length	99.9	60.3	···	core top ~0.6 m below surface
logged depth	101	61	···	after drilling [*Lüthi*, 2000, p. 40]
bottom depth	101.3	61.7	···	flow modeling [*Keck*, 2001]
GPR Ice Thickness				
CMP	···	60 [2]	···	
Profile 1	···	···	42 [2]	
Profile 2	···	58 [2]	···	
Profile 3	102 [5]	58 [5]	46 [5]	

Core and GPR depths are given in meters with respect to the 2000 surface. Accuracy of GPR ice thickness values in parantheses. $X_{1,3}$ denotes the crossover point of profiles 1 and 3.

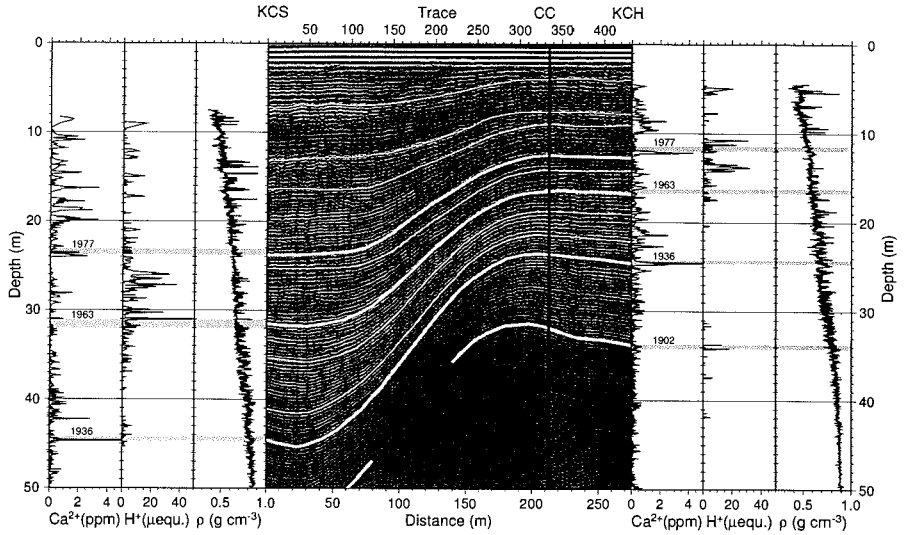

Figure 4. Comparison of ice core profiles from KCS (left), KCH (right), with internal GPR reflectors along connecting profile 3 (middle). Recorded are calcium, serving as proxy for the total mineral dust content, ice acidity, and high resolution densities, indicating the melt layer stratigraphy. Horizontal grey lines overlying the ice core records mark the depth of the 1902, 1936, 1963, and 1977 dating horizons. Thick white lines in the radargram indicate the depth of the dating horizons determined from tracking coherent phases starting from KCS, thin white lines mark strong continuous reflectors (see text for details). The line corresponding to the 1902 horizon is interrupted because of the reflector discontinuity.

Table 3. Comparison of age–depth relation at borehole locations from ice core and GPR data.

Time	Event	KCS		KCH	
		core	GPR	core	GPR
1977	dust	23.2–23.7	23.7	11.5–11.9	12.9
1963	Tritium	31.1–31.9	31.1	16.3–16.6	17.4
1936	dust	44.2–44.6	44.5	24.3–24.5	25.3
1902	dust	55.5–55.8	...	33.8–34.1	...

Ice core data are taken from *Armbruster* [2000] and converted to depth below the 2000 surface using accumulation measurements and flow modeling [*Keck*, 2001]. The depth of individual GPR reflector phases at KCH was determined as described in the text (compare Figure 4).

determine the accuracy of a time scale transfer from one core to another, we (i) associate absolut time horizons at KCS to strong corresponding phases of an internal reflector at the same depths; (ii) track and mark continuous coherent phases from KCS to KCH in a large scale, high resolution plot of the radargram; and (iii) compare the transferred age–depth relation to the chronology of KCH.

The transmitted radar pulse consists of approximately five half cycles, with the main energy being located in the first three ones. During propagation, the pulse is subject to phase shifts, distortions, and multiple reflections. In the recorded radargram, an internal reflector therefore does not consist of a single maximum peak, but of several phases. In the migrated depth domain radargram, each phase is then of the order of $\lambda/2$ (0.4 m in ice), and a sharp reflector is distributed over a depth range of approximately 2λ (1.6 m in ice).

The radargram shows a smooth steplike slope in the internal structure between KCS and KCH (Figure 4), steepening with depth, which is related to bedrock topography (Figure 2) as well as systematically varying submergence velocities [*Keck*, 2001]. About 100 m upslope of KCS, in the steepest part of the internal slope, the reflectors become discontinuous below a depth of 35 m.

Starting the tracking of internal horizons at KCS yields an higher accuracy, as the annual layer thickness, and therefore temporal resolution, is almost twice as large as at KCH. Tracking the reflectors corresponding to the 1936, 1963 and 1977 data from KCS to KCH results in depths that are about 0.8–1.0 m lower than the respective data in the KCH ice core profiles (Table 3). The last continuous reflector corresponds to about 1930. Older dating horizon, especially the 1902 event, cannot be used for tracking without significantly decreasing the accuracy because of discontinuities of the GPR horizons.

In addition to the calibrating horizons, we also tracked several other strong continuous internal reflections from KCS to KCH. Although some horizons seem to be linked to similar characteristic peak patterns in the ice core records, it is not possible to clearly identify the causes of prominent reflections from comparison with ice core records alone (see discussion in chapter 5).

4.4. Application of the age–depth relationship

The age–depth relation derived above uses information from KCS and KCH. Additional estimates for the accuracy of the lateral transfer of the age–depth information can be performed with independent information available from the CC ice core, e.g. by comparing modeled burial depth since core retrieval with depths derived from fastening the dated CC records to the KCS/KCH age–depth profiles.

The 1977 calibration signal is located 1.6–2.1 m below top edge of the CC core, the 1902 signal at 26.3–26.5 m. According to accumulation measurements and flow modeling results, the 1977 signal submerged to a depth range of 11.0–11.2 m below the 2000 surface, the 1902 signal to 30.5–30.6 m. Using the KCS/KCH/GPR age–depth relation, the lower limit of 1977 is 12.8 m (Figure 4), and, accounting for the systematic error of 1 m, the upper limit is 11.8 m. As the 1902 horizon is discontinous for some 50 m, we cannot use it for tracking from KCS, nevertheless from KCH. The 1902 depth at CC in 2000 results as 31.8 m. The resulting error interval (5–15%) is mainly made up by the uncertainties of the age–depth scenario (~1 m) and the uncertainty in the absolut depth scale arising from the non-consolidated upper core sections, which required to connect the top core to the actual surface at time of drilling via snow pit sampling.

5. Discussion

The EM propagation velocities are one of the key properties to derive a true picture of the subsurface structure from GPR surveys. Comparison of velocity–depth profiles derived from CMP survey data and ice core properties from polar regions show that the agreement in a flat area can be within a couple of percent [*Eisen et al.*, 2002]. The larger discrepancies in our case being on the order of 10% are probably related to the dipping of internal reflectors with respect to the surface and a curved ray path, which is neglected in the small spread approximation used here [*Yilmaz*, 1987].

Likewise, the inclination between surface and bedrock is probably the reason why the ice thicknesses determined at KCH is systematically smaller than borehole depth and core length. The 2D migration performed during post-processing only corrects the dipping component which is parallel to the profile. As the subsurface and bedrock gradients are non-parallel to the profile lines in our case (Figure 2) (i.e. out-of-plane) the bedrock dipping of around 7 degrees at KCH for profiles 2 and 3 relative to the surface implies that the depth is some 1.5% larger. To further improve the accuracy of the subsurface image, 3D survey setup and migration processing would be necessary, requiring, however, an extensive logistical and temporal effort during data acquisition [*Moran et al.*, 2000].

Another issue to be considered when comparing GPR ice thicknesses is the nature of the bottom reflector. If crystalline rock is in direct contact with the glacier bottom, a sharp reflection could be expected. However, if a sedimentary layer is present, the reflected echo becomes diffuse, thus increasing the error for ice thickness values. In our case, the bottom few metres of the ice cores all show entrainment of debris, but only at cores CC and KCS the silty layer forming the ice bedrock interface was penetrated. We may thus argue that the ice thickness from KCH borehole logging is underestimated by some 10 cm relative to CC and KCS cores. The silty layer of unknown depth indeed add to the uncertainty in the GPR ice thickness in comparison to borehole depths.

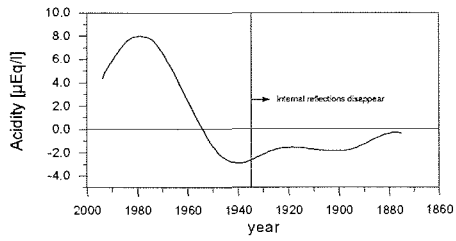

Figure 5. General acidity trend analysed in the CC Colle Gnifetti ice core by direct measurements and ion balance evaluations. Outliers related to extreme saharan dust deposits were removed prior to SSA smothing. The vertical line at 1935 marks the approximate transition from continuous to discontinuous and finally disappearing internal GPR reflections.

The internal structures of our radargrams are partially linked to ice thickness. This can be expected, as accumulation and flow field determine the submergence velocity, and thus the position of isochronic reflectors. Deep internal reflections towards KCS dissapear, as the main flow channel of Colle Gnifetti is entered (for a radar cross section of Colle Gnifetti see *Lüthi* [2000], Figure A.4). The matching of the age–depth profiles in the upper tens of meters between KCS and KCH by tracking internal reflections is encouraging. Errors are of the order of a wavelength, corresponding to a few years in the depth range under consideration.

Several features make it more diffcult to extend the transfer to larger depths: the signal-to-noise ratio decreases in the vicinity of boreholes, probably because of the disturbed firn and ice structure, making it more difficult to separate internal reflections from noise; the internal reflectors become more discontinuous with depth, especially in parts of larger inclination between reflector and surface; below approximately 25 m at KCS and 45 m at KCH, no continuous internal reflections are detected. Either too much energy is absorbed during propagation below this level to detect a distinct return signal at the surface, or the ice properties change.

The latter case is unlikely in the sense that flow features become irregular and disturb layering, as this would contradict age–depth relations established by *Armbruster* [2000] and *Keck* [2001] down to 40 and 70 m depth, respectively. However, physical and chemical properties show important transitions around these depths. Here, density reaches the value of glacier ice and melt layers are not outstanding anymore. Disregarding outstanding mineral dust layers, the ice matrix chemistry changes from acidic to slightly alkaline properties due to much smaller emissions prior to 1950 (Figure 5). Thus distinct acidic peaks can hardly be found below the critical depths. In general, decreasing variations in density would allow chemical horizons to become the primary reflection mechanism, but as both observed chemical and physical features reduce the overall reflection coefficient of distinct layers, the amount of energy reflected to the surface decreases as well.

To clearly identify the reason for missing reflectors in the lower part of the ice and to increase the accuracy of the age–depth transfer, the origin and structure of dominant reflectors has to be pinned down. Separating the effects of changes in density and chemical composition, as well as determining the influence of variations of layer thickness on the recorded signal, could best be achieved by forward modeling of radargrams, based on DEP data [*Eisen et al.*, 2003]. Unfortunately, no DEP measurements were carried out after retrieving the ice cores.

An illustrative example is the vanishing of weaker phases when tracking horizons from KCS to KCH. As layer thickness decreases by roughly 50% towards KCH, it can be expected that the characteristics of internal reflectors change as well. This has the important consequence that individual phases do not indicate isochronous surfaces. A bulk of phases, however, forming a distinguishable internal reflector, can be considered to correspond to a layer of distinct physical properties, extending over a small depth range, and thus being approximately isochronuous.

6. Conclusions

Internal reflections measured with GPR can be used to match and transfer age-depth relations of ice cores in cold alpine ice bodies over distances of at least several hundred meters. Successful application of GPR data requires, however, a rather smooth flow regime, the presence of strong continuous internal reflectors, and a GPR system capable to record weak reflections at high depth resolution. The GPR device should combine a powerful transmitter pulse with sub-meter resolution and large transmitter/receiver antenna gain. Given that GPR uncertainty is sufficently small, ice core interpretations profit from GPR surveys in several ways: age-depth relation can be transferred from one site to another; interpretation of ambigous peaks in core records can be complemented by matching clear signals from other cores via interal horizons; major transitions in physical-chemical properties can be remotely detected and continuously tracked to other parts of the region of interest; the combination of surface measurements of ice velocity, modeling, and reflection horizons at various depths provide a detailed picture of the 3D flow regime. Analyses of GPR surveys thus may help to assess upstream flow effects associated with strong longitudinal changes in the submergence velocity.

Despite the success of our study in the upper 30 to 50 m of the ice column at Colle Gnifetti, it fails to supplement the ice core age-depth relations and map the isochrone pattern at larger depth. Future radar activities at this site should therefore focus on the basal regime, being supported by high resolution DEP if new ice cores are being retrieved. Power limitations can partly be overcome by decreasing the antennae frequency to 100 MHz using the same GPR system, assuring lower absorption, sufficient resolution with a wavelength of 1.7 m, and still managable operation. Remaining limitations are set by the absorption properties of ice and the working conditions at this high altitude site.

Although the main reason for the limited sensitivity of the GPR data as well as the major ice properties leading to the observed GPR reflectors could not be unambiguously identified, yet a more clear prospect on dedicated GPR applications at cold mountain glacier could be given. The glaciological characteristics of other cold alpine drill sites, e.g. in the Andes, Himalayan, or north-west Canada, are not substantially different from Colle Gnifetti regarding geometry, firn fraction, melt layer occurence or mass balance. In this respect, they are expected to provide quite similar results in such GPR studies. On the other hand, (sub)tropical sites, which may experience much higher mineral dust but lower (anthropogenic) acid inputs may respond to potential acidic reflectors different to what is seen at Colle Gnifetti.

Acknowledgments. We are grateful for the invaluable logistic support by Air Zermatt and the staff of Cabanna Regina Margherita from the Club Alpino Italiano di Varallo. Field work profited from advice and assisstance by Stephan Sutter, support from Guðfinna Tolly Aðalgeirsdottir greatly sped up field measurements. The research was partially supported by the European Union Environment and Climate Programme under contract ENV4-CT97-0639 (ALPCLIM).

References

Alean, J., W. Haeberli, and B. Schädler, Snow accumulation, firn temperature and solar radiation in the area of the Colle Gnifetti core drilling site (Monte Rosa, Swiss Alps): distribution patterns and interrelationships, *Z. Gletscherkd. Glazialgeol.*, *19*, 131–147, 1983.

Armbruster, M., Stratigraphical dating of high-alpine ice cores over the last 1000 years (in German), Ph.D. thesis, Ruprecht-Karls-Universität Heidelberg, Germany, http://archiv.ub.uni-heidelberg.de, 2000.

Bogorodsky, V., C. Bentley, and P. Gudmandsen, *Radioglaciology*, D. Reidel Publishing Company, Dordrecht, Holland, 1985.

Döscher, A., H. Gäggeler, U. Schotterer, and M. Schwikowski, A 130 years deposition record

of sulfate and cloride from a high-alpine glacier, *Water, Air, and Soil Pollution, 85(2)*, 603–609, 1995.

Eisen, O., U. Nixdorf, F. Wilhelms, and H. Miller, Electromagnetic wave speed in polar ice: Validation of the CMP technique with high resolution DEP and γ-density measurements, *Ann. Glac., 34*, 150–156, 2002.

Eisen, O., F. Wilhelms, U. Nixdorf, and H. Miller, Identifying isochrones in GPR profiles from DEP-based forward modelling, *Ann. Glac., 37, -in press-*, 2003.

Garotta, R., and D. Michon, Continuous analysis of the velocity function and the move out corrections, *Geophysical Prospecting, 15*, 584–597, 1967.

Gudmandsen, P., Electromagnetic Probing of Ice, in *Electromagnetic Probing in Geophysics*, edited by J. Wait, pp. 321–348, Golem Press, 1971.

Haeberli, W., and M. Funk, Borehole temperatures at the Colle Gnifetti core-drilling site (Monte Rosa, Swiss Alps), *J. Glaciol., 37*, 37–46, 1991.

Hempel, L., F. Thyssen, N. Gundestrup, H. B. Clausen, and H. Miller, A comparison of radio-echo sounding data and electrical conductivity of the GRIP ice core, *J. Glaciol., 46*, 369–374, 2000.

Keck, L., Climate significance of stable isotope records from Alpine ice cores, Ph.D. thesis, Ruprecht-Karls-Universität Heidelberg, Germany, http://archiv.ub.uni-heidelberg.de, 2001.

Looyenga, H., Dielectric constant of heterogeneous mixtures, *Physica, 31*, 401–406, 1965.

Lüthi, M. P., *Rheology of cold firn and dynamics of a polythermal ice stream*, vol. 165 of *Mitteilungen*, Versuchsanstalt für Wasserbau, Hydrologie und Glaziologie der ETH Zürich, 2000.

Maupetit, F., D. Wagenbach, P. Weddeling, and R. Delmas, Recent chemical and isotopic properties of high altitude cold Alpine glaciers, *Atmos. Environ., 29*, 1–9, 1995.

Millar, D. H. H., Radio echo layering in polar ice sheets and past volcanic activity, *Nature, 292*, 441–443, 1981.

Moore, J., and J. Paren, New technique for dielectric logging of Antarctic ice cores., *Journal de Physique (Colloque C1), 48*, 155–160, 1987.

Moran, M. L., R. J. Greenfield, S. A. Arcone, and A. J. Delaney, Delineation of a complexly dipping temperate glacier bed using short-pulse radar arrays, *J. Glaciol., 46*, 274–286, 2000.

Murray, T., G. W. Stuart, P. J. Miller, J. Woodward, A. M. Smith, P. R. Porter, and H. Jiskoot, Glacier surge propagation by thermal evolution at the bed, *J. Geophys. Res., 105*, 13,491–13,507, 2000.

Preunkert, S., D. Wagenbach, M. Legrand, and C. Vincent, Col du Dme (Mt. Blanc Massif, French Alps) suitability for ice cores studies in relation with past atmospheric over Europe, *Tellus, 52B*, 993–1012, 2000.

Preunkert, S., M. Legrand, and D. Wagenbach, Sulfate Trends in a Col du Dôme (French Alps) Ice Core: A Record of Anthropogenic Sulfate Levels in the European Mid-Troposphere over the 20th Century, *J. Geophys. Res., 106*, 31,991–32,004, 2001.

Robin, G. d. Q., S. Evans, and J. T. Bailey, Interpretation of radio echo sounding in polar ice sheets, in *Philosophical Transactions of the Royal Society of London*, vol. 146 of *A*, pp. 437–505, Royal Society of London, 1969.

Shumskii, P. A., *Principles of structural glaciology: the petrography of fresh-water ice as a method of glaciological investigation*, Dover Publications Inc., New York, 1964.

Siegert, M., On the origin, nature and uses of Antarctic ice-sheet radio-echo layering, *Progress in Physical Geography, 23*, 159–179, 1999.

Suter, S., *Cold firn and ice in the Monte Rosa and Mont Blanc areas: spatial occurrence, surface energy balance and climatic evidence*, vol. 172 of *Mitteilungen*, Versuchsanstalt für Wasserbau, Hydrologie und Glaziologie der ETH Zürich, 2002.

Vincent, C., M. Vallon, F. Pinglot, M. Funk, and L. Reynaud, Snow accumulation and ice flow at Dôme du Goûter (4300 m), Mont Blanc, French Alps, *J. Glaciol., 43*, 513–521, 1997.

Wagenbach, D., Environmental records in alpine glaciers, in *The environmental record in glaciers and ice sheets*, pp. 69–83, Dahlem Konferenzen, John Wiley and Sons, Chichester, 1989.

Wagenbach, D., Special problems of mid latitude glacier ice core research, in *Greenhouse gases,*

isotopes and trace elements in glaciers as climatic evidence for the Holocene, pp. 10–14, Report of the ESF/EPC Workshop, Zürich, 27-28 October 1992, Arbeitsheft No 14, VAW-ETH Zürich, Switzerland, 1994.

Wagenbach, D., S. Preunkert, J. Schäfer, and W. Jung, Northward Transport of Saharan Dust Recorded in a Deep Alpine Ice Core, in *The Impact of African Dust Across the Mediterranean*, pp. 291–300, Kluwer Academic Publishers, 1996.

Wagner, S., *Three-dimensional modeling of two glaciers and deformation analysis of ice-rich permafrost (in German)*, vol. 146 of *Mitteilungen*, Versuchsanstalt für Wasserbau, Hydrologie und Glaziologie der ETH Zürich, 1996.

Wilhelms, F., *Measurement of dielectric properties of polar ice cores (in German)*, vol. 367 of *Berichte zur Polarforschung*, Alfred-Wegener-Institut für Polar- und Meeresforschung, 2000.

Yilmaz, O., *Seismic data processing*, vol. 2 of *Investig. Geophys.*, Society of Exploration Geophysicist, 1987.

Olaf Eisen, Alfred-Wegener-Institut für Polar- und Meeresforschung, Postfach 120161, 27515 Bremerhaven, Germany. (e-mail: oeisen@awi-bremerhaven.de)

PAPER V

PAPER V is in review at the Journal of Geophysical Research – Solid Earth

Radar reflection characteristics and ice core synchronization: advantages of combined analyses of survey and synthetic radar data

Olaf Eisen, Uwe Nixdorf, Frank Wilhelms, and Heinrich Miller

Alfred-Wegener-Institut für Polar- und Meeresforschung Bremerhaven, Bremerhaven, Germany

Abstract. Ice core records and ice penetrating radar data contain mutual information on glacial subsurface structure and composition, providing various opportunities for interpreting past and present environmental conditions. To exploit the full range of possible applications, accurate dating of internal radar reflection horizons (IRHs) and knowledge about the constituting features is required. With records of three ice cores from Dronning Maud Land (DML), Antarctica, surface-based radar profiles connecting the drilling locations, and the successful reproduction of measured radar data by forward modeling of electromagnetic wave propagation, we investigate the accuracies involved in transferring age–depth relationships obtained from ice cores to continuous radar reflections. Three specific questions are considered: How accurate can we date IRHs between ice cores? Is it possible to unambiguously identify the origin depth of reflections? Which concept minimizes errors involved in ice core synchronization and extrapolation of prominent features along IRHs? To this end we use various methods, including conventional geophysical techniques to connect radar data and subsurface features, but also perform novel sensitivity studies with altered ice core records to reveal characteristic composition of individual radar reflections. For our radar operations at 200 and 250 MHz in the upper 100 m of the ice sheet, comprising some 1000–1500 years of deposition history, dating and synchronization errors are 8 a in favourable cases and 19 a at the limit of feasibility. About one third of the uncertainty is associated with the initial ice core dating, the remaining part to radar data quality and analysis. In addition to the immediate significance of our results to experiments related to the ongoing deep drilling in DML, we consider this study to provide a roadmap for future studies on the origin, characteristic, and interpretation of radar reflections, especially also in respect to deeper parts of the ice sheets.

Introduction

Interpretation of ice cores as paleoclimate archives requires detailed knowledge about their past and present geophysical environment. Different techniques have been developed that facilitate the determination of the present state as well as the reconstruction of past glaciological settings surrounding the drilling locations, but the raising number of deep ice cores being retrieved in Antarctica and Greenland yielding high quality records comes along with an increasing demand for ice core synchronization, improved numerical ice sheet modeling, and extended surface observations.

In this context, ice penetrating radar (IPR) provides a powerful tool to investigate properties of glaciers and ice sheets, having lead to its widespread application in glaciology. Studies of dielectric properties of ice and internal radar reflection horizons (IRHs) suggested for long that most processes forming electromagnetic reflectors take place at the glaciers surface at approximately the same time, with the submergence rate of the isochronic surface being determined by interaction of the flow field and surface accumulation [*Robin et al.*, 1969; *Gudmandsen*, 1975; *Clough*, 1977; *Millar*, 1981; *Bogorodsky et al.*, 1985; *Moore*, 1988]. In general,

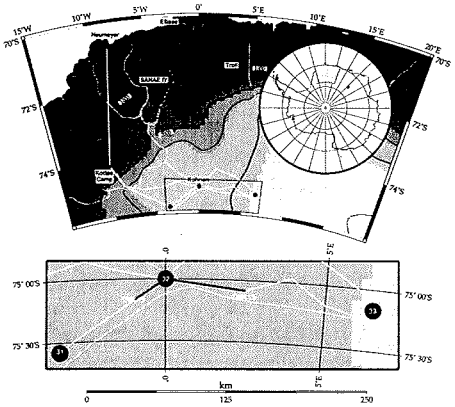

Figure 1. Location map of study area in DML, showing ice core drill sites (B31-33), summer camps, and research stations. Thick white lines are traverse surface-based radar profiles, thin white lines are major ice divides. The upper right inset shows the location of DML on the Antarctic continent, the lower inset indicates the IPR profiles from DML19 to B32 at DML05 in 2000/01 and from DML05 to DML15 1998/99 (black), shown in Figure 5.

the reflection of electromagnetic waves occurs where the complex dielectric constant changes. Discontinuities in the real part, the permittivity, are basically related to density and dominate reflections in the upper hundreds of meters. Variations in the imaginary part, proportional to conductivity and related to acidity, are the governing cause in deeper regions of the ice. A third mechanism, proposed by *Harrison* [1973], involves dielectric anisotropy of the crystal fabric, but its significance is still heavily discussed.

The main application of IPR in polar environments has been ice thickness probing in relation to ice core deep drilling projects [*Hempel and Thyssen*, 1992; *Dahl-Jensen et al.*, 1997; *Nixdorf and Göktaş*, 2001; *Steinhage et al.*, 1999; *Kanagaratma et al.*, 2001, among others]. As a matter of principle, IPR is used as well to establish the stratigraphy of IRHs, and thus isochronic layers. Such IPR-based mapping of englacial isochrones on a quasi-continuous scale may allow to match ice core records [*Siegert et al.*, 1998; *Jacobel and Hodge*, 1995], depict vertical strain rates [*Jacobel et al.*, 1993; *Raymond et al.*, 1995; *Hodgkins et al.*, 2000], reconstruct snow and firn genesis [*Frezzotti et al.*, 2002], determine spatial distributions of accumulation [*Richardson-Näslund and Holmlund*, 1999; *Nereson and Raymond*, 2001], and validate numerical ice sheet models [*Huybrechts et al.*, 2000; *Baldwin et al.*, 2003].

The importance of accurate interpretations of IRHs for these applications in terms of the underlying physical processes and the possibility to determine physical properties along ice cores have motivated for some time several studies on forward modeling of radar data, which in principle provide the best means to directly investigate reflection mechanisms [e.g. *Moore*, 1988; *Blindow*, 1994; *Miners et al.*, 1997]. The distribution of the dielectric constant with depth can be derived from dielectric profiling (DEP) [*Moore and Paren*, 1987], the direct current conductivity can be determined from electric conductivity measurements (ECM) [*Hammer*, 1980]. Mainly because of shortcomings of ice core data and computational resources earlier forward modeling approaches were only of minor success. The development of an improved calibrated DEP device for simultaneous measurements of the real and imaginary part of the complex dielectric constant [*Wilhelms*, 2000] provides the basis for recent advances of modeling results [*Kohler et al.*, 2003; *Eisen et al.*, 2003b]. By combining high resolution DEP data with multi-dimensional finite-difference (FD) numerical modeling techniques *Eisen et al.* [2003c] demonstrated that reproduction of surveyed radar data can be achieved to a considerable degree.

Based on their approach this study aims at evaluation of IRH analysis techniques. Datings of ice cores, obtained from annual layer counting or wiggle matching, are usually transferred to IRHs by mere comparison or correlation techniques. Although the connection of

volcanic events with deeper IRHs might be unambiguous in special cases [*Hempel et al.*, 2000], the grade of uncertainty depends in general on location, considered depth range, and IPR system properties. To improve quantitative interpretation and utilization of isochrones we examine which error is related to conventional IRH dating, how accurate the synchronization of ice cores and the extrapolation of ice core properties along IRHs can be performed, and if the combination of ice core dating and forward modeling of radar data provides advantages to conventional techniques.

We first present the used data sets, obtained during several EPICA pre-site surveys in Dronning Maud Land (DML), Antarctica, which comprise DEP records from three shallow ice cores and an extensive set of surface-based radar surveys (Figure 1). In the second part of this paper we introduce the numerical FD forward modeling technique in respect to radar reflection origin and characteristics and perform comparison of surveyed and synthetic radar data. Finally, we join the different data sets and techniques to investigate and answer the main questions in the third part.

Data Base

This study makes use of two data sets. One is based on dielectric profiling of ice cores, the other on surface-based ice penetrating radar surveys. Although both methods depend on the dielectric properties of the ice column, they are independent in the sense that they are autonomous and represent different pictures of the subsurface, as introduced in this section.

Ice core DEP data

The complex relative dielectric constant of snow and ice can be written as

$$\varepsilon = \varepsilon' - i\varepsilon'' = \varepsilon' - i\frac{\sigma}{\varepsilon_0\omega} = |\varepsilon|e^{-i\delta}, \quad (1)$$

where the real part ε' is the ordinary relative permittivity and the imaginary part ε'' is the dielectric loss factor of the medium. The latter can be expressed as a function of conductivity σ, angular frequency ω, and the permittivity of vacuum ε_0. The last expression defines the loss tangent, $\tan\delta = \varepsilon''/\varepsilon'$. The electromagnetic wave speed in snow and ice is related to the dielectric constant by

$$c = c_0/\sqrt{\varepsilon}, \quad (2)$$

with c_0 being the electromagnetic wave speed in vacuum.

The ice cores B31, B32, and B33 were retrieved in the field season of 1997/98 during the EPICA pre-site survey [*Oerter et al.*, 2000]. DEP of the complex ε with a calibrated guarded scanning capacitor and γ-absorption density measurements were performed simultaneously along the 1 m long core sections immediately after retrieval. The combined DEP-density device, developed by *Wilhelms et al.* [1998] and improved by *Wilhelms* [2000], operated at a frequency of 250 kHz with an electrode length of 1 cm and data points taken in 5 mm increments, providing systematic accuracies for each ε-component of 1% and statistical errors of 0.1% after correcting the raw data to an ambient temperature of -15°C. An depth error of 1 cm results from the positioning of the core sections in the measuring bench. *Sommer et al.* [2000] performed dating by annual layer counting of multi-parameter chemical records combined with identification of volcanic horizons, resulting in an age–depth relationship for each ice core with an accuracy between ±5 and ±8 a.

For identification of sections with poor core quality we follow the scheme tested and applied by *Eisen et al.* [2003b]. The running mean and standard deviation of ε' is calculated within a 2.5 m window along the core. DEP values that show a permittivity which is more than one standard deviation below the window mean are rejected, as the lower permittivity values are most likely caused by cracks in the ice. Together with data gaps from drilling operation the total percentage of missing data of the different cores is around 5% (Table 1).

Table 1. Properties of ice core DEP data.

	B31	B32	B33
core length	115.1	148.9	129.6
missing data	0.84	1.02	0.32
rejected data	5.81	7.04	5.82
total	6.65	8.06	6.14

All values in m.

Surface-based ice penetrating radar

Usually two types of measurements are performed for radar data acquisition: common-midpoint (CMP) and common-offset (CO) surveys. The CMP recording technique basically yields information about the vertical reflection properties of a single column of small horizontal extend and the velocity–depth profile, as the distance between transmitter (TX) and receiver (RX) is symmetrically increased relative to the stationary center point. For CO surveys, TX and RX are kept at a fixed distance and moved across the surface, providing a picture of the subsurface structure along the survey profile in the time domain.

Radar measurements analyzed here result from CO measurements between various borehole locations (Figure 1) and were performed with a commercial RAMAC radar set of the Swedish company Malå Geoscience. The monopulse bistatic radar system was operated with antennae at 200 and 250 MHz, unshielded dipoles in a fixed distance of 60 cm in the first and shielded antennae at a distance of 36 cm in the latter case. Both setups are permanently mounted in skid-boxes and connected with the central processing unit via light conducting cables, thus avoiding noise from ohmic conductors. The processing unit was operated by a Husky FC PX5 personal computer, using the radar system software. The 200 MHz survey was carried out in 1999 between B32 and B33, using a snow tractor for pulling at an average speed of 8 km h^{-1}. Traces were recorded every 1.5 m, triggered by a distance wheel, in a 1500 ns time window consisting of 2400 samples. The 250 MHz data were recorded in 2001 between B32 and B31, pulling the device by a skidoo at 12 km h^{-1} with traces recorded every meter in a 1570 ns time window with 2048 samples. For either measurement setup the stored traces consist of 8 vertically stacked pulse recordings.

Whereas the comparison of surveyed and synthetic radargrams, carried out in the next section, is based on raw traces, the tracking of coherent patterns in adjacent traces can best be achieved in processed IPR profiles. Processing was performed using Paradigm Geophysical FOCUS version 4.2 software and includes 5-fold horizontal stacking, bandpass filtering, and automatic gain control (AGC). Internal reflection horizons were semi-automatically tracked in the processed data with the Landmark OpenWorks release 2003.0 software. The tracking algorithm exploits the coherency of signal features (e.g. minimum, maximum or zero amplitude) above noise to automatically detect this feature in a prescribed time window in adjacent traces and follows it as long as a similarity criteria is fulfilled. The tracking process is observed by the user and requires manual interaction in case of a low signal-to-noise ratio (SNR). Several IRHs were observed at numerous depths and tracked continuously in the whole region, forming the basis of the results presented in a later section.

Forward Modeling of Radargrams

Our interest in numerical modeling of electromagnetic wave reflections aims at the reproduction of surveyed radargrams for glaciological applications. The approach described here profits from the utilization of the in-situ complex dielectric constant and the implicit inclusion of wave phenomena occuring during propagation, especially multiple reflections and interferences, in the finite-difference time domain (FDTD) model.

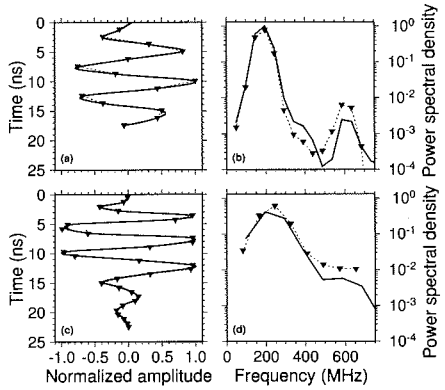

Figure 2. Radar wavelets used for FDTD modeling: time domain signals of the 200 (a) and 250 MHz antennae (c) and their corresponding power spectra in (b) and (d), respectively. Thin dashed lines with triangles indicate the raw data wavelets taken from the direct air wave, the thick lines denote the Akima spline interpolated resampled wavelets used for modeling.

Implementation of IPR characteristics

Different schemes were developed over the decades to employ FD techniques for computational electrodynamics. Whereas several approaches are based on wave equation formulations of only the electric or magnetic field, the algorithm introduced by *Yee* [1966] solves for both electric and magnetic fields in time and space using the coupled Maxwell's curl equations. This provides a robust basis with several advantages over other realizations [*Taflove*, 1995]. We implement the two-dimensional transverse electric (TE) version of the Yee algorithm on a staggered grid with leapfrog time integration. The TX is an infinite electric line source close to the surface (E_y-polarized), the y-component of the electric field E at a preselected position represents the signal recorded by the RX.

Two sets of IPR parameters are considered for the modeling experiments: the 250 MHz setup at B31 and B32 and the 200 MHz setup at B32 and B33. For each experiment the DEP data are linearly interpolated onto the cartesian space grid, assuming lateral homogeneous values in ice and air, with $\varepsilon_{air} = 1$ and $\sigma_{air} = 0$. Considering the results found by numerous authors on the crucial role of the transmitted radar wavelet on forward modeling [*Moore*, 1988; *Arcone et al.*, 1995; *Hildebrand*, 1996], we use duration and shape of the air waves determined from survey data as the source wavelets (Figure 2) and adopt the IPR TX and RX geometry also for modeling.

Calculations were performed with a parallelized version of the FD model on a NEC SX-6 supercomputer at the Deutsches Klimarechenzentrum (DKRZ, Hamburg, Germany). Model dimensions for standard runs are 10 m in horizontal and 120 m in vertical direction with an isotropic space increment $\Delta = 0.01$ m and a time increment $\Delta t = 0.01$ ns, thus providing high resolution of the interpolated source pulse (Figure 2), satisfying the stability criterion, and avoiding numerical diffusion [*Taflove*, 1995].

Evaluation of model results

The value of numerical modeling of synthetic radargrams lies in the opportunity to investigate the connection between medium properties and radar observations. Before transferring modeling results to in-situ problems the validity of modeling approach has to be proven.

Different radar setups, data processing, and display methods were examined to evaluate the truth content of synthetic radargrams, e.g. comparison of raw single traces [*Hildebrand*, 1996; *Miners*, 1998], embeddment of synthetic traces in raw CO profiles displayed in variable density representation [*Kohler et al.*, 2003], or confronting synthetic traces with stacked CO data in wiggle format [*Eisen et al.*, 2003b]. Most successful comparisons were so far achieved by exploiting the SNR improving properties of CMP processing [*Eisen et al.*, 2003c]. For the goals aimed at in this study, however, it is necessary to directly compare synthetic radargrams

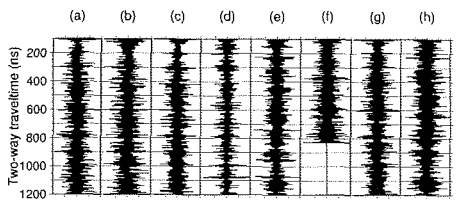

Figure 3. Single trace comparison of different data sets from B32, demonstrating the difficulty to reproduce individual reflection characteristics. Traces in (a)–(c) are from 30-fold stacked 200 MHz CO data, (d) is derived from a normal moveout-corrected CMP survey. CO data from different years, recorded at 250 MHz and also processed with 30-fold horizontal stacking, are shown in (f) and (g). The synthetic radar traces are plotted in (e) and (h), representing 200 MHz and 250 MHz experiments, respectively. Automatic gain control has been applied to 100 ns windows.

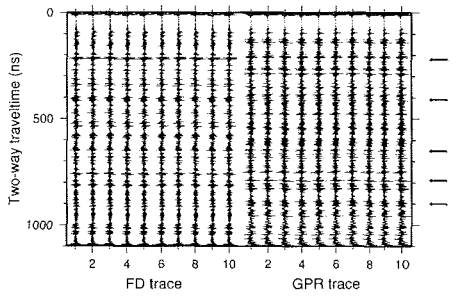

Figure 4. Evaluating the agreement of surveyed and synthetic radar data by comparison of multi-trace representations. The synthetic trace calculated by FD modeling (left) and the reference trace from CO data (right) are each plotted 10 times. The coherency of reflection signals in both data sets indicates internal reflection horizons that are reproduced by the synthetic data. Position of five selected IRHs discussed in the text are indicated by arrows. Automatic gain control has been applied to 100 ns windows.

with CO profiles of interest to associate properties investigated by numerical sensitivity studies with IRHs. Utilization of CMP data as an intermediate step between synthetic and surveyed CO data represents an additional source of uncertainties.

Small scale variability of physical properties of firn imposes the most severe problem on the objective reproducibility of surveyed data. Not only does processing of measured radar data by means of horizontal stacking only partly increase SNR, as demonstrated in Figure 3, also does the utilization of dielectric properties of one core ignore lateral inhomogeneities [L. Karlöf, personal communication, 2002]. Instead of trying to achieve the best agreement of single traces, we decide to make use of a data representation that usually reveals lateral coherencies in radar data. The reference trace derived from the CO profile of interest at a borehole location, consisting of 30 horizontally stacked traces, is reproduced 10 times, as is the synthetic radar trace. Plotting both data sets of multiple traces in variable amplitude wiggle format simulates two CO profiles from the same data point and makes it easier to identify those reflections that are reproduced by the synthetic data (Figure 4). In general we propose to use single-trace evaluations of CO data (Figure 3) only if specific structures are to be investigated, like anisotropic features in deeper ice, as it is by no means possible to achieve the same degree of agreement of CO with synthetic data as was demonstrated for CMP surveys. Multi-trace evaluations, on the other hand, emphasize the variations with depth, instead of individual reflector amplitude characteristics, and are more suitable for regional interpretations (Figure 4).

We perform the multi-trace comparison for each synthetic trace with the corresponding CO profile, that is the 250 MHz data connecting B31 and B32, and the 200 MHz data connecting B32 and B33. It is possible to identify at least five reflections that are continuous throughout the region and are reproduced to approximately

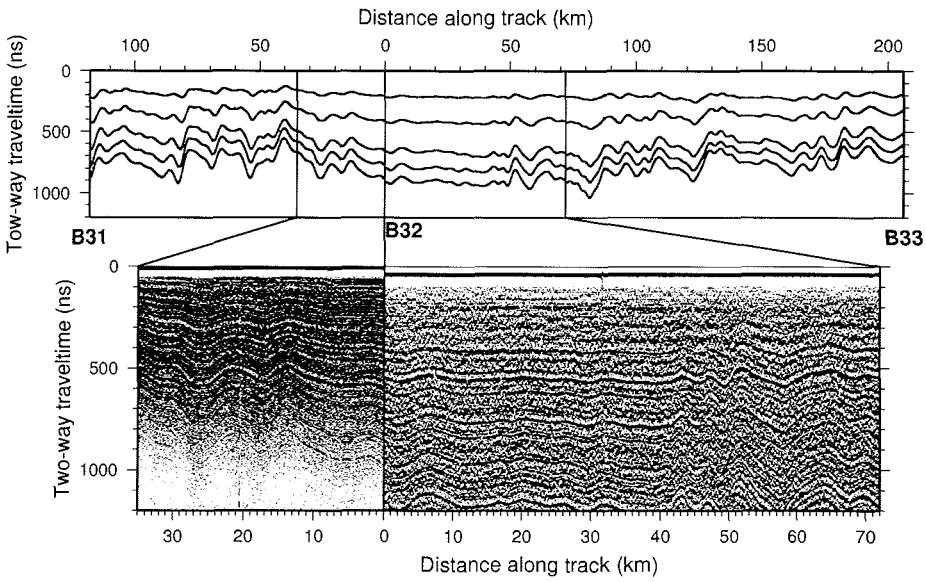

Figure 5. Internal reflections tracked from B31 via B32 to B33 (Figure 1), starting at B32 at TWTs of around 210, 420, 650, 780, and 900 ns. Below, two examples of processed common offset profiles are shown, recorded at 250 MHz (B32–B31) and 200 MHz (B32–B33). The greyscale indicates the signal envelope, i.e. magnitude, resulting in an emphasized contrast, but lower vertical resolution. Detection limits are around 1000 and 1200 ns for the 250 and 200 MHz signal, respectively. In regions with steeper internal topography, however, signals faint at shallower depths, posing a problem for tracking deeper reflections continuously.

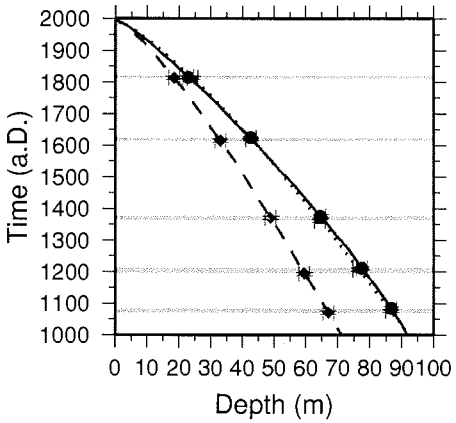

Figure 6. Dating of tracked internal reflection horizons at the three boreholes based on ice core data. The curves indicate the age–depth relation of the three ice cores B31 (solid), B32 (stippled), and B33 (dashed) [*Sommer et al.*, 2000]. The symbols represent the position of the depth-converted IRHs. Vertical error bars are the uncertainty of the ice core dating (5–8 a), horizontal error bars are the errors of the IRH tracking in m. The horizontal grey bars indicate the range between the oldest and youngest age of each IRH transferred from the ice core records.

the same degree by each of the different modeling experiments. The analyses described in the next section will focus on these IRHs for application purposes.

Analyses and Interpretations

Our main goals are the dating of IRHs, the identification of their constituting dielectric signals, and the synchronization of ice cores. In this section we present different methods to find appropriate solutions for the individual formulation of questions.

The common heart to approach either problem is the continuous tracking of IRHs between drilling locations (Figure 5), already introduced above. However, whereas dating of IRHs is most accurate if dated ice cores are available at either end of the profile, as laid out next, the analyses of reflection causes moreover profits from FD modeling in most cases. Finally, we join both results to estimate accuracies of and discuss conditions necessary for successful ice core synchronization.

Dating internal reflection horizons

As radar data are recorded in the time domain (reflection amplitude as a function of TWT) they have to be converted to depth domain before transferring ice core age–depth relationships to prominent radar signals. The most precise TWT–depth function is obtained from integration of the DEP-based wave speed (2), accurate to within 1% [*Eisen et al.*, 2002]. After conversion, each tracked IRH is associated with a specific depth at the borehole location for which an age dating is available. Performing TWT–depth–age conversions at all drill sites yields three age datings for each tracked signal (Figure 6).

Theoretically, tracking of single phases of an IRH is accurate to within $\lambda/4$. However, this value can only be achieved if the data is recorded at a high sampling rate which is in general in contrast to long recording windows and efficient field work. Although system settings during our radar surveys fulfil requirements to reach this accuracy, measurement noise and lateral variations of the reflection properties do not allow tracking of coherent signals to this limit.

For low noise content the continuous tracking of a single phase can be as accurate as $\pm\lambda/2$, that is $\pm$ 0.5 m or 2.5 ns for the 200 MHz data in firn (assuming $c_{firn} = 2 \cdot 10^8$ m s^{-1}). In respect to the ice core datings this corresponds to an age error of $\pm$6.5 a at B31 and B32 and $\pm$8.5 a at B33 below 40 m depth, with slightly lower values above. If the reflector is rather faint or the internal structure is subject to strong changes, continuous tracking of a single phase might not be possible. Nevertheless, the reflector itself might still be continuous and trackable at

Table 2. Dating of IRHs at borehole locations.

ice core	210 ns	415 ns	650 ns	780 ns	890 ns
IRH tracking					
B31	1815	1624	1376	1212	1085
B32	1822	1619	1362	1208	1075
B33	1813	1615	1371	1194	1071
mean	1817	1619	1370	1205	1077
error	±5	±5	±7	±10	±7
FD Sensitivity Studies					
B31	1819 – 1809	1645 – 1632	1394 – 1382	1233 – 1215	1097 – 1081
B32	1819 – 1807	1645 – 1627	1374 – 1360	1229 – 1210	1092 – 1078
B33	1820 – 1808	1647 – 1633	1395 – 1364	1213 – 1185	1093 – 1067
mean	1819 – 1808	1646 – 1631	1388 – 1369	1225 – 1204	1094 – 1075
error	±1 ± 1	±1 ± 3	±12 ± 12	±11 ± 16	±3 ± 7

All values in a. The IRHs are identified by their TWT at B32. Age–depth relationships for each core are taken from *Sommer et al.* [2000], rounded to whole years and accurate to 5–8 a. The listed errors are the standard deviations in respect to the three datings of each IRH. The total standard deviation referred to in the text is based on the 15 values for IRH tracking and 30 values for the FD sensitivity studies and result as 7 a and 8 a, respectively.

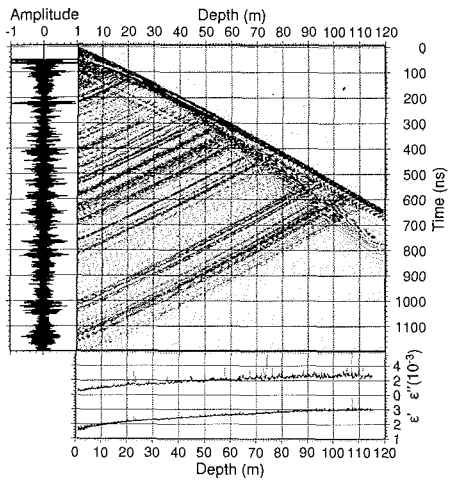

Figure 7. Depth–time slice of the modeled E_y wave field at the receiver position, showing the propagation of the wavelet transmitted at the surface (to the left) through the medium (depth to the right) with time (downwards). Reflections occur at discontinuities of ε and travel back to the surface. Greyscale indicates signal amplitudes. The lower figure shows the ε-distribution with depth, the radargram to the left displays the signal as it is recorded at the surface.

a lower accuracy, limited by the length of the energetic part of the source wavelet, which is around 10 ns in our case (Figure 2). Tracking of these low quality reflectors is then accurate to within some 5 ns (1 m), corresponding to an age uncertainty of approximately 13 a at B31 and B32 and 17 a at B33.

The agreement of this theoretical error analysis and the statistical values calculated from the IRH data set are on the same order of magnitude (Table 2). The standard deviation of the mean age of the tracked signals varies between 5 and 10 a, the total standard deviation derived from all values results as 7 a.

The theoretical estimates, however, do rely on the assumption that a single feature in ε causes the reflection. The problem is less well behaved if several features occur on a short vertical distance. If the traveltime from one reflecting feature to the next is less than the length of the source wavelet λ_w, the individual reflected wave trains superimpose, leading to constructive and destructive interferences, recorded reflections that can hardly be separated in the radargram, and which might moreover be noisy because of strong multiple reflections. In this context, FD forward modeling of radargrams provides a mighty tool to reveal the constituting components of such blurred reflections, as demonstrated next.

Origin of reflection horizons

From simplistic information-theoretical point of view the FD program basically encodes and transforms the information contained in the ε-depth distribution to the time domain format of the radargram. The embedded basic traveltime–depth conversion is in principle already possible with a velocity–depth function. However, only the knowledge of the wave field at every time step allows for investigation of complicated processes occuring during reflection and propagation. These lead to a much different depth structure of the final radargram than the one evident from original physical properties of the medium.

For instance, combination of the depth–time slice of the wave field at the receiver location with the medium properties and the synthetic radargram nicely illustrates at which depth reflections originate, which ice core signals might be involved in the reflection process, and what the reflection looks like for the receiver at the surface (Figure 7). Unfortunately, it is still difficult to directly observe interfering signals and multiple reflections in this representation because of the at least two orders of magnitude difference in signal amplitude of the primary (transmitted) and secondary (reflected) wave trains.

We therefore perform two types of sensitivity experiments with changed DEP data to directly

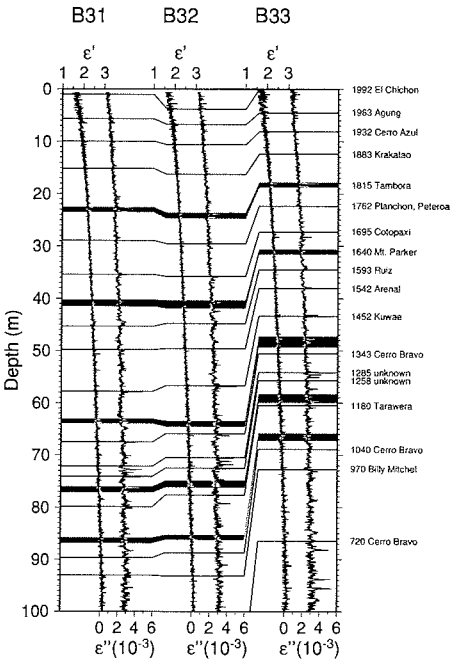

Figure 8. Measured ordinary relative permittivity ε' and dielectric loss factor ε'' as a function of depth of the ice cores B31, B32, and B33. Selected volcanic events are indicated on the right, their depth at the different locations is indicated by the thin solid lines. Datings are taken from *Sommer et al.* [2000], volcanic events at B32 from *Göktaş* [2002]. The dark gray horizontal bars indicate the depth sections for which DEP values are removed and linearly interpolated for sensitivity studies.

investigate the influence of individual DEP features on the radargram: the first type aims at the origin of the tracked IRHs used earlier for dating purposes; the second examines the influence of closely spaced and neighboring DEP signals on an observed broad reflection.

The datings obtained from the IRH tracking described above result from following only individual signals from core to core [*Bogorodsky et al.*, 1985], but lacks evidence that the same signals were tracked continuously. Additional information for verification and error estimates can be obtained by forward modeling. Only those surveyed reflections are selected for tracking that are reproduced by the 250 MHz synthetic data at B31 and B32 as well as by the 200 MHz data at B32 and B33. This makes sure that changes in DEP data, confined to the sections constituting these reflections, will also be evident in forward modeling results. For this purpose the DEP data of all three ice cores are removed in the vicinity of the depths where the tracked IRHs originate (Figure 8). Forward modeling computations based on the altered DEP data lead to distributions of reflections that are different from the original ones. Ideally, the modeling results should exactly remove the selected reflections and, at the same time, should get by with least removed DEP data as possible. As this cannot be expected a priory, the identification of the depth sections responsible for reflections is a rather iterative process carried out manually.

The final results clearly demonstrate the connection between removed DEP sections and vanishing reflections (Figure 9). The quality depends on several factors: the reproducibility of the surveyed reflections by DEP-based forward modeling – gapy DEP sections produce synthetic radargrams of poorer agreement; the resolution of the radar data – reflection properties strongly depend on the source wavelet (compare the reflection characteristic at 790 ns at B32 for 200 and 250 MHz); the strength of the surveyed reflection – lower SNR decreases accuracies (e.g. the 200 MHz reflections at 650 and 480 ns at B32 and B31, respectively).

The datings obtained from the IRH-related sensitivity studies provide an additional means to date the origin of reflections, as they associate a depth – and thus age – range instead of just one value for each IRH (Table 2). The statistical analyses of this additional data set yields dating errors that show larger scatters, but the total standard deviation of 8 a derived from the whole set is just slightly larger than

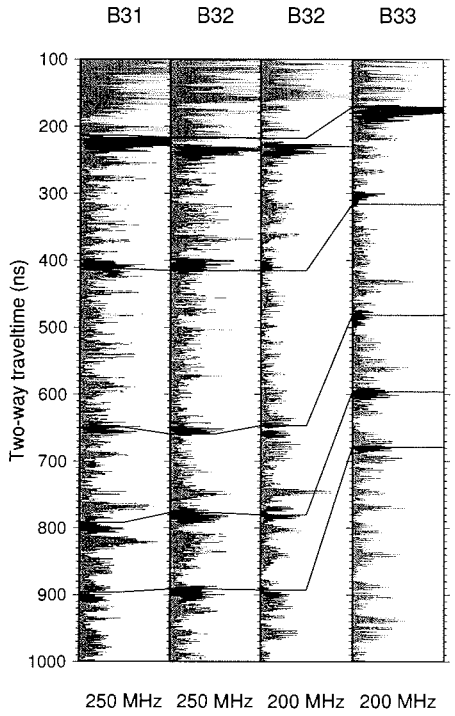

Figure 9. Results of IRH sensitivity studies at B31, B32, B33 with 250 and 200 MHz. The envelope of the original synthetic radargrams are plotted in black, with the results of the sensitivity studies plotted in grey on top. The reflections appearing in black are missing in the sensitivity results because of removed DEP data (Figure 8). The horizontal step-like black lines indicate the depth of the tracked IRHs at each location.

the 7 a obtained earlier from IRH tracking, accentuating the validity of both error estimates.

The second type of sensitivity experiment investigates the variation of reflection characteristics. Removing sections of the DEP data and performing forward modeling with the interpolated ice core record yields a different reflection structure. The part of the now missing signals is caused by the removed section of the DEP data. In total we carry out three sensitivity runs with 200 MHz signals at B32 and B33, focusing on the region in the age range between 1150 and 1280 a. The DEP data in both core profiles is removed in three stages increasing the age range by 20 a intervals: 1210–1230, 1210–1250, and 1190–1250 a. The series of reflections shown in Figure 10 (a) at a TWT of 740–840 ns originates from a group of permittivity peaks at a depth range of around 71–81 m at B32. At B33 the signals are located between 54 and 62 m with partly different parameter values and peculiarities (Figure 10 (d)). The series of sensitivity studies reveals that the strong reflection signals originating at 1240, 1220, 1200 a (centered at ~770, 783, and 803 ns TWT, respectively) can be separated and almost unambiguously attributed to the corresponding DEP sections. At B33 the DEP signals at the same age cause the reflections to be differently structured: only the signal at 1200 a (600 ns) is clearly visible, the 1220 and 1240 a reflections (558 and 575 ns TWT, respectively) are either small and not outstanding anymore or show a broadened phase characteristic (Figure 10 (b)). The sensitivity runs demonstrate that only the 1200 a reflection really has the same constituting features at B33 as at B32, whereas the other two signals result from a superposition of several reflections partly originating at other depths (Figure 10).

The reason for the different appearance of the same DEP signal in the modeled radargrams is simple: the accumulation rate at B33 is lower than at B32, the ε-peaks are closer together, resulting in superposition and interference of the reflected waves and changed properties of probable multiple reflections. Tracking single phases of the 1240 IRH from B33 to B32, for instance, leads to a point where first single phases and then the reflector as a whole split up. Because of this ambiguity the signal tracked to B32 might be of different origin than the signal we started from at B33, increasing the uncertainty of subsequent dating attempts if additional information from forward model-

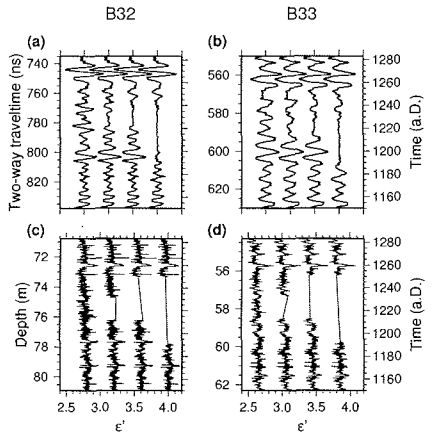

Figure 10. Example for detailed signal decomposition, modeled with the 200 MHz signal at B32 (a) and B33 (b). The permittivity of the constituting DEP signals are shown in (c) and (d) and shifted by +0.4 in respect to the first profile; straight parts indicate removed data. The right-hand y-axes are time a.D. in the same scale for all graphs, the left-hand y-axes are scaled differently because of the varying depth and traveltime range at B32 and B33 of the same age window.

ing is not available.

Synchronizing ice core records

The scheme developed so far profits from the presence of several synchronized ice core records, dated independently from radar-based information. Nevertheless, one can think of several applications with only one dated ice core that take advantage of this preparatory work, e.g. extrapolation of age–depth relationships, synchronization of ice cores of minor quality, or preliminary studies for future projects. Based on an existing ice core with profiled dielectric properties we propose the following implementation:

- calculate a synthetic radar trace from the DEP data using appropriate modeling parameters and wavelet functions
- determine a survey reference trace at the drilling location from radar profiles connecting to the new region of interest and evaluate the agreement of survey and synthetic radar trace
- if correspondence of both trace types is significant, localize reflections that are prominent in either trace and perform sensitivity studies to identify the constituting DEP features
- track the corresponding internal reflection horizons to the region of interest
- at the final destination perform a CMP-based traveltime–depth conversion of the radar data
- scale the initial DEP data to the new reflector–depth distribution and perform forward modeling (again including evaluation of surveyed and synthetic results as well as IRH sensitivity studies)
- if the reflector characteristics are reproduced synthetically, ice core properties of the starting point can be extrapolated to the new destination

Feasibility of this concept implies several assumptions: processes forming isochronous reflectors leave a signature at the surface of the whole study area (e.g. meteorological events, deposits of volcanic origin or storm advected oceanic or terrestrial materials); the IRHs are continuous, although not necessarily of laterally stable internal characteristics; synthetic radargrams reproduce the surveyed reference traces. Whereas the first and second assumption are obviously knock-out criteria, the unsuccessful forward modeling at the starting or final destination only reduces accuracies of the aspired synchronization.

Two types of errors are involved in the extrapolation of ice core datings and synchronization: first, the accuracy of the dating of the

initial core, and, second, the uncertainties involved in the IRH tracking. The ice cores used in this study are dated with errors of around 5–8 a [*Sommer et al.*, 2000]. With the IRH tracking errors discussed above, the total statistical error of a best case scenario – continuous tracking of single phases and highly accurate ice core datings – is on the order of 8 a. The worst case – highly variable but still continuous reflectors and lower accuracy of the age–depth relation – yields an accuracy of some 19 a in the depth range below 40 m. If several ice cores are available, the IRH tracking error can be minimized if the site with higher accumulation is chosen as the starting point. Decreasing annual layer thickness, and therefore temporal resolution, along track generally insure more stable tracking than vice versa, as already demonstrated for alpine ice bodies [*Eisen et al.*, 2003a].

It has to be kept in mind that variations with depth of the two error components (IRH and age–depth) have an opposite sign. The physical limit for IRH tracking accuracy is wavelength (respective wave speed) and lateral signal coherency. As most decrease of the wave speed occurs in the upper tens of meters of the ice column, the tracking accuracy increases in the upper part and is then basically constant for the rest of the ice column, given that the SNR remains sufficiently high, as is the case for airborne radio echo sounding data down to several km [*Nixdorf et al.*, 1999]. The accuracy of the core-based age–depth relation, on the other hand, strongly decreases with depth. Firstly, the firn (and later ice) densification process increases the age rate (age per depth), thereby decreasing resolution of distinct features, annual layers and dominant signal; secondly, in deeper parts ice dynamics smooth out additional features which might not be preserved in ice core records. All in all, the accuracy of dating extrapolation is limited by IRH properties in the upper hundreds of meters of the ice sheet, but the large increase of the age rate with depth due to ice dynamics are the limiting factors in deeper regions.

Outlook

The findings developed in this study emphasize the complementary character of ice core records and radar data, providing mutual information on the glacial subsurface structure and composition. A common problem in ice core interpretation is the different quality of age scales, derived from various techniques. Merging ice cores, radar data, and the analysis methods utilizing FD modeling on larger horizontal and vertical scales might partly remedy ambiguous interpretations.

Pinning down the age of isochronic IRHs from association with datings of several ice cores is the preferred approach in terms of minimizing accuracy, but age–depth profiles are in fact not a necessary criteria. In fact, as long as the physical process constituting a radar reflector can be revealed and the assumption holds that it remains also responsible over larger distances, any property can be transferred along the IRH. Good core quality, however, implying high SNR in physical and chemical records with distinct features, and preferably high accumulation rates, that is high temporal resolution, is one key ingredient for good agreement between synthetic and measured radargrams. We are well aware that sensitivity studies with FD forward modeling are a kind of trial-and-error scheme. The ultimate goal, of course, is the direct accurate inversion of radar data to yield DEP-distributions as a two-dimensional profile, a goal that probably might not be achieved for quite a while but should nevertheless be kept in mind.

In this context, the concept laid out here also promises useful application for analyses of still remaining problems in deeper parts of the ice sheet. The present study is a first step, as more or less unambiguous in upper layers, but will become even more important if the technique is extended to deeper regions of the ice sheet where several physical processes leading to reflections of comparable magnitude show up. Namely the contribution of fabric orientations and rapid changes therein on the elec-

tromagnetic reflectivity can be investigated in further detail as soon as high resolution DEP profiles, corresponding radar surveys, to be expected within the next years from the EPICA ice core in DML, and a numeric model covering several kilometers of ice column are available.

Acknowledgments. The original version of the FDTD model was developed by Volker Mayer and Jupp Sandmeier as a module for the commercial radar and seismic analysis PC software Reflex (Sandmeier Software, Karlsruhe, Germany). They gave helpful advice for decoupling the module from the PC software for our special purposes. Debugging and optimization greatly profited from support by Stephan Frickenhaus, AWI computing centre, and Klaus Ketelsen, DKRZ. Preparation of this work was supported by the Deutsche Forschungsgemeinschaft grant Ni493/1 and two scholarships of the Studienstiftung des Deutschen Volkes. This work is a contribution to the "European Project for Ice Coring in Antarctica" (EPICA), a joint ESF (European Science Foundation)/EC scientific programme, funded by the European Commission and by national contributions from Belgium, Denmark, France, Germany, Italy, the Netherlands, Norway, Sweden, Switzerland and the United Kingdom.

References

Arcone, S., D. Lawson, and A. Delaney, Short-pulse wavelet recovery and resolution of dielectric contrasts within englacial and basal ice of Matanuska Glacier, Alaska, U.S.A., *J. Glaciol.*, *41*, 68–86, 1995.

Baldwin, D. J., J. L. Bamber, A. J. Payne, and R. L. Layberry, Using internal layers from the Greenland Ice Sheet, identified from radio echo sounding data, with numerical models, *Ann. Glac., 37, -in press-*, 2003.

Blindow, N., Reflection amplitudes of 40 MHz monopulse radio echo sounding: correlation with ice core data and ice dynamics, *Filchner-Ronne Ice Shelf Programme, Report No.8 (1994)*, pp. 5–8, 1994.

Bogorodsky, V., C. Bentley, and P. Gudmandsen, *Radioglaciology*, D. Reidel Publishing Company, Dordrecht, Holland, 1985.

Clough, J. W., Radio echo sounding: reflections from internal layers in ice sheets, *J. Glaciol.*, *18*, 3–14, 1977.

Dahl-Jensen, D., et al., A search in North Greenland for a new ice-core drill site, *J. Glaciol.*, *43*, 300–306, 1997.

Eisen, O., U. Nixdorf, F. Wilhelms, and H. Miller, Electromagnetic wave speed in polar ice: Validation of the CMP technique with high resolution DEP and γ-density measurements, *Ann. Glac.*, *34*, 150–156, 2002.

Eisen, O., U. Nixdorf, L. Keck, and D. Wagenbach, Alpine ice cores and ground penetrating radar: Combined investigations for glaciological and climatic interpretations of a cold Alpine ice body, *Tellus*, *55B*, 1007–1017, 2003a.

Eisen, O., F. Wilhelms, U. Nixdorf, and H. Miller, Identifying isochrones in GPR profiles from DEP-based forward modelling, *Ann. Glac., 37, -in press-*, 2003b.

Eisen, O., F. Wilhelms, U. Nixdorf, and H. Miller, Revealing the nature of radar reflections in ice: DEP-based FDTD forward modeling, *Geophys. Res. Letters*, *30*, 2003c.

Frezzotti, M., S. Gandolfi, and S. Urbini, Snow megadunes in Antarctica: Sedimentary structure and genesis, *J. Geophys. Res.*, *107*, ACL X-1–X-12, 2002.

Göktaş, F., *Characterisation of glacio-chemical and glacio-meteorological parameters of Amundsenisen, Dronning Maud Land, Antarctica*, vol. 425 of *Berichte zur Polarforschung*, Alfred-Wegener-Institut für Polar- und Meeresforschung, 2002.

Gudmandsen, P., Layer echoes in polar ice sheets, *J. Glaciol.*, *15*, 95–101, 1975.

Hammer, C., Acidity of polar ice cores in relation to absolute dating, past volcanism, and radio-echoes, *J. Glaciol.*, *25*, 359–372, 1980.

Harrison, C. H., Radio echo sounding of horizontal layers in ice, *J. Glaciol.*, *12*, 383–397, 1973.

Hempel, L., and F. Thyssen, Deep Radio Echo Soundings in the vicinity of GRIP and GISP2 Drill Sites, Greenland, *Polarforschung*, *62*, 11–16, 1992.

Hempel, L., F. Thyssen, N. Gundestrup, H. B. Clausen, and H. Miller, A comparison of radio-echo sounding data and electrical conductivity

of the GRIP ice core, *J. Glaciol.*, *46*, 369–374, 2000.

Hildebrand, A., Untersuchung der Laufzeit- und Amplitudenverhalten elektromagnetischer Impulse bei glaziologischen Radarmessungen, Ph.D. thesis, Westfälische Wilhelmsuniversität Münster, 1996.

Hodgkins, R., M. J. Siegert, and J. A. Dowdeswell, Geophysical investigations of ice-sheet internal layering and deformation in the Dome C region of central East Antarctica, *J. Glaciol.*, *46*, 161–166, 2000.

Huybrechts, P., D. Steinhage, F. Wilhelms, and J. Bamber, Balance velocities and measured properties of the Antarctic ice sheet from a new compilation of gridded data for modeling, *Ann. Glac.*, *30*, 52–60, 2000.

Jacobel, R., and S. Hodge, Radar internal layers from the Greenland summit, *Geophys. Res. Letters*, *22*, 587–590, 1995.

Jacobel, R. W., A. M. Gades, D. L. Gottschling, S. M. Hodge, and D. L. Wright, Interpretation of radar-detected internal layer folding in West Antarctic ice streams, *J. Glaciol.*, *39*, 528–537, 1993.

Kanagaratnа, P., S. P. Gogineni, N. Gundestrup, and L. Larsen, High-resolution radar mapping of internal layers at NGRIP, *J. Geophys. Res.*, pp. 33,799–33,812, 2001.

Kohler, J., J. C. Moore, and E. Isaksson, Comparison of modelled and observed responses of a glacier snowpack to ground-penetrating radar, *Ann. Glac., 37, -in press-*, 2003.

Millar, D. H. H., Radio echo layering in polar ice sheets and past volcanic activity, *Nature*, *292*, 441–443, 1981.

Miners, W., A. Hildebrand, S. Gerland, N. Blindow, D. Steinhage, and E. Wolff, Forward Modelling of the Internal Layers in Radio Echo Sounding Using Electrical and Density Measurements from Ice Cores, *J. Phys. Chem. B*, *101*, 6201–6204, 1997.

Miners, W. D., Electromagnetic reflections inside ice sheets, Ph.D. thesis, Open University, 1998.

Moore, J., Dielectric variability of a 130 m Antarctic ice core: implications for radar sounding, *Ann. Glac.*, *11*, 95–99, 1988.

Moore, J., and J. Paren, New technique for dielectric logging of Antarctic ice cores., *Journal de Physique (Colloque C1)*, *48*, 155–160, 1987.

Nereson, N. A., and C. F. Raymond, The elevation history of ice streams and the spatial accumulation pattern along the Siple Coast of West Antarctica inferred from ground-based radar data from three inter-ice-stream ridges, *J. Glaciol.*, *47*, 303–313, 2001.

Nixdorf, U., and F. Göktaş, Spatial depth distribution of the subglacial bed and internal layers in the ice around NGRIP, Greenland, derived with airborne RES, *J. Appl. Geophys.*, *47*, 175–182, 2001.

Nixdorf, U., D. Steinhage, U. Meyer, L. Hempel, M. Jenett, P. Wachs, and H. Miller, The newly developed airborne RES-system of the AWI as a glaciological tool, *Ann. Glac.*, *29*, 231–238, 1999.

Oerter, H., F. Wilhelms, F. Jung-Rothenhäusler, F. Göktas, H. Miller, W. Graf, and S. Sommer, Accumulation rates in Dronning Maud Land as revealed by dielectrical-profiling measurements at shallow firn cores, *Ann. Glac.*, *30*, 27–34, 2000.

Raymond, C. F., N. Nereson, A. M. Gades, H. Conway, R. Jacobel, and T. Scambos, Geometry and stratigraphy of Siple Dome, Antarctica, *Antarct. J. U.S.*, *30*, 91–93, 1995, 1996 Review.

Richardson-Näslund, C., and P. Holmlund, Spatial variablility in shallow snow-layer depths in central Dronning Maud Land, East Antarctica, *Ann. Glac.*, *29*, 10–16, 1999.

Robin, G. d. Q., S. Evans, and J. T. Bailey, Interpretation of radio echo sounding in polar ice sheets, in *Philosophical Transactions of the Royal Society of London*, vol. 146 of *A*, pp. 437–505, Royal Society of London, 1969.

Siegert, M. J., R. Hodgkins, and J. A. Dowdeswell, A chronology for the Dome C deep ice-core site through radio-echo layer correlation with the Vostok ice core, Antarctica, *Geophys. Res. Letters*, *25*, 1019–1022, 1998.

Sommer, S., et al., Glacio-chemical study covering the past 2 kyr on three ice cores from Dronning Maud Land, Antarctica 1. Annually resolved accumulation rates, *J. Geophys. Res.*, *105*, 29,411–29,421, 2000.

Steinhage, D., U. Nixdorf, U. Meyer, and H. Miller, New maps of the ice thickness and subglacial

topography in Dronning Maud Land, Antarctica, determined by means of airborne radio echo sounding, *Ann. Glac.*, *29*, 267–272, 1999.

Taflove, A., *Computational Electrodynamics: The Finite-Difference Time-Domain Method*, Artech House, Boston, 1995.

Wilhelms, F., *Measurement of dielectric properties of polar ice cores (in German)*, vol. 367 of *Berichte zur Polarforschung*, Alfred-Wegener-Institut für Polar- und Meeresforschung, 2000.

Wilhelms, F., J. Kipfstuhl, H. Miller, K. Heinloth, and J. Firestone, Precise dielectric profiling of ice cores: a new device with improved guarding and its theory, *J. Glaciol.*, *44*, 171–174, 1998.

Yee, K. S., Numerical solution of initial boundary value problems involving Maxwell's equations in isotropic media, *IEEE Transactions on Antennas and Propagation*, *14*, 302–307, 1966.

Olaf Eisen, Uwe Nixdorf, Frank Wilhelms, Heinrich Miller, Alfred-Wegener-Institut für Polar- und Meeresforschung, Postfach 120161, 27515 Bremerhaven, Germany. (e-mail: oeisen@awi-bremerhaven.de)